

Comparison-Benchmarking of three DWM-based wake models at below-rated wind speeds

Øyvind Waage Hanssen-Bauer¹, Paula Doubrawa², Helge Aa. Madsen³, Henrik Asmuth⁴, Jason Jonkman², Gunner C. Larsen³, Stefan Ivanell⁴, and Roy Stenbro¹

¹Institute for Energy Technology, Instituttveien 18, 2007 Kjeller, Norway

²National Renewable Energy Laboratory, Golden, CO 80401, USA

³Department of Wind Energy, Risø Campus, Technical University of Denmark, DK-4000 Roskilde, Denmark

⁴Wind Energy Division, Department of Earth Sciences, Uppsala University, 621 67 Visby, Sweden

Correspondence: Øyvind Waage Hanssen-Bauer (oyvind.hanssen-bauer@ife.no)

Abstract. Wind turbine wake models are essential tools for predicting power losses and structural loads in wind farms. Among ~~them~~these, the dynamic wake meandering (DWM) model, included as a recommended approach in the International Electrotechnical Commission design standard, is a widely used engineering-fidelity method that balances accuracy and computational cost. This study compares the performance of three DWM-based wake model implementations (from the Technical University of Denmark, the National Renewable Energy Laboratory, and the Institute for Energy Technology) under below-rated wind speed conditions. Model predictions of wake flow, power output, and structural loads for a four-turbine row are evaluated across different ambient turbulence levels and wind-direction misalignments, and compared against high-fidelity large-eddy simulation results. All three models captured the overall wake evolution and mean turbine performance with reasonable accuracy; their predicted time-averaged thrust and power were typically within ~~5–10~~5–10 % of the large-eddy simulation benchmark. However, notable differences emerged in wake structure and unsteady load predictions, with discrepancies increasing for turbines further downstream. These differences highlight the importance of modelling choices such as wake summation and turbulence treatment, which strongly influence power-deficit and fatigue-load predictions. Comparison with large-eddy simulations reveals ~~the each approach's~~ strengths and weaknesses ~~of each approach~~, indicating where improvements are needed. ~~In general~~Overall, the findings ~~suggest directions for refining DWM models and improving~~ point to specific refinements for DWM models to improve their fidelity, ultimately enabling more robust wake predictions for wind farm design and operation.

1 Introduction

The wind energy industry has undergone significant development ~~in recent decades~~since its beginning, evolving from isolated, low-efficiency turbines to large-scale, modern wind farms. In these farms, spatial constraints and the need to minimize infrastructure and maintenance costs often lead to farm layouts with tightly spaced turbines. This evolution has increased the focus on turbine–turbine interactions, as wake effects have been identified as a major contributor to energy losses and elevated structural loads throughout the farm.

To ~~maximise~~maximize energy yield, the industry commonly employs simplified engineering models for steady-state wake prediction during design and operational planning. However, wakes from upstream turbines not only reduce wind speeds but also generate unsteady turbulence, which impacts the performance and ~~fatigue-loading~~fatigue loading of downstream machines. Because steady-state models are inherently unable to capture these unsteady flow phenomena, they are not suitable for load assessments. Instead, the industry commonly relies on the effective turbulence model (International Electrotechnical Commission, 2019) for structural load calculations, which does not simulate individual wakes explicitly but approximates their impact by artificially increasing the ambient turbulence intensity. The alternative approach to consider wake effects on turbine loads according to international wind turbine design standards is the dynamic wake meandering (DWM) model ~~(Larsen et al., 2008)~~(Larsen et al., 2008; Madsen et al., 2010; Larsen et al., 2013). This approach explicitly simulates individual wakes as convecting, meandering flow fields, where the ~~velocity-deficit~~velocity deficit is advected downstream with stochastic lateral and vertical motion driven by ambient large-scale turbulence, superimposed on an ambient wind field. By capturing key unsteady wake dynamics such as meandering and advection, DWM-based models include physical phenomena that are absent from simpler steady-state models, yet remain orders of magnitude more computationally efficient than high-fidelity large-eddy simulations (LES). Recent work by Doubrawa et al. (2023) showed that even though ~~on-average~~the effective turbulence model and the DWM model predict similar intra-farm flow characteristics and, when coupled with aeroelastic solvers, turbine structural loads on average, much more insight and ~~direction-variability-arises~~directional variability arise from the DWM model that the effective turbulence model cannot resolve. DWM models enable realistic load predictions under ~~wake conditions~~ — waked conditions — an essential capability for wind farm design and certification.

Since its introduction in the early 2000s, the DWM model has undergone continuous refinement. Several research groups have proposed enhancements or modifications to the original formulation, including alternative meandering algorithms, variations in wake-deficit shapes ~~(Doubrawa et al., 2017; Branlard et al., 2023)~~(Doubrawa et al., 2017; Branlard et al., 2023; Bernard et al., 2023), improved wake superposition techniques (Machefaux et al., 2016; de Vaal and Muskulus, 2021), and more advanced treatments of wake-added turbulence (Madsen et al., 2005; Keck et al., 2015; Branlard et al., 2024). These efforts have led to a range of DWM-based implementations, such as the original model integrated with DTU's aeroelastic software HAWC2, NREL's FAST.Farm tool (Jonkman et al., 2017), and the more recent WIFET wake model (Hanssen-Bauer et al., 2020; de Vaal and Muskulus, 2021), each incorporating unique sub-models. While grounded in the same core physical principles, their predictions can differ substantially due to implementation choices.

DWM-based models have been calibrated and compared with high-fidelity large-eddy simulations coupled with LES actuator-line turbine models (LES-ALM) (Madsen et al., 2010; Jonkman et al., 2018; Doubrawa et al., 2018; Shaler and Jonkman, 2021; Hanssen-Bauer et al., 2020) and also validated with full-scale field measurements (Madsen et al., 2010; Larsen et al., 2013, 2015, 2017). ~~Yet direct~~Direct intercomparisons between different DWM implementations remain limited. ~~A notable exception is the~~ with a few notable exceptions. The benchmarking study by Asmuth et al. (2022) ~~, which~~ compared six numerical ~~models—including models – including~~ DWM implementations from DTU and NREL, and the LES-ALM software ~~Ellipsys3D—with Ellipsys3D – with~~ full-scale measurements from the DanAero experiment. That study focused on a two-turbine setup under below-rated wind conditions, ~~analysing~~analyzing one full-wake and one partial-wake case. However, the

scope was limited to the response of two turbines and the wake flow behind only the upstream rotor, leaving the effects of multiple interacting wakes unexamined. In another benchmarking study, Bernard et al. (2024) compared three different DWM implementations, together with the effective turbulence model and LES, against measurement data from an offshore wind farm with 6 MW turbines located in the North Sea. This comparison presented the response of one turbine in the second row of the wind farm for below-rated wind speeds and different inflow directions, resulting in both free inflow and inflow partially affected by the wake of a single upstream turbine.

Our recent comparison of DWM-based models extended the benchmarking to an above-rated wind speed case, involving a four-turbine row aligned with the incoming wind and a single ambient turbulence condition (Hanssen-Bauer et al., 2023). That study revealed substantial discrepancies between the model implementations. While time-averaged ~~wake-deficits~~ wake deficits and power outputs were generally consistent across models and in reasonable agreement with LES, fatigue-load predictions diverged significantly further downstream, with differences reaching up to 25 % of reference values. These results underscore how implementation details, such as wake-merging methods and turbulence modelling, can critically affect load predictions, even under otherwise comparable conditions. They also highlight the need for continued evaluation and improvement of engineering-fidelity wake models before they can be fully relied upon in design and certification workflows.

In the present study, we extend the earlier above-rated comparison to systematically evaluate three DWM-based wake models under below-rated wind speed conditions, while introducing two further variables: ambient turbulence intensity and wind-direction misalignment. Specifically, we ~~analyse~~ analyze three inflow conditions representative of low to moderately high turbulence environments and two wind alignment scenarios — one with flow aligned with the turbine row, resulting in a full-wake configuration, and another with a small offset angle introducing a partial-wake condition. A high-fidelity LES-ALM is used as the reference benchmark, following the methodology of our previous study (Hanssen-Bauer et al., 2023). This setup enables an in-depth assessment of wake evolution, power production, and structural load indicators along a row of turbines for each DWM model, across all combinations of wind speed, turbulence, and alignment.

The primary objectives of this study are twofold: (1) to evaluate each DWM model’s accuracy relative to LES predictions, identifying ~~the~~ deviations in wake behaviour and turbine fatigue response; and (2) to investigate how differences in sub-modelling strategies — such as wake meandering formulations, velocity-deficit profiles, multi-wake superposition methods, and wake-added turbulence treatments — affect model performance. By isolating and ~~analysing~~ analyzing these factors, we aim to explain the observed differences and identify the most influential modelling assumptions, thereby informing future development of accurate, robust engineering-fidelity wake models for wind farm applications.

85 2 Methodology

In this study, we compare three different DWM-based wake models with high-fidelity LES-ALM. The original DWM model developed at the Technical University of Denmark (DTU) is referred to as DWM_{DTU}. The second DWM model uses the National Renewable Energy Laboratory (NREL) DWM implementation in FAST.Farm, named DWM_{NREL} in this study. The third model, named DWM_{IFE}, uses the DWM implementation WIFET Farm from the Institute for Energy Technology (IFE).

90 This model is newly developed in the NEXTFARM project (RCN, 2025) and is an extension to the aeroelastic tool 3DFloat (Nygaard et al., 2016). The LES-ALM simulations were performed by Uppsala University and are hereafter called LES_{UU}.

2.1 Test cases

In this study, we consider the same simple farm layout as in Hanssen-Bauer et al. (2023), a row of four NREL ~~5-5~~ MW reference turbines (Jonkman et al., 2009) spaced 7.5 diameters (~~7.5D~~7.5D) apart. The NREL ~~5-5~~ MW turbine has a rotor diameter of ~~D = 126~~D = 126 m, a hub height of 90 m, a rated speed of 11.4 ms^{-1} , and a rated aerodynamic power of 5.3 MW. All numerical models, both DWM and LES, use the same incoming wind field, the LES-generated precursor described in Sect. 2.3. In ~~that way~~this way, we exclude the effect of different inflow models, ~~and enable to~~and can investigate the differences in the wake models and their isolated impact on power and ~~fatigue loads~~fatigue loads. However, an important exception is the computation of the meandering in the DWM_{DTU} model, which is derived from a Mann turbulence box with a grid size of one diameter (Madsen et al., 2008, 2010). As this approach is an integrated part of the model and its calibrated ~~model parameters~~model parameters, ~~it was found~~parameters, we found it necessary not to deviate from this setup.

Three wind fields with varying ambient turbulence intensity (TI_a) were generated, representing low, medium, and high turbulence inflow conditions. Table 1 ~~gives~~provides details about the flow at hub height for the different cases. While the aim was to have three wind ~~boxes~~fields with identical below-rated mean wind speed at hub height, ~~we see that in fact in practice~~the mean wind ~~speed varies~~speeds differ slightly. For the highest TI_a case, the mean wind speed is close to, but still below, the rated wind speed. The inflow data provided to the DWM models ~~was~~were sampled in a separate precursor run of the main LES without turbines, in a plane ~~4D-1D~~4D-1D upstream of the position of the most upstream turbine, ~~(hereafter referred to as turbine 1. This way, it is ensured 1). This approach ensures~~ that the inflows seen by the turbines are as similar as possible. For the DWM simulations, the LES-generated wind field was ~~then imposed 4D~~imposed 1D upstream of turbine 1, and the simulations were run for 52.5 min. To exclude ~~any~~ transient effects at the beginning of the simulations, the first 7.5 min were ~~excluded from the results~~discarded, resulting in an effective simulation length of $t_{\text{sim}} = 45 \text{ min}$. This corresponds to $6.7L_x/U_\infty \leq t_{\text{sim}} \leq 8L_x/U_\infty$ for the different cases, where L_x is the longitudinal length of the flow ~~regime~~domain, and U_∞ is the mean undisturbed ambient wind speed.

In total, four simulation cases were run in this study. ~~For three of the cases, the mean wind direction was in line with the row of turbines. Three cases had the mean wind direction aligned with turbine row~~ but with varying inflow ~~condition~~turbulence conditions, yielding fully waked configurations. Here, the turbines downstream of turbine 1 were operating in fully waked conditions. The fourth case was run with medium ambient turbulence conditions, ~~but with an offset angle of 5° between the mean wind direction~~wind direction and the turbine row, resulting in a ~~ease~~scenario where turbines 2–4 operated under partially waked conditions. ~~However, as for all cases in this study. In all cases,~~ the rotors were aligned with the mean ~~wind direction~~wind direction (i.e. no ~~yaw misalignment relative to the mean wind occurred~~intentional yaw misalignment). Due to an error in the setup of the LES-ALM simulation ~~of for~~ the first case, the rotor was run with 0° tilt ~~angle, and not rather than~~ the correct 5° tilt angle of the NREL ~~5-5~~ MW turbine. As the LES-ALM simulations are ~~rather~~ computationally expensive, it was decided

Table 1. Inflow conditions at hub height, resulting pre-defined RPM values, and rotor tilt angle for the simulation cases

	U_{hub} [ms ⁻¹]	TI_{hub} [%]	RPM turbine 1 [min ⁻¹]	RPM turbine 2 [min ⁻¹]	RPM turbine 3 [min ⁻¹]	RPM turbine 4 [min ⁻¹]	Rotor tilt [°]
Low TI_a	8.86	4.6	10.23	8.43	8.36	8.35	0
Medium TI_a	8.98	8.8	10.51	8.76	8.57	8.54	5
High TI_a	10.63	12.0	11.86	10.76	10.44	10.38	5
Medium TI_a / Skewed inflow	8.98	8.8	10.36	9.40	9.32	9.27	5

to keep a 0° tilt angle for the first case and adjust the DWM simulations accordingly, while for the remaining ~~simulations cases~~ the tilt angle was ~~adjusted-set~~ to 5° (see table 1).

125 As in Hanssen-Bauer et al. (2023), the turbines were forced to operate at fixed rotor speeds and blade pitch angles in all simulations. These predefined values were set by first running the DWM_{IFE} and DWM_{NREL} models with variable rotor ~~speeds~~ ~~speed~~ and blade pitch ~~with-using~~ the same inflow ~~and-subsequently-using~~, ~~then taking~~ the mean of the time-averaged values from ~~the-two-those~~ runs for the final simulations. The resulting rotor speeds are given in table 1, while the blade pitch angles were 0° for all turbines, as expected for below-rated conditions. ~~The-approach-for~~ ~~As described in Sect. 2.2.4,~~ DWM_{DTU} ~~is~~
130 ~~to-run~~'s approach for multiple-wake situations is to consider the meandered wake deficit from each upstream turbine as if operating in isolation (i.e. experiencing free-stream velocity). The DWM_{DTU} approach thus differs from the other models by ~~running~~ all upstream wake-generating turbines at ~~free-inflow-conditions~~, ~~except-free-stream-velocity~~, ~~except-for-the-turbine~~ whose loads are being calculated. For example, when computing the ~~turbine-where-the-loads-are-simulated~~. So when the loads of turbine 4 ~~were-simulated~~, turbines 1 to 3 ~~were-are~~ set to the rotor ~~speeds-speed~~ given for turbine 1 in table 1, while turbine 4
135 ~~was-is~~ set to the RPM specified for that turbine.

To ~~get-results-comparable-to-the-ALM-in-LES_{DTU}~~, ~~it-was-decided-to-run~~ ~~ensure-comparability-with-the-LES-ALM~~, we ran the aeroelastic solvers coupled to the DWM wake models with rigid rotors and ~~exclude-all-the-effects-from-the-tower-excluded-all~~ ~~tower-effects~~. Aerodynamic forces, including gravity forces, along the ~~radial-span-of-the-blade-were-reported~~ ~~blade-span-were~~ ~~output~~ from all simulations, and power and loads were calculated from these forces using ~~the-same-identical~~ algorithms. This
140 is the same procedure used in Hanssen-Bauer et al. (2023).

To compare fatigue-damage calculations ~~using-for~~ the different wake models, ~~45-45~~ min ~~damage-equivalent-loads~~ (~~DEL~~ ~~damage-equivalent~~ ~~loads~~ (DELs) were calculated. Based on the Palmgren–Miner damage-summation rule with Goodman’s correction, a DEL is a load that, at a chosen equivalent number of ~~eyes—here-cycles—here~~ $N_{eq} = 45 \cdot 60 = 2700$ (i.e. a load at 1 Hz for 45 min) ~~—will-give-the-same—~~ ~~produces-the-same-fatigue~~ damage as the summation of ~~the-k-cycles~~ ~~damage-from-the-K~~ different load
145 ~~ranges~~ S_k with N_k of load ~~ranges~~ S_k^m ~~cycles~~, determined using rainflow counting (Rychlik, 1987):

$$\text{DEL} = \left(\frac{1}{N_{eq}} \left(\sum_{k=1}^{N_k} \tilde{K} N_k S_k^m \right) \right)^{\frac{1}{m}}, \quad (1)$$

where the material-specific Wöhler coefficient m in Eq. (1) is set to $m = 3$ for calculations on the tower and to $m = 10$ for the blade.

2.2 The DWM models

150 The original DWM model is based on the assumption that the quasi-steady ~~wake-deficit~~wake deficit, obtained from a thin shear-layer approximation of the ~~Navier-Stokes~~Navier-Stokes equations, meanders in a stochastic manner due to the large-scale turbulent structures in the wind, and that the self-generated turbulence field in the wake can be superimposed onto the ~~wake-deficit~~wake deficit and exposed to the same dynamics. In this study, we compare three DWM-based wake models from DTU, NREL, and IFE. An overview of the differences between these three DWM model implementations ~~are~~is given in
 155 Hanssen-Bauer et al. (2023). What follows is a summary of the most important differences needed to understand the discrepancies in the results.

2.2.1 Initial ~~wake~~ velocity ~~profile~~deficit

DWM_{DTU} and DWM_{NREL} obtain the initial velocity profile behind the turbine from the blade element momentum (BEM) model (Madsen et al., 2008, 2010), but the wake profile is adjusted by including a simple closed-form modification ~~taking~~
 160 ~~care of the~~to account for pressure recovery in the ~~wake-near-field~~near-wake region. DWM_{IFE} on the other hand, assumes a Gaussian wake-deficit profile ~~for all positions downstream of the turbine~~at all downstream positions, and the initial ~~wake-centre~~wake-centre deficit is obtained from $C_T(U)$ tables ~~with of~~ thrust coefficient as function of wind speed for the specific turbine.

2.2.2 Thin shear-layer approximation and eddy viscosity model

All ~~the~~three DWM implementations build on the same assumption of an axisymmetric wake with a thin shear-layer approx-
 165 imation of the ~~Navier-Stokes~~Navier-Stokes equations, where the pressure term is neglected. As a turbulence closure~~of the~~ ~~equations~~, an eddy viscosity model consisting of two terms ~~;~~is applied. The first term models the contribution related to the ambient wind shear and scales with the turbulence intensity, while the second term is related to the wake shear. The model includes filter functions to adjust the model in the near-wake region where the assumption of negligible pressure variations is not valid. The details of the eddy viscosity model, ~~with the~~along with its associated filter functions and calibration constants, vary
 170 ~~between~~among the DWM implementations (for details, see Madsen et al., 2010; Jonkman et al., 2017; de Vaal and Muskulus, 2021).

2.2.3 Wake transport velocity

The ~~wake-deficit~~ wake deficit is transported downstream by the wind, but since the ~~free-stream velocity is disturbed by this deficit itself~~ free-stream velocity is itself disturbed by the deficit, the choice of wake transport velocity is not trivial. While
 175 DWM_{DTU} applies a transport velocity of U_∞ , DWM_{IFE} uses the approximation ~~of~~ $0.8U_\infty$, estimated by Keck et al. (2013). DWM_{NREL}, on the other hand, ~~is calculating~~ calculates the local velocity at the position of each wake slice, which varies in both time and space; therefore, the wake accelerates from near-wake to far-wake, because the ~~wake-deficits~~ wake deficits are stronger in the near-wake and weaken further downwind.

2.2.4 Wake summation

180 For ~~multiple wake situations~~ situations with multiple wakes, where a turbine's incoming flow field is affected by more than one ~~wake of upstream turbines~~ upstream wake, DWM_{DTU} ~~distinguish~~ distinguishes between below- and above-rated wind speed conditions (Larsen et al., 2015):

$$U_w(x, y, z) = U_\infty - \begin{cases} \max_i (U_\infty - u_w^i(x, y, z)), & U_\infty \leq U_r \\ \sum_i (U_\infty - u_w^i(x, y, z)), & U_\infty > U_r \end{cases} \quad (2)$$

Here, U_∞ is the undisturbed free-stream velocity, u_w^i is the wake velocity induced by turbine i , and U_r is the turbine's rated
 185 wind speed. In this study the wind speed is always below rated, ~~therefore so~~ the upper expression is used. ~~The~~ This maximum deficit operator looks at the meandered ~~wake-deficit~~ wake deficit from each upstream turbine ~~when~~ operating in isolation (i.e. ~~-, experiencing under~~ free-stream velocity conditions), and assumes that the total incoming ~~wake-deficit~~ wake deficit can be approximated ~~to be the maximum single wake deficit~~ by the maximum single wake deficit, evaluated at each radial position of the turbine of interest.

190 ~~In~~ DWM_{NREL} ~~the~~ superimposes axial velocity-deficits ~~are superimposed~~ using a local root-sum-square method, where the wake of each ~~individual~~ turbine is calculated using ~~the that turbine's~~ local incoming wind velocity ~~of that turbine, meaning that,~~ In other words, the wakes are calculated ~~in a sequential way~~ sequentially from upstream to downstream (Jonkman et al., 2017):

$$U_w(x, y, z) = U_\infty - \sqrt{\sum_i (u_0^i - u_w^i(x, y, z))^2} \quad (3)$$

Here, U_∞ is again the undisturbed free-stream velocity, u_0^i is the local incoming wind velocity ~~of at~~ turbine i , and u_w^i is the
 195 wake velocity induced by turbine i .

Radial velocity-deficit fields are superimposed using a linear summation method ~~-, where the wake of each individual turbine is calculated~~ in the same sequential way as for manner as the axial component.

DWM_{IFE} uses the ~~momentum conserving~~ momentum conserving summation method derived by Zong and Porté-Agel (2020a) for wake superposition. This is an iterative method ~~-, where the velocity-deficits in which the velocity deficits~~ from

200 the upstream turbines are summed ~~weighted with weights based~~ on the ratio of ~~the each individual wake's~~ mean convection velocity ~~of the individual wake, $u_c^i(x)$, and the convection velocity of the combined wakes,~~ ~~to the combined wakes' convection velocity~~ $U_c(x)$:

$$U_w(x, y, z) = U_\infty - \sum_i \frac{u_c^i(x)}{U_c(x)} (U_\infty - u_w^i(x, y, z)), \quad (4)$$

~~where~~

205 $u_c^i(x) = \frac{\iint u_w^i(x, y, z) \cdot (u_0^i - u_w^i(x, y, z)) dydz}{\iint (u_0^i - u_w^i(x, y, z)) dydz}, \quad (5)$

~~and~~

$$U_c(x) = \frac{\iint U_w(x, y, z) \cdot (U_\infty - U_w(x, y, z)) dydz}{\iint (U_\infty - U_w(x, y, z)) dydz}. \quad (6)$$

~~The integrals in Eqs. (5) and (6) are solved numerically over a cross-section with 64 grid points in each dimension, spaced $\Delta y = \Delta z = 10$ m apart and centred on the wake centre.~~

210 2.2.5 Tilt and yaw misalignment

The ~~implementations by~~ DWM_{DTU} and DWM_{IFE} ~~implementations~~ used in this study do not ~~take into account any impact on the flow~~ ~~account for any flow effects~~ due to tilt ~~and or~~ yaw misalignment between the rotor and the flow. However, ~~in~~ the latest version of DWM_{DTU} ~~a model to account~~ ~~includes a model~~ for flow effects due to yaw misalignment ~~using a Hills~~, ~~using a Hill's~~ vortex analogy (Larsen et al., 2020) ~~the implementations by DWM_{DTU} and DWM_{IFE} used in this study do not take into~~ ~~account any impact on the flow due to tilt and yaw misalignment between the rotor and the flow.~~ ~~In~~. ~~By contrast~~, DWM_{NREL} ~~accounts for~~ tilt and yaw misalignments ~~are accounted for and affect~~, ~~which thereby influence~~ wake deflection (Jonkman et al., 2017). The wake planes in the DWM_{NREL} model are oriented by the rotor centreline ~~and not the wind direction~~ ~~rather than the wind direction~~, causing the wake to deflect based on tilt and yaw misalignment because ~~the wake deficit a wake deficit~~ normal to the ~~tilted/yawed~~ rotor introduces a velocity component that is not parallel to the incoming flow. DWM_{NREL} ~~has in~~ ~~addition also has~~ a newly implemented curled-wake model with improved accuracy for large rotor misalignments (Branlard et al., 2023), but this ~~model extension~~ is not used in ~~this the present~~ study.

225 2.2.6 Ground effects

DWM_{NREL} does not yet have a model to account for ground effects on the flow field. ~~For both~~ ~~Both~~ DWM_{DTU} and DWM_{IFE} ~~such a model is implemented, but do include ground-effect models, but these were~~ not used for the simulations in this study. ~~For~~ ~~In the case of~~ DWM_{IFE} 's part, ~~the mirroring model to handle ground effects~~, ~~a mirror-based ground effect model~~ was used in the simulations in Hanssen-Bauer et al. (2023), but it was later ~~seen that this gave found to produce~~ unrealistically high deficits ~~close to the ground, and near the ground~~. DWM_{IFE} ~~performed better when turning off this model~~ ~~showed better agreement when this model was turned off~~.

2.2.7 Wake-added turbulence and turbulence build-up

230 Wake-added turbulence is the self-generated small-scale turbulence in the wake of the turbines a turbine's wake due to wake shear and the breakdown of the wake tip vortices, and comes in addition to the conventional atmospheric boundary layer turbulence. DWMOf the three DWM implementations, DWM_{DTU} is the only DWM implementation one including a wake-added turbulence model in the simulations performed in for this study. At an early stage in the In the early development of the DWM model at DTU, it became clear from the comparison of model simulations with detailed inflow measurements on a full-
235 scale turbine with, including angle of attack and relative velocity to at a blade section , were used for validation. Comparisons between model simulations and these measurements made it clear that additional turbulence to what is generated from wake meandering was necessary to model beyond that generated by wake meandering had to be modelled (Madsen et al., 2005). In practice the wake, the wake's self-generated turbulence, which is of particular importance in case of particularly important under stable stratification of the atmospheric boundary layer, is modelled based on an isotropic Mann turbulence box with
240 smaller length scale ¹ than the conventional inflow turbulence, ambient turbulence and transformed into an inhomogeneous turbulence field by a scaling factor k_{mt} varying that varies radially based on the wake-deficit strength and the wake shear-layer velocity gradient:

$$k_{mt} = \left| \frac{u_w(r)}{U_\infty} \right| k_{m1} - \left| \frac{\partial(u_w(r)/U_\infty)}{\partial r} \right| k_{m2}. \quad (7)$$

Here $k_{m1} = 0.6$ and $k_{m2} = 0.35$ are empirical factors tuned by comparison with inflow and load measurements on a full-scale
245 full-scale turbine (Madsen et al., 2008) and with actuator-line simulations (Madsen et al., 2010). Later, an improvement to the original model to account for the turbulence build-up of turbulence inside a wind farm was suggested (Keck et al., 2015), but this is not included in the current DWM_{DTU} model.

The results by DWM_{NREL} are not including results do not include any wake-added turbulence model in this study. However, an improved wake-added turbulence model has recently been implemented in FAST.Farm (Branlard et al., 2024).

250 DWM_{IFE} does not include a wake-added turbulence model for load calculations analogous to the one formulated in the original DWM model. However, the increased TI turbulence intensity in the wake due to the turbulence-generating wake-deficit wake deficit shear is modelled based on the eddy viscosity through the eddy-viscosity formulation in the wake-deficit model, and the total contribution of increased TI turbulence from all upstream wakes is estimated by a root-sum-square summation (de Vaal and Muskulus, 2021). Thus, the increased effective TI felt turbulence intensity experienced by a turbine operating un-
255 der waked conditions is taken into account and affects the development of its own wake downstream. Note that this summation of turbulence contributions from upstream wakes differs from the momentum-conserving method in Eq. (4) used for summation of the velocity deficits.

¹ $L = D/8$, where L is the length scale of the spectral velocity tensor and D is the turbine diameter, as opposed to $L = 33.6$ m, which is recommended for atmospheric turbulence above 60 m (International Electrotechnical Commission, 2019).

2.2.8 Aeroelastic solvers

All DWM models are coupled to an aeroelastic solver for calculating blade forces. DWM_{DTU} is coupled to HAWC2 (Madsen et al., 2020), DWM_{NREL} to OpenFAST (NREL, 2025), and DWM_{IFE} to 3DFloat (Nygaard et al., 2016). In all these aeroelastic solvers the blade forces are obtained from BEM, although in different implementations, with Prandtl blade tip correction (Glauert, 1935). DWM_{NREL}'s OpenFAST ~~has in addition a blade root~~ additionally includes a blade-root correction.

2.3 Large-eddy simulations

The LES-ALM reference case ~~is (LES_{UU}, and)~~ as well as the three inflow wind fields used by all ~~the~~ numerical models in this study, ~~is~~ are computed using the ~~numerical framework EllipSys3D~~ EllipSys3D numerical framework (Michelsen, 1994a, b; Sørensen, 1995), and is identical to the solver used in our ~~recent comparison at above-rated wind conditions (Hanssen-Bauer et al., 2023). The solver was also participating in the mentioned comparison (Hanssen-Bauer et al., 2023). This solver also participated in the aforementioned~~ benchmarking study against full-scale measurements (Asmuth et al., 2022), ~~however~~ although under the name LES-EllipSys3D or LES_{DTU}.

The three inflow wind fields are generated using a bi-periodic precursor simulation of a pressure-driven isothermal boundary layer. The computational domain extends $L_z = 1280$ m in the vertical direction, $L_x = 6L_z$ in the streamwise direction, and $L_y = 4L_z$ in the lateral direction. The grid is uniform in all coordinate ~~direction~~ directions, with $\Delta x = 20$ m and $\Delta y = \Delta z = 10$ m. A symmetry boundary condition is imposed at the domain top. At the surface, shear stress is prescribed using the Monin-Obukhov similarity theory (Monin, 1954) and the local instantaneous velocity sampled at the first grid point above the boundary. Inflow data for the main LES-ALM simulation, which are also ~~employed~~ used by the DWM models, are extracted after a spin-up time of 30 000 ss.

The domain of the LES_{UU} simulation (~~i.e.~~ including wind turbines) has the same dimensions $L_{x,y,z}$ as the precursor ~~field~~. The inlet is located $6D$ upstream of turbine 1. In the turbine and wake region, the grid is uniform with a resolution of $\Delta x = \Delta y = \Delta z = D/32 = 3.9375$ m, starting $3D$ upstream of turbine 1 and extending $33D$ in the streamwise direction, and $4D$ in both the lateral and vertical directions. Outside this inner region, the grid is smoothly stretched towards the boundaries. The turbine rotors are represented using ALMs (Sørensen and Shen, 2002), with each blade discretized into 32 elements. The ALM body forces are projected onto the grid with a three-dimensional Gaussian smearing function of width $\epsilon = 2\Delta x$. To mitigate spurious induction effects arising from the finite ~~core-size~~ core size of root and tip vortices, the smearing correction proposed by Meyer Forsting et al. (2019) is applied. Following a spin-up of 30 min, the main simulation is run for 45 min.

2.4 Wake tracking

From the flow field generated by LES_{UU}, ~~the~~ wake centre positions were tracked using ~~the python toolbox SAMWICH developed at NREL~~ NREL's Python toolbox SAMWICH. The wake centres were identified ~~in the plane 5D for each time step in a plane 5D~~ downstream of each turbine (normal to the wind-direction, for each time step) using the two-dimensional Gaussian fit method (Trujillo et al., 2011) as implemented in ~~the SAMWICH toolbox~~ SAMWICH. To minimize algorithm error, the search

290 area was limited to $\pm 1.25D$ ~~of laterally from~~ the turbine location ~~laterally~~, and between $-0.5D$ and D ~~relative to the hub~~
~~height~~ ~~vertically~~. ~~After vertically relative to hub height. After obtaining~~ the wake centre time series ~~were obtained~~ for each tur-
bine and downstream location, four post-processing steps were applied to reduce error in the wake centre estimates. These ~~post~~
~~processing~~ ~~post-processing~~ steps were determined based on a separate analysis ~~conducted on~~ ~~of~~ DWM_{NREL} simulation results,
where SAMWICH wake centre detections were compared to actual wake centre values output directly from DWM_{NREL}.

- 295
1. Edge Detection Removal: wake centres detected at the ~~search area edge~~ ~~edge of the search area~~ were discarded and filled
~~back in with~~ ~~in by~~ linear interpolation.
 2. Spike Removal 1: a median filter with ~~a~~ kernel size of 15 ~~seconds~~ was applied to remove spurious spikes in the wake
centre time series.
 3. Jump removal: ~~To to~~ remove remaining jumps in the wake centre time series, a ~~rolling mean was applied on moving~~
300 ~~average was applied to~~ segments starting 20 ~~seconds~~ before the first ~~;~~ and 20 ~~seconds~~ after the last consecutive points
~~;~~ ~~exceeding the exceeding~~ a maximum allowable gradient of $0.2D/sD$ s^{-1} .
 4. Spike Removal 2: ~~A final step a final median filter~~ (identical to step 2) ensured that any spikes introduced by ~~previous~~
~~steps~~ ~~step 3~~, primarily due to the arbitrary ~~length of segment selected in step 3~~ ~~selected segment length~~, were reduced
~~from the final, in the~~ post-processed wake centre time series.

305 Despite the improvements ~~seen~~ after post-processing the raw wake centres, the ~~SAMWICH~~ ~~SAMWICH-derived~~ centres did
still at times ~~differ differed~~ from the centres computed by DWM_{NREL}. This ~~could happen because SAMWICH was tracking~~
~~discrepancy could occur because SAMWICH tracks~~ the aggregate deficit ~~;~~ made up of more than one wake deeper ~~into in~~ the
farm. The difference between the standard deviation of the ~~the~~ wake centre time series tracked by SAMWICH and ~~the one that~~
obtained directly from DWM_{NREL} ~~stayed remained~~ below $0.06D$ (i.e. 6 % of the rotor diameter) ~~. This value considers for~~ all
310 inflow cases ~~;~~ ~~and and for~~ both lateral and vertical wake centre coordinates.

3 Results

3.1 Fully waked cases with varying ambient turbulence

In this section, we present a detailed comparison of the three DWM-based models under fully waked conditions for a row of
four turbines exposed to aligned inflow. Three cases corresponding to low, medium, and high ambient turbulence conditions
315 are considered, while maintaining below-rated wind speeds. We assess time-averaged flow fields, wake centre positions, power
production, thrust forces, blade loads, and fatigue to identify key differences between the models and examine the influence of
sub-modelling strategies.

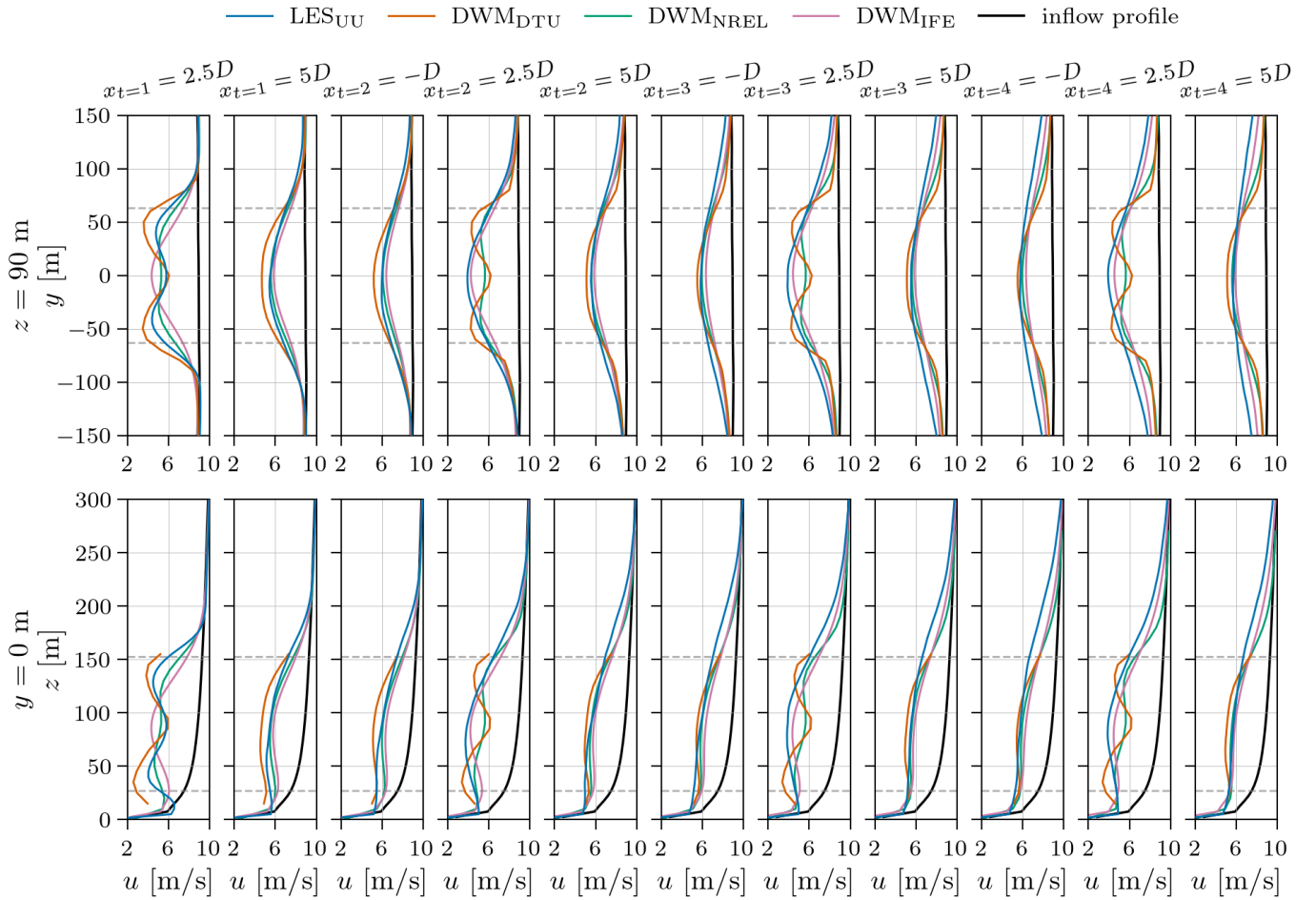


Figure 1. Time-averaged velocity profiles for the aligned incoming wind case with low ambient turbulence ($TI_a = 4.6\%$). Horizontal dashed lines indicate the rotor swept area.

3.1.1 Mean velocity profiles

Figure 1 shows time-averaged velocity profiles at $-1D$, $2.5D$, and $5D$ relative to the ~~4-turbine's~~ four turbines' streamwise
 320 positions for the low ambient turbulence case ($TI_a = 4.6\%$). The upper row shows horizontal profiles at hub height and the
 lower row shows vertical profiles at the ~~turbine's~~ turbines' lateral centre. Horizontal dashed lines indicate the range of the
 turbine~~rotor's~~ swept's rotor-swept area. In the ~~near-wake~~ near wake of turbine 1, at $x_{t=1} = 2.5D$, all ~~the~~ models except
~~DWM_IFE~~ show velocity profiles with two minima reflecting the rotor thrust distribution. For ~~DWM_DTU~~, this characteristic
 near-wake profile is more ~~distinct~~ pronounced than the LES profile, ~~while the opposite goes with lower velocities at the~~
 325 ~~minima and higher velocity near the hub height, whereas the opposite is true~~ minima and higher velocity near the hub height, whereas the opposite is true for ~~DWM_NREL~~. Both ~~DWM_DTU~~ and ~~DWM_NREL~~

predict the initial velocity profile downstream of the turbine ~~by using~~ the BEM model. ~~DWM_{IFE}, on the other hand by contrast,~~ assumes a Gaussian wake-deficit profile for all x downstream of the turbine. For LES_{UU} , DWM_{DTU} , and DWM_{NREL} , the velocity-deficit profiles have ~~nearly~~ reached a Gaussian-like shape ~~at by~~ $x_{t=1} = 5D$. While all ~~the~~ models show similar shapes ~~of for~~ the horizontal profiles at $x_{t=1} = 5D$ and $x_{t=2} = -D$, the vertical profile of LES_{UU} differs ~~slightly~~ in shape from the ~~other models with relatively higher~~ ~~others, with relatively larger~~ deficits at the lower part of the rotor ~~spanswept area compared to the upper~~. For turbines 2–4, both DWM_{NREL} and DWM_{DTU} estimate the transition from BEM to Gaussian shape later than LES_{UU} ~~which, which already~~ shows a Gaussian ~~shape already~~ ~~profile~~ at $x = 2.5D$. While the DWM models show symmetric horizontal ~~velocity-deficits~~ ~~velocity deficits~~ for the developed profiles, the LES_{UU} deficit has its maximum at $y < 0$. This small asymmetry ~~for in~~ LES_{UU} , which becomes more pronounced for ~~the~~ higher ambient turbulence cases, will be discussed in Sect. 3.1.2 ~~where plots showing when~~ wake centre positions are presented. At the wake centre, DWM_{IFE} ~~in general tends to under-predict~~ ~~generally tends to underpredict~~ the deficit slightly compared to LES_{UU} . DWM_{NREL} shows good agreement ~~to with~~ LES_{UU} at the wake centre at $x = 5D$ and $x = -D$, while DWM_{DTU} tends to slightly ~~over-predict the wake centre~~ ~~overpredict the centreline~~ deficit at these positions.

DWM_{DTU} and DWM_{NREL} show ~~minor differences comparing only minor differences in~~ the flow downstream of turbines 2–4 ~~with compared to~~ turbine 1. ~~The~~ ~~By contrast, the~~ wakes of DWM_{IFE} and LES_{UU} ~~, however,~~ show significant development as the deficit outside the rotor ~~span increases~~ ~~swept area increase~~ along the row of turbines. Hence, DWM_{IFE} and LES_{UU} show lower ~~gradients compared to~~ ~~DWM_{DTU} and DWM_{NREL}~~ ~~velocity gradients~~ in the wake shear layer between the ~~wake-deficit and ambient for all turbines operating under waked conditions, and~~ ~~deficit and the ambient flow for all waked turbines,~~ especially for turbine 4. ~~The momentum conserving~~ ~~4, compared to~~ ~~DWM_{DTU} and DWM_{NREL}~~ . ~~The momentum-conserving~~ wake summation method ~~applied in~~ DWM_{IFE} ~~, equation (4) (Eq. (4))~~, seems to capture the impact of ~~the wakes from far upstream, which has far-upstream wakes, which have~~ expanded over a long distance, but still ~~the deficits are weaker to produces~~ ~~weaker deficits towards~~ the sides and above the rotor ~~span~~ compared to LES_{UU} . ~~The~~ ~~By contrast, the~~ wake-deficit profiles predicted by DWM_{DTU} and DWM_{NREL} ~~, however,~~ ~~show less~~ ~~show less lateral and vertical~~ spreading. The ~~maximum deficit~~ ~~maximum-deficit~~ operator in the DWM_{DTU} model derives the ~~turbine's~~ incoming deficit at each radial position as the smallest deficit ~~scanning through the meandered deficits of found among~~ all upstream turbines' ~~meandered deficits (see Eq. (see equation (2) and Larsen et al. (2013)).~~ This ~~seems to cause~~ ~~causes~~ DWM_{DTU} to predict only small variations in the incoming velocity ~~fields~~ ~~field~~ for turbines 2–4, resulting in similar ~~wakes~~ ~~wake profiles along the row~~. The fact that DWM_{NREL} predicts only minor variations in the wake flow for turbines 2–4 is more surprising given the sequential ~~method for multiple wake handling applied by this DWM version (see equation~~ ~~multi-wake handling in this model (see Eq. (3)).~~ However, the closer agreement of DWM_{IFE} with LES_{UU} in predicting wake development along the turbine row may also stem from ~~the fact that~~ DWM_{IFE} ~~is being~~ the only DWM implementation that incorporates a turbulence build-up model. This model accounts for the elevated incoming turbulence levels experienced by turbines 2–4 ~~due to the 2–4 due to~~ added turbulence in ~~the turbine upstream~~ wakes, leading to faster wake recovery through enhanced mixing and momentum entrainment from the ambient flow.

Figures 2 and 3 show time-averaged velocity profiles for the ~~eases with~~ medium ($TI_a = 8.8\%$) and high ($TI_a = 12\%$) ambient turbulence ~~cases~~, respectively. The wake development behind each turbine is similar to the ~~previous low-turbulent~~

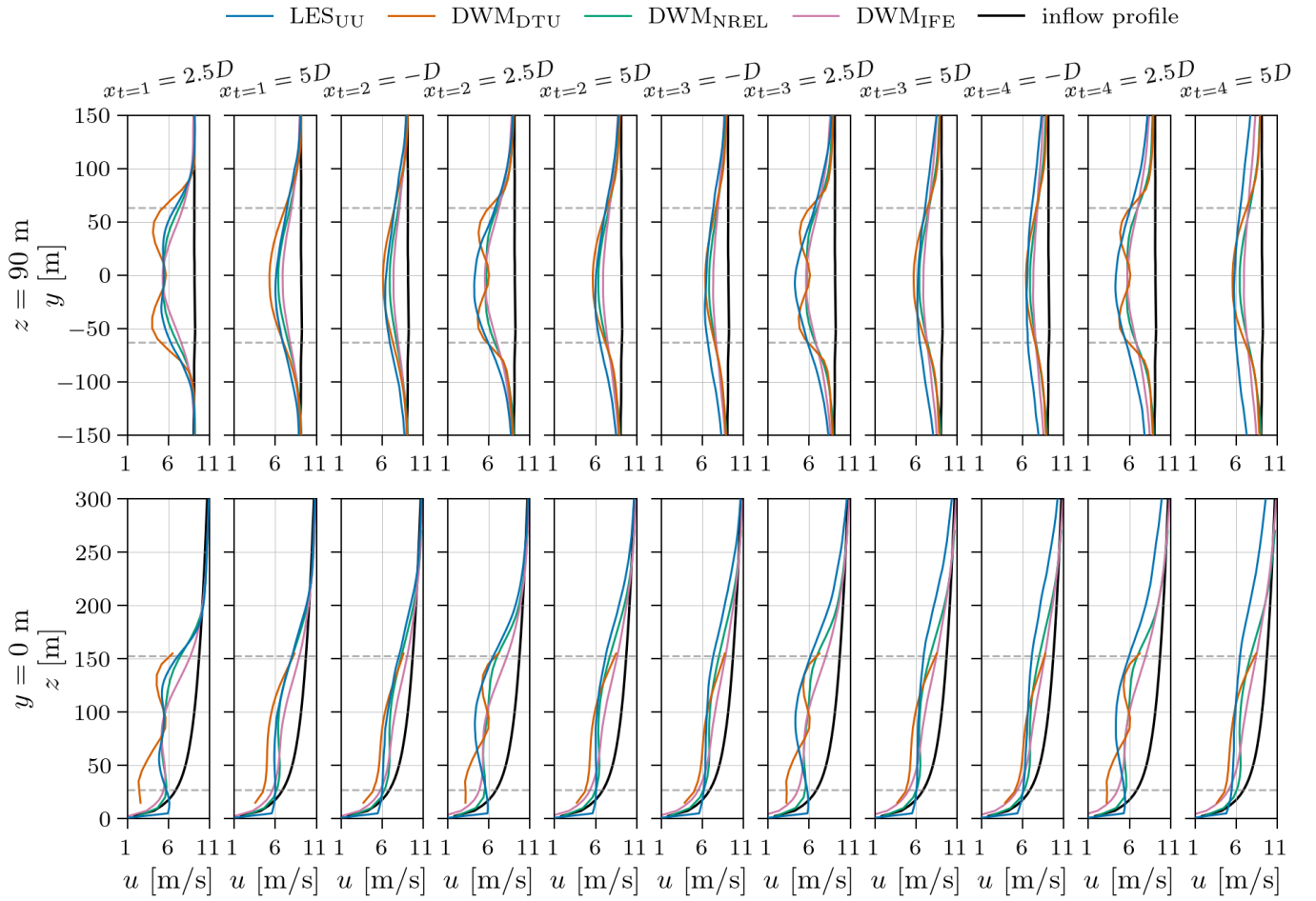


Figure 2. Time-averaged velocity profiles for the aligned incoming wind case with medium ambient turbulence ($TI_a = 8.8\%$). Horizontal dashed lines indicate the rotor swept area.

low-turbulence case, but due to higher turbulence levels and thus stronger meandering, the wakes show faster recovery and transition towards a Gaussian-like profile. As for lead to faster wake recovery and a quicker transition toward Gaussian profiles. As in the low-turbulence case, DWM_{DTU} shows a more distinct near-wake profile than the other models at $x = 2.5D$ for all turbines and for both $TI_a = 8.8\%$ and $TI_a = 12\%$. For Under medium ambient turbulence conditions, only traces of the characteristic near-wake profile is are visible in the wake wakes of DWM_{NREL} and LES_{UU} . For DWM_{NREL} it is evident for (evident at $x = 2.5D$ downstream of all the turbines, while for LES_{UU} it can be seen only turbines for DWM_{NREL} , and only at $x_{t=1} = 2.5D$ downstream of turbine 1, at $x_{t=1} = 2.5D$ for LES_{UU}). For the high ambient turbulence case, the wakes predicted by both DWM_{NREL} and LES_{UU} have developed to a Gaussian profile at Gaussian profiles by $x = 2.5D$ downstream

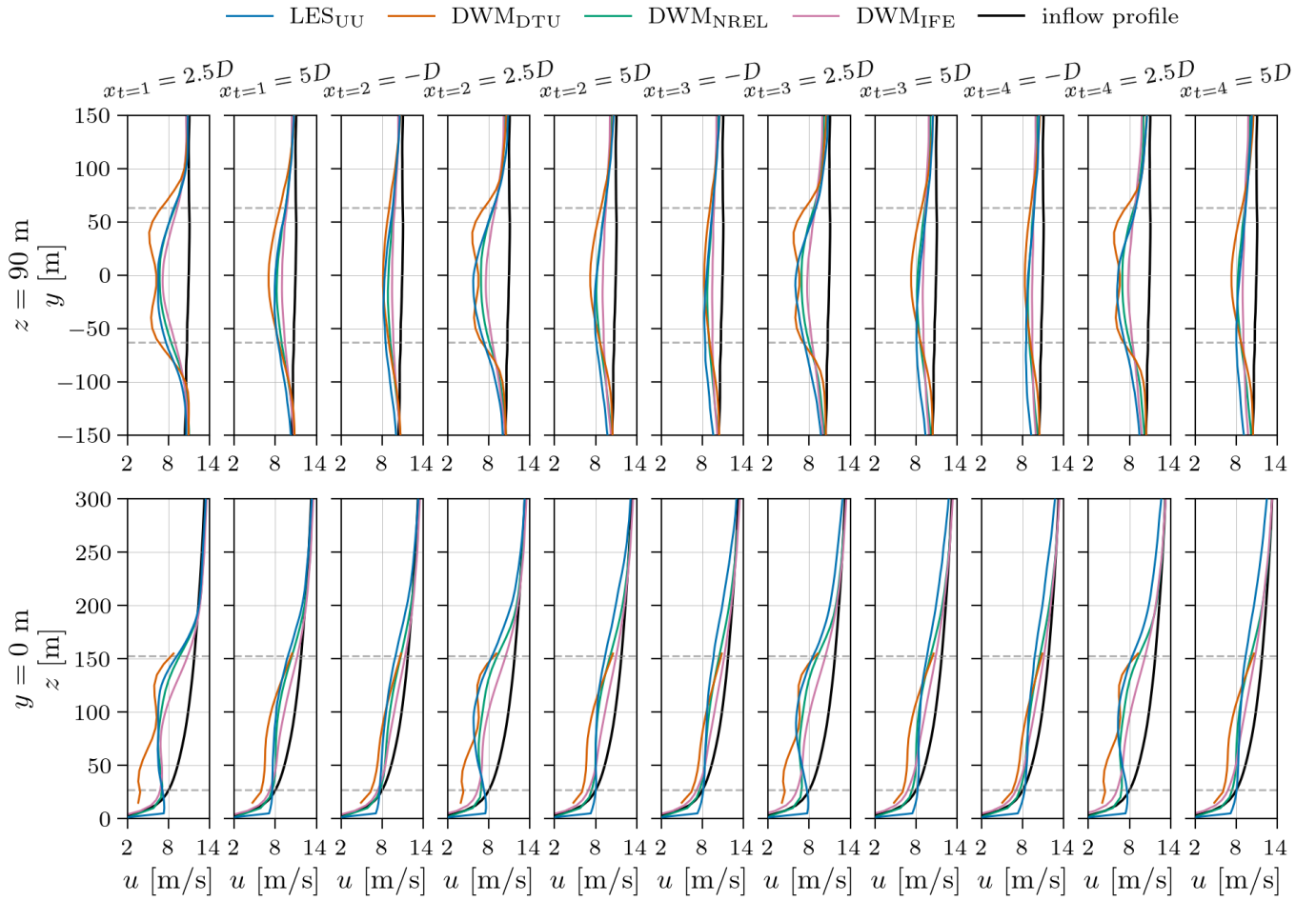


Figure 3. Time-averaged velocity profiles for the aligned incoming wind case with high ambient turbulence ($TI_a = 12\%$). Horizontal dashed lines indicate the rotor swept area.

of behind all turbines. However, it should be noted, however, that for power and loads generation, the the load predictions
 370 the near-wake at $x = 2.5D$ is of has minor importance.

More relevant are the profiles at $x = 5D$ downstream and $x = -D$ just upstream the next turbine in the row. Here, DWM_{IFE} ,
 and to a minor lesser degree DWM_{NREL} , tend to under-predict the deficit at the wake centre tends to underpredict the centreline
 deficit, while DWM_{DTU} slightly over-predicts overpredicts the deficit, compared to LES_{UU} . As for in the $TI_a = 4.6\%$ case,
 375 DWM_{IFE} is the only DWM model capturing the increased that captures the increase in deficit outside the rotor span for in the
 horizontal profiles along the turbine row, but not at the same level although not to the same extent as LES_{UU} . For the vertical
 profiles, however, no such increase is evident for DWM_{IFE} in the plots does not show such an increase along the row. Again,

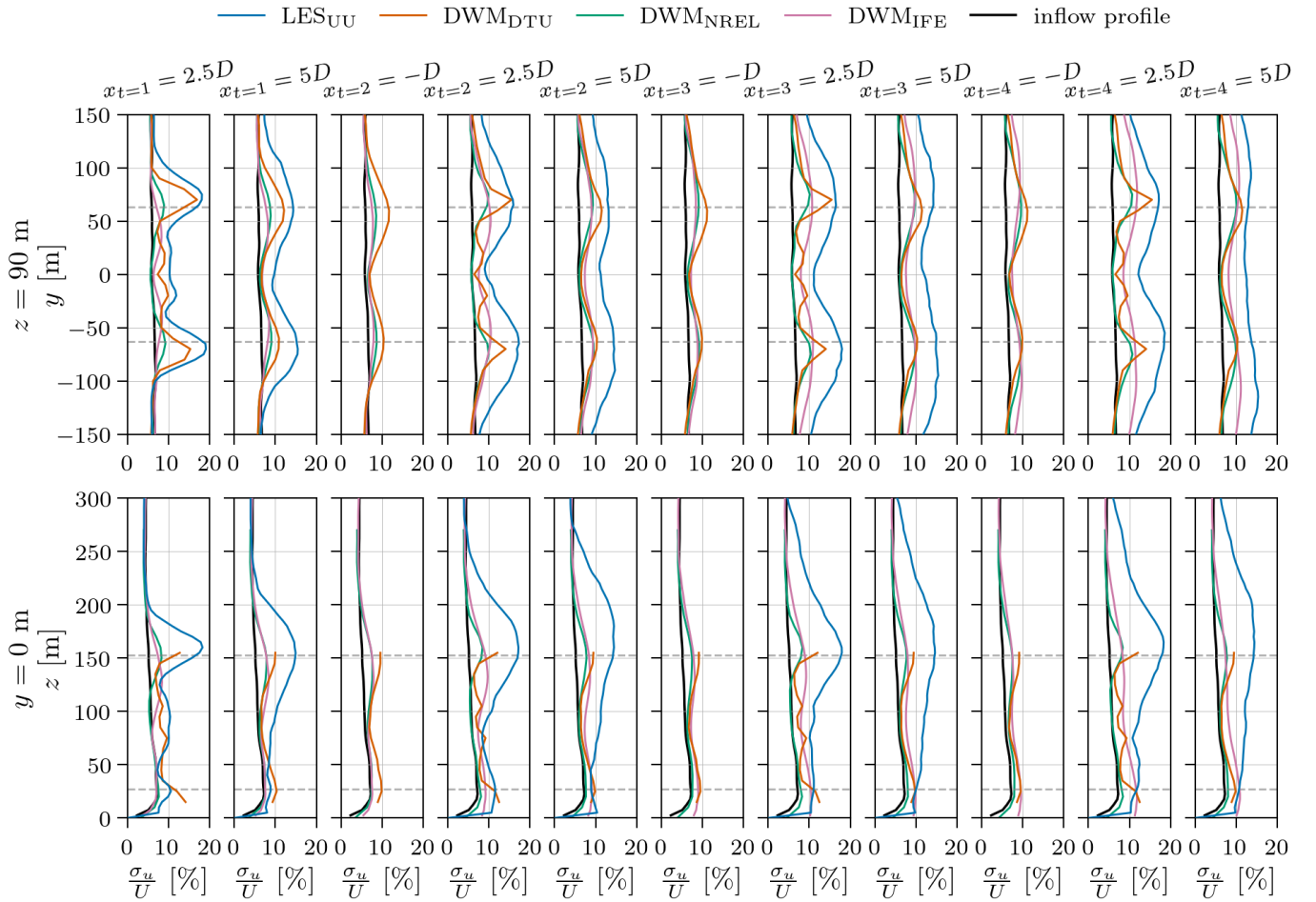


Figure 4. Profiles of [velocity](#) standard deviation [of velocity](#) for the aligned incoming wind case with low ambient turbulence ($TI_a = 4.6\%$). Horizontal dashed lines indicate the rotor swept area. [LES_{UU} data are not available at \$x_{t=i} = -D\$, \$i = 2, 3, 4\$ due to lack of time-resolved data at this axial position.](#)

DWM_{DTU} and DWM_{NREL} show [only](#) minor development in the flow along the turbine row, when comparing the wakes of turbine 1 and turbine 2 [and especially when comparing the wakes of turbines 2–4.](#)

LES_{UU} shows some notable differences in the flow field as the ambient turbulence level [increase: as already increases: as](#) mentioned, the asymmetry about $y = 0$ [gets becomes](#) more pronounced for higher ambient turbulence, and [a](#) strong acceleration of the flow [is seen appears](#) near the surface behind all turbines. In addition, the wake moves slightly [away from ground, which is visible upward, noticeable](#) behind turbine 2 and further downstream. This [upward deflection](#) is likely due to the non-zero turbine tilt angle for the $TI_a = 8.8\%$ and $TI_a = 12\%$ cases, [causing which causes](#) the wakes to deflect upwards. [Only the DWM model from NREL takes the turbine tilt into account NREL is the only DWM model that accounts for rotor tilt](#) when

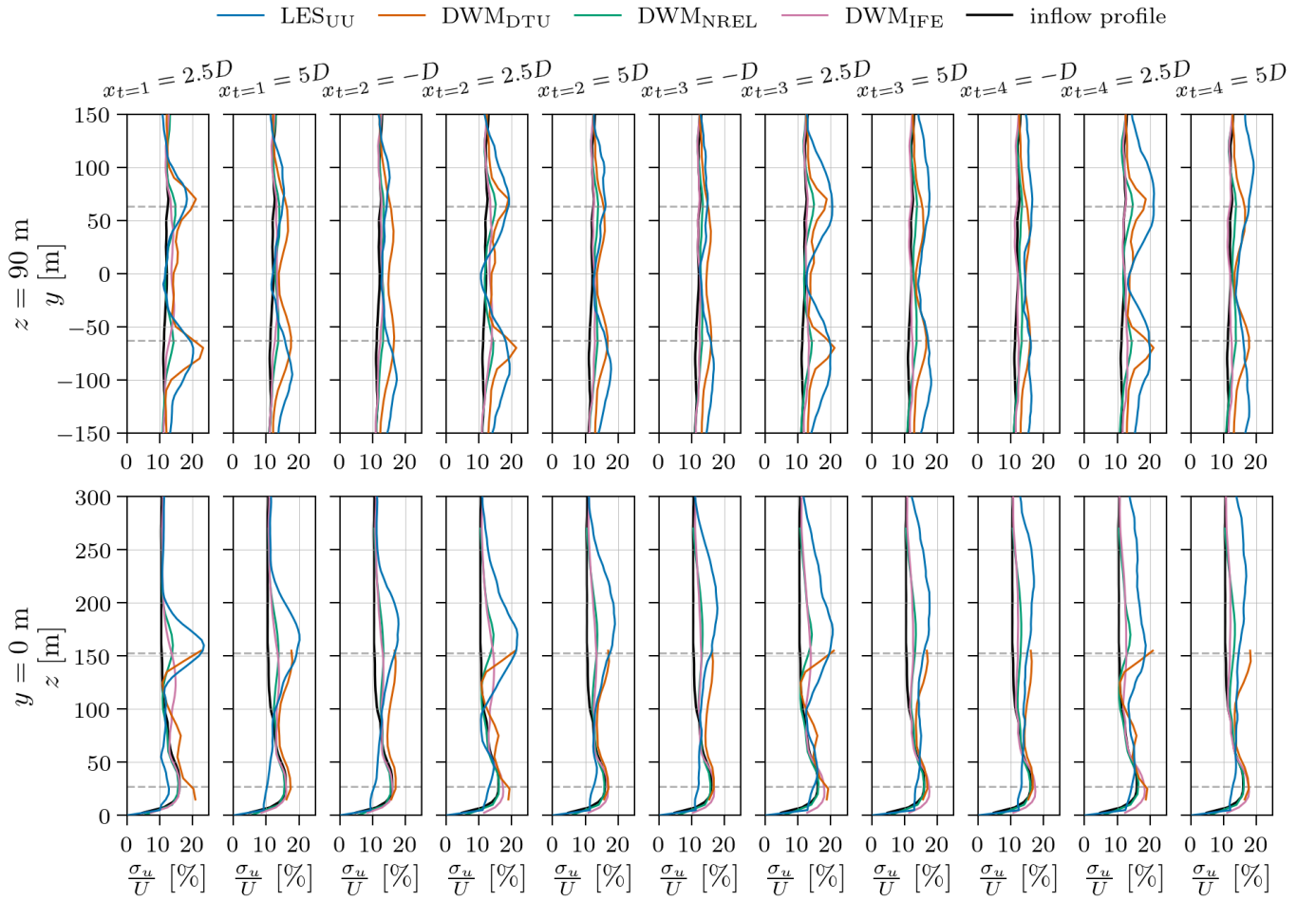


Figure 5. Profiles of velocity standard deviation of velocity for the aligned incoming wind case with medium ambient turbulence ($TI_a = 8.8$ %). Horizontal dashed lines indicate the rotor swept area.

385 calculating the flow. Even though the-an upward wake deflection is not evident for DWM_{NREL} in the velocity profiles, it becomes visible in the wake centre position plots in Sect. 3.1.2.

390 Figures 4–6 show profiles of axial velocity standard deviation, σ_u , for the three different ambient turbulence levels investigated. In general, LES_{UU} shows much higher levels of exhibits much higher σ_u than the DWM models, with the exception for DWM D_{TU} showing levels than DWM_{NREL} and DWM_{IFE}. DWM_{DTU}, however, the only DWM implementation in this study that includes a wake-added turbulence model, shows comparable levels to , and higher levels than, LES_{UU} for the at $TI_a = 8.8$ % and , and even higher at $TI_a = 12$ % cases, respectively. DWM_{DTU} is the only DWM implementation with a wake added turbulence model applied in this study. For $TI_a = 4.6$ and $TI_a = 8.8$ %. For all ambient turbulence levels, the shapes of the DWM_{DTU} profiles at $x_{t=1} = 2.5D$ are in good agreement to-'s σ_u profiles downstream of turbine 1 are in fairly good agreement with LES_{UU}

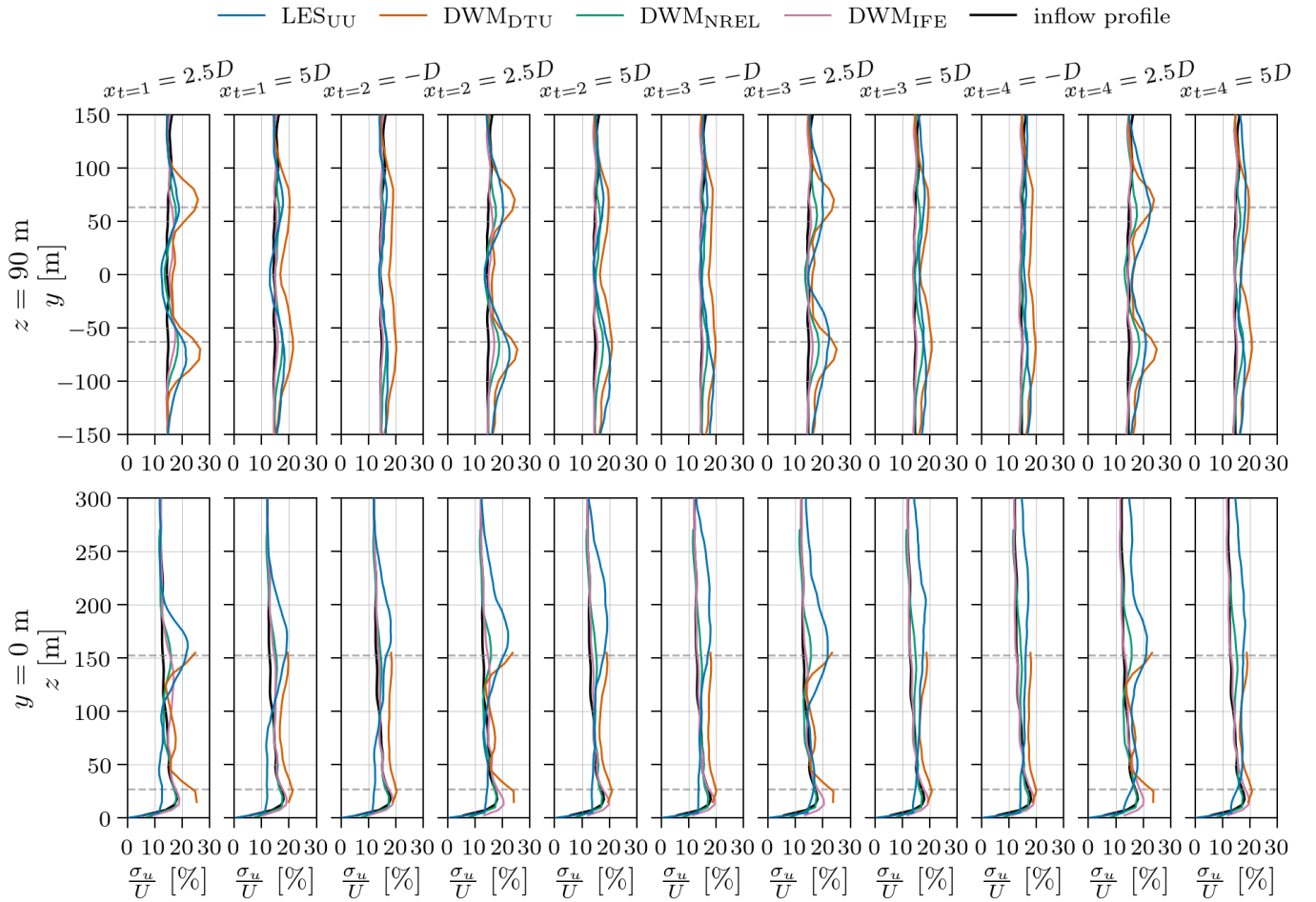


Figure 6. Profiles of velocity standard deviation of velocity for the aligned incoming wind case with high ambient turbulence ($TI_a = 12\%$). Horizontal dashed lines indicate the rotor swept area.

except close to near the surface. In this regime, and also at $x_{t=1} = 5D$, the This deviation from LES_{UU} is likely not due to the

395 wake added turbulence formulation itself, but because of the deviation in wake shape seen in Figs. 1 and 2 could stem directly
from the wake added turbulence formulation, but also from differences in predicted wake shape, since the shape relates to
the wake added turbulence formulation wake shape affects the wake added turbulence via the velocity gradient. Deviation in
predicted wake shape compared to LES_{UU} also impact the levels of The instantaneous wake shape also impacts σ_u for the
400 DWM models predict in all models through wake meandering, since areas with higher velocity gradients compared to LES_{UU}
to also experience higher variations in velocity in the wake experience larger temporal velocity fluctuations as the wake me-
anders. This is highly visible around the lower part of the rotor's swept area in the wake of turbines 1 and 2 for the cases

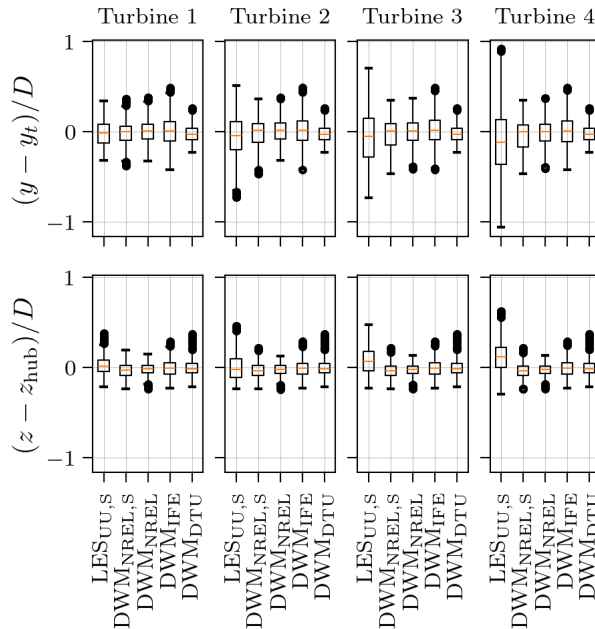


Figure 7. Box ~~plot-plots~~ of horizontal (upper row) and vertical (lower row) wake centre ~~position-positions~~ at $x = 5D$ behind the turbines, for the aligned incoming wind case with low ambient turbulence ($TI_a = 4.6\%$).

with higher ambient turbulence, $TI_a = 8.8$ and $TI_a = 12$. Here the DWM models show higher vertical velocity gradients, and consequently higher levels of σ_u , compared to LES_{UU} which shows an almost flat vertical velocity profile in this regime. Also
405 for the turbines deeper into the turbine row, the deviation in predicted wake shape can to a large extent explain the difference in σ_u seen between the DWM models and LES_{UU}. However, it gets Deeper into the farm, it becomes clear that the lack of a model for absence of a turbulence build-up model in DWM_{DTU}, as addressed in Keck et al. (2015) and Branlard et al. (2024), amplifies the difference-differences along the turbine row. Even though not including a wake-added-wake-added turbulence
410 bient turbulence case shown in Fig. 4, where for σ_u levels in DWM_{IFE} the levels of σ_u along the turbine row increase and become closer to the levels increase along the row and approach those of LES_{UU} in the wake of turbine 4. The same-This increase is not seen-observed in Figs. 5–6, possible due to the already high ambient turbulence in these cases, thus making the because the ambient turbulence is already high in those cases, making the relative wake turbulence build-up relatively smaller.

3.1.2 Wake centre positions

415 Figures 7 -and 8 show distributions of horizontal and vertical wake centre positions relative to the hub positions, at axial positions $5D$ downstream of each turbine in the row for the, under low and high ambient turbulence levels-conditions (the medium ambient turbulence case is shown in Fig. A3 in Appendix A). The distributions are shown as box-and-whisker box-and-whisker

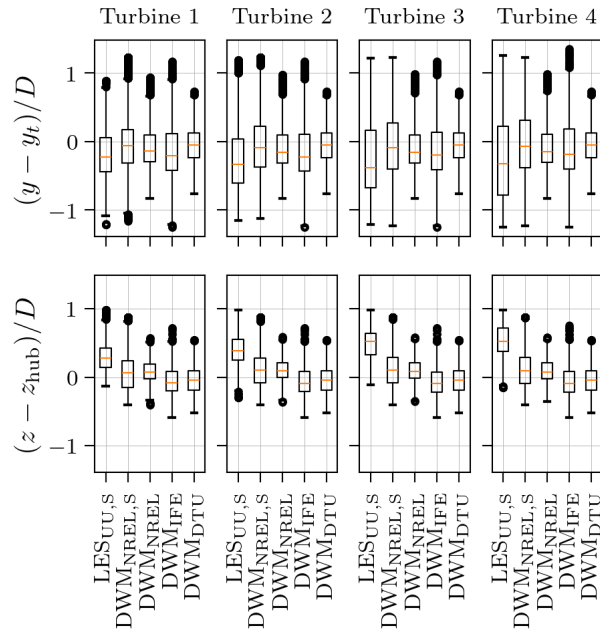


Figure 8. Box ~~plot-plots~~ of horizontal (upper row) and vertical (lower row) wake centre ~~position-positions~~ at $x = 5D$ behind the turbines, for the aligned incoming wind case with high ambient turbulence ($TI_a = 12\%$).

plots, where the box ~~indicate the range of the spans the~~ first and third quartiles and the orange line ~~shows the within the box~~ denotes the median wake centre position. Whiskers ~~are extending extend~~ to the most extreme ~~non-outlier data point~~, and
 420 outliers, shown as circles ~~are defined to be points located~~, are defined as points outside the box ~~with more than beyond~~ 1.5 times the box size ~~($1.5(Q_3 - Q_1)$)~~. For ~~the models marked with subscript S~~ those models labelled with a subscript "S", the wake centre positions are tracked using the python toolbox SAMWICH developed at NREL centres were tracked using NREL's SAMWICH toolbox, described in Sect. 2.4. For the ~~rest of the models, the wake centre positions are taken directly from the meandering algorithm in the DWM simulations~~ other models, wake centres come directly from each DWM model's own
 425 ~~meandering algorithm~~. For DWM_{NREL} , we show both the wake centres from SAMWICH and directly from DWM ~~are included in the figures to give an indication of the differences between the~~, to illustrate differences between these two approaches.

For ~~At~~ $TI_a = 4.6\%$ all models predict the median wake centre ~~position~~ of turbine 1 to ~~be around the hub remain near the hub position~~, (0,0) ~~For in the plots. In~~ this low ambient turbulence case, the turbines are modelled with zero rotor tilt. The DWM models ~~also predict the median positions of the wakes of~~ similarly keep the median wake positions of turbines 2–4 to
 430 ~~be close to near~~ (0,0), while the wake of ~~whereas in~~ LES_{UU} moves slightly upwards ~~the wakes shift slightly upward~~ and to the right (negative y) ~~deeper into further down~~ the turbine row. ~~The At~~ $TI_a = 12\%$ case shows similar results as $TI_a = 4.6\%$, the trends are similar, except that the ~~wake of~~ LES_{UU} wake moves further upwards, and the DWM_{NREL} ~~also moves wake also shifts~~ slightly above hub height. A rotor-misalignment is well-known to deflect a wind turbine wake (Clayton and Filby, 1982)

~~and the 5° tilt for the~~ In the $TI_a = 12\%$ case ~~is the~~ turbines were operated with a 5° rotor tilt. Notably, any misalignment
 435 of the rotor with the inflow is known to deflect the wake (Clayton and Filby, 1982), so a positive tilt is expected to deflect
 the wake ~~upwards~~ upward. DWM_{NREL} is the only DWM model that ~~take the effect of wake deflection due to tilt and yaw~~
~~misalignment into account.~~ For ~~accounts for~~ wake deflection from tilt or yaw misalignment, which is reflected in the results. At
 $TI_a = 12\%$, the median positions of the wake centres ~~are clearly moving~~ clearly shift to the right (negative y) ~~when looking~~
~~downstream with downstream distance~~ for all models except DWM_{DTU}, where the meandering ~~as mentioned above is derived~~
 440 ~~from~~ is driven by a separate Mann box ~~and not by the LES inflow~~. The LES precursor has a small mean ~~velocity component~~
~~in y direction~~ ~~velocity component~~ of -0.23 ms^{-1} at hub position for the $TI_a = 12\%$ case. If ~~we assume that the wakes follow~~
~~this velocity in y direction as a passive tracer, the wake will have moved~~ the wakes simply advected with this lateral velocity
~~like passive tracers, they would move about~~ $\sim -17\text{m} \sim -0.13D$ in y direction at $5D$ downstream. This is ~~in on~~ the same order
~~of magnitude the DWM models predict the median wake centre position to be~~ as the median wake displacements predicted by
 445 the DWM models at $5D$ downstream for all ~~the~~ turbines, and ~~can therefore explain the asymmetry seen for the DWM cases.~~
~~With thus likely explains the slight lateral asymmetry seen in those cases. By~~ the same reasoning, ~~the wake centre should move~~
 ~~$\sim -0.043D$ vertically due to a mean velocity component in z direction~~ a mean vertical velocity of -0.076 ms^{-1} in the inflow
~~would move the wake centre by $\sim -0.043D$ over $5D$.~~ This is in the same order ~~of magnitude as~~ the upward shifts predicted
 by DWM_{DTU} and DWM_{IFE} ~~predict the median wake centre position to be, while for,~~ whereas LES_{UU} and DWM_{NREL} the
 450 ~~upward deflection due to the rotor tilt has a larger contribution~~ show upward deflection since the contribution from rotor tilt is
 dominating.

The asymmetry in the ~~In~~ LES_{UU}, the wakes show a horizontal displacement in all cases: the largest in the high turbulence
~~case, consistent with the -0.23 ms^{-1} mean y -velocity, but even in the low and medium turbulence cases where the mean~~
 ~~y -velocity are near zero (0.0126 and -0.0710 ms^{-1} , respectively). These asymmetries in the LES_{UU} ~~deficit flow~~ becomes~~
 455 more pronounced ~~for the higher ambient turbulence case and deeper into the~~ further down the turbine row. ~~Wake deflection for~~
~~turbines with no~~ Notably, even without any rotor misalignment between the rotor and the incoming wind ~~has,~~ wake deflections
~~have~~ been observed previously in both experiments (Bartl et al., 2018; Bossuyt et al., 2021) and LES ~~studies~~ (Fleming et al.,
 2014). As ~~thoroughly explained by Zong and Porté-Agel (2020b)~~ it follows from the streamwise momentum equation that for
~~a counter-clockwise~~ explained in detail by Zong and Porté-Agel (2020b), for a anti-clockwise rotating wake in an undisturbed
 460 shear layer ~~where the~~ with a positive vertical velocity gradient ~~is positive~~ in the rotor area, it follows from the streamwise
~~momentum equation that the momentum balance causes the wake to deflect to the left. Conversely, the momentum balance will~~
~~cause a wake deflection towards the left~~ while the difference in tip vortex strength ~~on~~ between the upper and lower ~~part~~ half of
 the wake will ~~have the opposite effect.~~ These non-axisymmetric effects ~~due to wake rotation and tip vortices are only captured~~
~~by~~ tend to deflect it to the right. These two opposing effects, which are not captured by the axisymmetric DWM wake models,
 465 likely explains why LES_{UU} ~~and not by~~ predicts a greater wake deflection than the DWM models. Similarly, differences in tip
~~vortex strength between the left and right sides of the wake, captured in the three-dimensional LES_{UU} flow, can drive the wake~~
~~upward, explaining the larger upward wake deflections in LES_{UU} compared to DWM.~~

All models show ~~more meandering in horizontal than vertical direction, and also increased meandering for grater horizontal~~ meandering than vertical, and all show increased meandering at higher TI_a . For turbine 1 ~~there is good agreement between~~ the models in terms of, the models agree well on the meandering level. However, ~~there is a tendency that DWM_{IFE} shows~~ tends to produce slightly more meandering than the other DWM models, ~~with better match to LES for.~~ It matches LES more ~~closely in~~ the low ambient turbulence case ~~and slightly too high level of but slightly overestimates~~ meandering at high ambient turbulence. According to Keck et al. (2013), a lower wake transport velocity ~~increases the level leads to increased levels~~ of meandering, ~~which is in line consistent~~ with the higher meandering levels ~~seen for DWM_{IFE} compared relative~~ to DWM_{DTU}.

~~DWM_{NREL} and DWM_{NREL,S} show excellent agreement in median wake positions for all ambient turbulence cases, and in~~ meandering levels for the low ambient turbulence case. However, at high ambient turbulence, DWM_{NREL,S} predicts a larger ~~wake position spread than DWM_{NREL}. This is expected as the SAMWICH algorithm becomes less accurate with increasing~~ background turbulence, since the turbulence effectively acts as noise for the tracking algorithm.

For ~~the wakes of~~ turbines 2–4, the box plots show larger discrepancies ~~wake position distributions diverge more~~ between the models. While the wake of LES_{UU} shows a $\sim 50\%$ increase in ~~spreading wake spread~~ from turbine 1 to 2, there is no significant ~~change for~~ the DWM models ~~show no significant change.~~ The wake meandering ~~for of~~ LES_{UU} continue continues to increase from turbine 2 to 4. ~~The constant wake meandering predicted by the DWM models for all turbines is due to the meandering~~ algorithm used by these models. DWM assumes that the wakes of all turbines are meandered by ~~In DWM, however, all turbine~~ wakes are subjected to the same ambient turbulence field ~~without wake added turbulence included.~~ with no contribution

~~from wake-added turbulence to meandering. Therefore, the meandering does not increase for downstream turbines.~~ It is also worth noting that ~~the wake tracking algorithm in the SAMWICH toolbox~~ SAMWICH tracks the combined wake effect from all upstream ~~turbines; for wakes; for example at turbine 4 this means it identifies~~ the sum of the wakes from turbine 1 to 4. ~~Since~~ Because the meandering of an isolated wake increases grows with downstream distance, the ~~impact from the wakes of~~ the upstream turbines ~~upstream turbine wakes, which have travelled further can possibly contribute to an increased meandering~~ level of the combined wakes farther, might contribute additional meandering to the combined wake tracked downstream of turbines 2–4 ~~tracked by SAMWICH. In fact, DWM_{NREL,S} shows a small slight increase in meandering along the row~~ for both $TI_a = 4.6\%$ and $TI_a = 12\%$ ~~along the turbine row. We therefore cannot rule out that parts of the differences we see in that is~~ not present in DWM_{NREL}, suggesting that tracking the combined wake can capture some growth in meandering. Therefore, ~~some differences in the apparent~~ wake meandering between LES_{UU} and the DWM models ~~comes may arise~~ from the different

~~methodologies used to identify the wake centres~~ wake-centre identification methods.

3.1.3 Power and thrust

Figures 9 and 10 show time-averaged thrust ~~force~~ and aerodynamic power for the three levels of ambient turbulence investigated. While all models ~~show good agreement on the thrust force for~~ are in good agreement for the thrust of turbine 1, LES_{UU} ~~shows predicts~~ about 10% higher power ~~compared to than~~ the DWM models for this turbine. As expected, ~~there is all models~~ show a significant drop in both thrust and power ~~for all models~~ from turbine 1 to turbines 2–4 ~~operating (which operate~~ under waked conditions). For DWM_{NREL}, DWM_{IFE}, and LES_{UU}, ~~both~~ thrust and power ~~continue to~~ decrease slightly from turbine

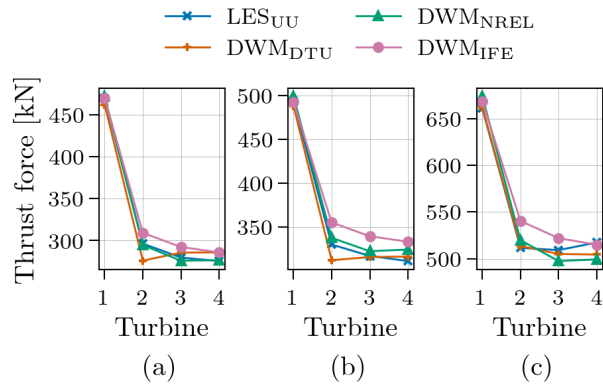


Figure 9. Mean thrust force for the aligned incoming wind case with (a) low ($TI_a = 4.6\%$), (b) medium ($TI_a = 8.8\%$), and (c) high ($TI_a = 12\%$) ambient turbulence.

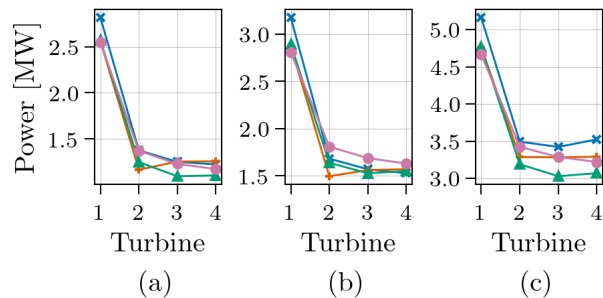


Figure 10. Mean power for the aligned incoming wind case with (a) low ($TI_a = 4.6\%$), (b) medium ($TI_a = 8.8\%$), and (c) high ($TI_a = 12\%$) ambient turbulence. For legend, see Fig. 9.

2 to through 4 for in the low and medium ambient turbulence cases. By contrast, DWM_{DTU} on the other hand shows a larger decrease initial drop in thrust and power from turbine 1 to 2 for both thrust and power compared to the two other DWM models, followed by. It then predicts an increase in power and thrust these quantities from turbine 2 to turbine turbines 3 and 4. This
505 A similar effect has been seen in a row of turbines from observed in full-scale measurements like e. g. at the Lillgrund wind farm with similar inflow under comparable conditions (below-rated wind speeds and low ambient turbulence) but with the turbines more closely spaced (see e.g., Madsen et al., 2016). For turbines (see e.g., Madsen et al., 2016). At $TI_a = 12\%$, the drop from turbine 1 to 2 is smaller for all models, as expected for with higher ambient turbulence, smaller for all models due to faster wake recovery. From For turbine 2 to 4, DWM_{DTU} shows constant values of nearly constant thrust and power, and not
510 the increase as was seen for the instead of the increase seen at low and medium ambient turbulence cases. LES_{UU} on the other hand shows a small, however, shows a slight increase in thrust and power from turbine 3 to 4 for at $TI_a = 12\%$. This could

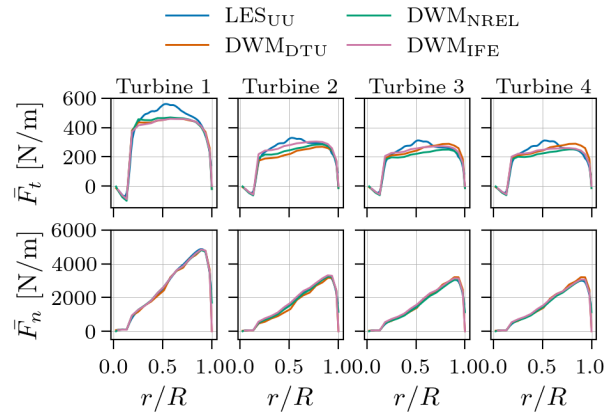


Figure 11. Time-averaged blade force as function of blade radius for the aligned incoming wind case with low ambient turbulence ($TI_a = 4.6\%$).

be explained by a behaviour could be due to turbulence build-up along the turbine row accelerating-, which accelerates wake recovery deeper into the farm.

3.1.4 Blade forces

515 The Figure 11 shows the time-averaged tangential and normal force distribution distributions along the radial positions of the blades in Fig. 11 show good agreement between the models. Results are shown for the low ambient turbulence case, but. The results are qualitatively similar for the higher ambient turbulence cases (not shown here). The largest deviations are seen in the middle section of the blades. Here Figs. A4 and A5 in Appendix A). Overall, the models are in good agreement. However, LES_{UU} gives predicts higher tangential forces compared to than the DWM models, which explains the higher levels of power
520 that was found in the middle section of the blades, consistent with its higher power predictions in Fig. 10. These figures also reveal that for the Since turbine 1 experiences the same inflow in all models, the differences observed for that turbine must come from differences in the turbine aerodynamic models (ALM in LES_{UU} and BEM variants in the DWM models; see Sect. 2.2.8 for details). Similar differences in the shape of the tangential force distribution between ALM and BEM have been reported in previous studies (Liu et al., 2022), though not as pronounced as observed here. The force-distribution plots further show that
525 for the $TI_a = 4.6\%$ and $TI_a = 8.8\%$ cases, where DWM_{DTU} showed predicts increased thrust and power for turbine turbines 3 and 4 relative to turbine 2, both normal and tangential forces tend to be higher compared to the other models at the outer part of the blade ($r/R > 0.5$) for the two last turbines in the row. For the normal forces that are almost, which are nearly an order of magnitude larger than the tangential forces, the relative difference differences between the models are small.

Figures 12 and 13 show the azimuthal variation of the normal component of the blade force at four radial positions along
530 the blade blade positions for the low and high ambient turbulence cases, respectively. (the medium ambient turbulence case is given in Fig. A6 in Appendix A). The time-averaged normal force at each radial position, \bar{F}_n (given in from Fig. 11), is has been

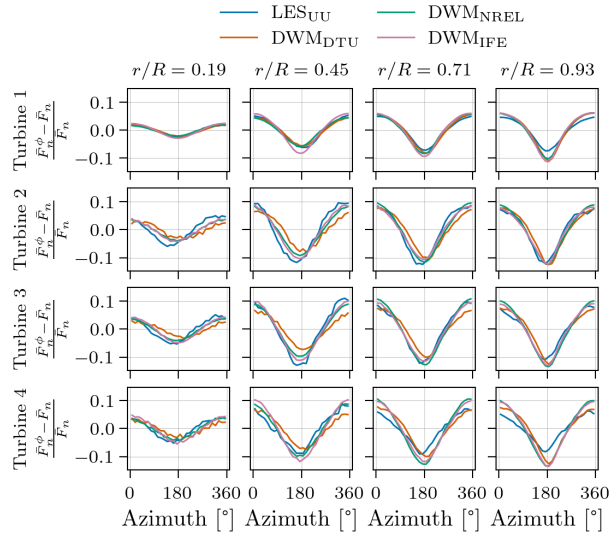


Figure 12. Relative difference between mean normal blade force per azimuthal bin \bar{F}_n^ϕ and total normal force \bar{F}_n , for the aligned incoming wind case with low ambient turbulence ($TI_a = 4.6\%$).

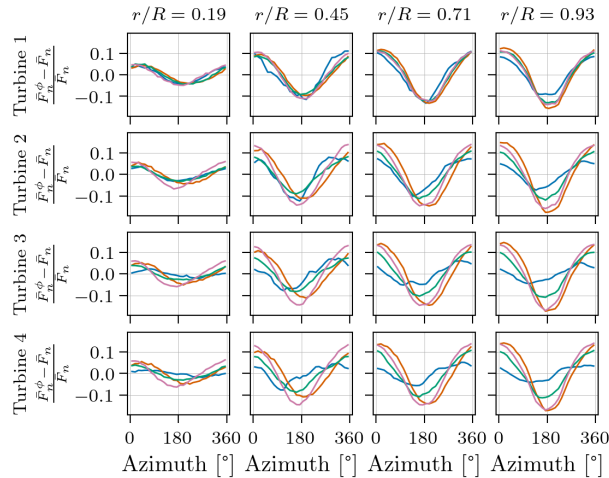


Figure 13. Relative difference between mean normal blade force per azimuthal bin \bar{F}_n^ϕ and total normal force \bar{F}_n , for the aligned incoming wind case with high ambient turbulence ($TI_a = 12\%$). For legend, see Fig. 12.

535 subtracted from the azimuthally varying force, and finally the result normalized by \bar{F}_n , to show only the relative force variation the blade experiences over the over a rotation. \bar{F}_n^ϕ is azimuthally binned with by $\Delta\phi = 12^\circ$ over using all blade rotations during the 45- from the 45 min simulations simulation. The maximum blade force occurs around $\phi = 0^\circ$. -This is- when the blade points upwards, which corresponds to when the blade and experiences the highest wind speeds. Equivalently Conversely, the

minimum blade force occurs around $\phi = 180^\circ$. As ~~mentioned~~ noted in Sect. 2.1, the tower is not modelled ~~in the simulations,~~ and the difference in wind, so any variation in wind speed experienced by the blades ~~are purely is solely~~ due to wind shear and, ~~in addition~~ for turbines 2–4, the influence ~~from of~~ upstream wakes. ~~All models show increasing amplitudes in force variation~~ In all models, the amplitude of force variation increases towards the blade tip ~~for all turbines, for every turbine.~~

540 For the low ambient turbulence case ~~given~~ in Fig. 12, the models generally agree on the shape of the force ~~variations shows~~ good agreement between the models, even though the variation. However, the phase of the DWM_{DTU} ~~force variations are~~ slightly shifted towards ϕ 's force variation is slightly shifted to higher ϕ for turbines 2–4 compared to the other models. ~~Also~~ the amplitudes of the force variations are generally in good agreement The force variation amplitudes also generally agree well between the models, however, LES_{UU} shows slightly smaller amplitudes than the DWM models at $r/R = 0.93$. ~~Since, even~~ for turbine 1 ~~experiences the same incoming wind profile for all models,~~ differences in force variations where all models share the same inflow. As before, differences observed for this turbine ~~are purely due to arise from~~ differences in the turbine aerodynamic models. In particular, the deviations at $r/R = 0.93$ is likely related to the tip corrections. The ALM in LES_{UU} uses an ALM with a vortex-based tip/smearing correction by Meyer Forsting et al. (2019), while all tip-smearing correction, whereas BEM in the DWM models uses BEM with applies the Prandtl tip correction (Glauert, 1935) for calculating blade forces (see Sect. 2.2.8). ~~Different tip corrections are likely causing the deviations at $r/R = 0.93$. for details).~~

For high ambient turbulence, Fig. 13, the ~~deviations between the models are more prominent~~ model differences are more pronounced. For the turbines operating under waked conditions, LES_{UU} exhibits a phase shift ~~towards lower to smaller~~ ϕ ($< 180^\circ$), ~~while i.e., peaks occur at $\phi < 180^\circ$),~~ whereas DWM_{DTU} again shows a ~~small shift towards higher~~ slight shift to larger ϕ ($> 180^\circ$). ~~For peaks at $\phi > 180^\circ$).~~ In LES_{UU} , the shift is largest this shift is greatest for turbine 3 and 4, ~~where the maxima have moved from:~~ the maxima move from about 0° to $\sim 300^\circ$ 300° , and the minima from $\sim 180^\circ$ to $\sim 150^\circ$. ~~As discussed, the box plots in around 180° to 150° . As noted earlier (Fig. 8 show that the wakes move),~~ the wakes shift slightly to the right when looking downstream (~~to negative~~ negative y). ~~This also,~~ which shifts the regime of highest wind to the left. Equivalently, the ~~area region~~ area region of lowest wind ~~will shift shifts~~ to the right, to $\phi < 180^\circ$. As ~~for in~~ the $TI_a = 4.6\%$ case, LES_{UU} predicts smaller force ~~variations~~ variation amplitudes than the DWM models at the blade tip for turbine ~~1.~~ This supports 1, supporting the conclusion that there are differences in the turbine aerodynamic models. For the turbines operating under waked conditions (2–4), the models show large deviations in amplitude. LES_{UU} ~~shows smaller amplitudes in force variations~~ compared to yields smaller force variation amplitudes than the DWM models, with DWM_{NREL} ~~being coming~~ closest. While the amplitudes of the force variations ~~stay remain~~ approximately constant for all turbines ~~for in~~ DWM_{DTU} and DWM_{IFE} , ~~it is decreasing deeper into~~ they decrease downstream along the turbine row for LES_{UU} and DWM_{NREL} .

565 For turbines 2–4 ~~operating under waked conditions, the varying incoming wind for the different models is the,~~ differences in their incoming wind fields are the main source of the ~~differences seen in the force variations~~ discrepancies in blade force variations between the models. The amplitudes of the force variations depend on the ~~variations in velocity~~ variation in velocity that the blades experience over a rotation. ~~A For instance, a~~ vertical velocity profile with less smaller variations over the ~~rotor's swept rotor-swept~~ rotor-swept area, as ~~typically seen for seen in~~ LES_{UU} at $x_{t=3} = -D$ and $x_{t=4} = -D$ in Figs. 2 and 3, ~~means a less~~

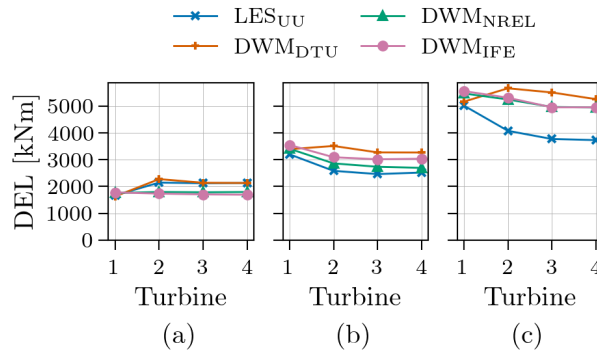


Figure 14. Fatigue of blade-root flapwise bending moment for the aligned incoming wind case with ambient turbulence of (a) $TI_a = 4.6\%$, (b) $TI_a = 8.8\%$, and (c) $TI_a = 12\%$.

570 force-variations-for-yields-smaller-force-variations-on the blades of turbine 3 and 4. EquivalentlyConversely, the higher velocity gradients in the profiles-estimated-by-DWM_{DTU} and DWM_{IFE} give-larger-profiles-result-in-larger-force-variation amplitudes.

3.1.5 Fatigue

Figure 14 shows 45-45 min damage-equivalent-damage-equivalent loads (DELs, see Sect. 2.1 for details) of-blade-root-for-the-blade-root flapwise bending moment, where-using-a Wöhler coefficient of 10 is-used for the blades. For the low ambient turbulence case, Fig. 14 (a), LES_{UU} shows a significant-large increase in DEL from turbine 1 to 2, followed by a constant level deeper-into-further-down the turbine row. DWM_{DTU} is-in-very-good-agreement-agrees-very-well with LES_{UU} for-in this case, except for-it-gives-a slightly higher DEL for-at turbine 2. By-contrast, DWM_{NREL} and DWM_{IFE} on-the-other-hand do not capture the-this increase in DELs from turbine 1 to 2, but gives-DELs-on-the-same-level-predict-nearly-the-same-DEL for all turbines.

580 Figure 14 shows-that-blade-root-also-shows-that-blade-root flapwise bending moment DELs increase with higher-TI_a-for-all-the-ambient-turbulence-for-all models. DWM_{DTU} shows a consistent-development-similar-trend from turbine 1 to 4 for-at all TI_a 's, with-levels: an increase from turbine 1 to 2, and a-small-then-a-slight decrease for the turbines further downstream. The other models have-show a different development for-the-along-the-turbine-row-at higher TI_a cases-compared-to-TI_a=4.6-For-. At $TI_a = 8.8\%$ and $TI_a = 12\%$, LES_{UU} shows-a-considerable-estimates-a-substantial decrease (about 15–20%) from turbine 1 to-turbine-2, and-then-fairly-followed-by-roughly constant levels from turbine 2 to 4. DWM_{NREL} and DWM_{IFE} show a similar development-trend along the turbine row but-with-higher-levels-of-DELs, but-at-higher-overall-DEL-levels.

To understand-the-differences-in-DELs, we-look-at-investigate-these-DEL-differences, Fig. 15 presents the power spectral density (PSD) of blade-root-the-blade-root flapwise bending moment presented-in-Fig-15, shown as cumulative integrals. All models show-jumps-at' spectra exhibit jumps at the $1P$ and-higher-harmonies, and-also-frequency-and-its-harmonics, as-well as-in-the-low-frequency-range below f_c . $1P$ corresponds to the frequency of one blade revolution, and the jumps seen in the

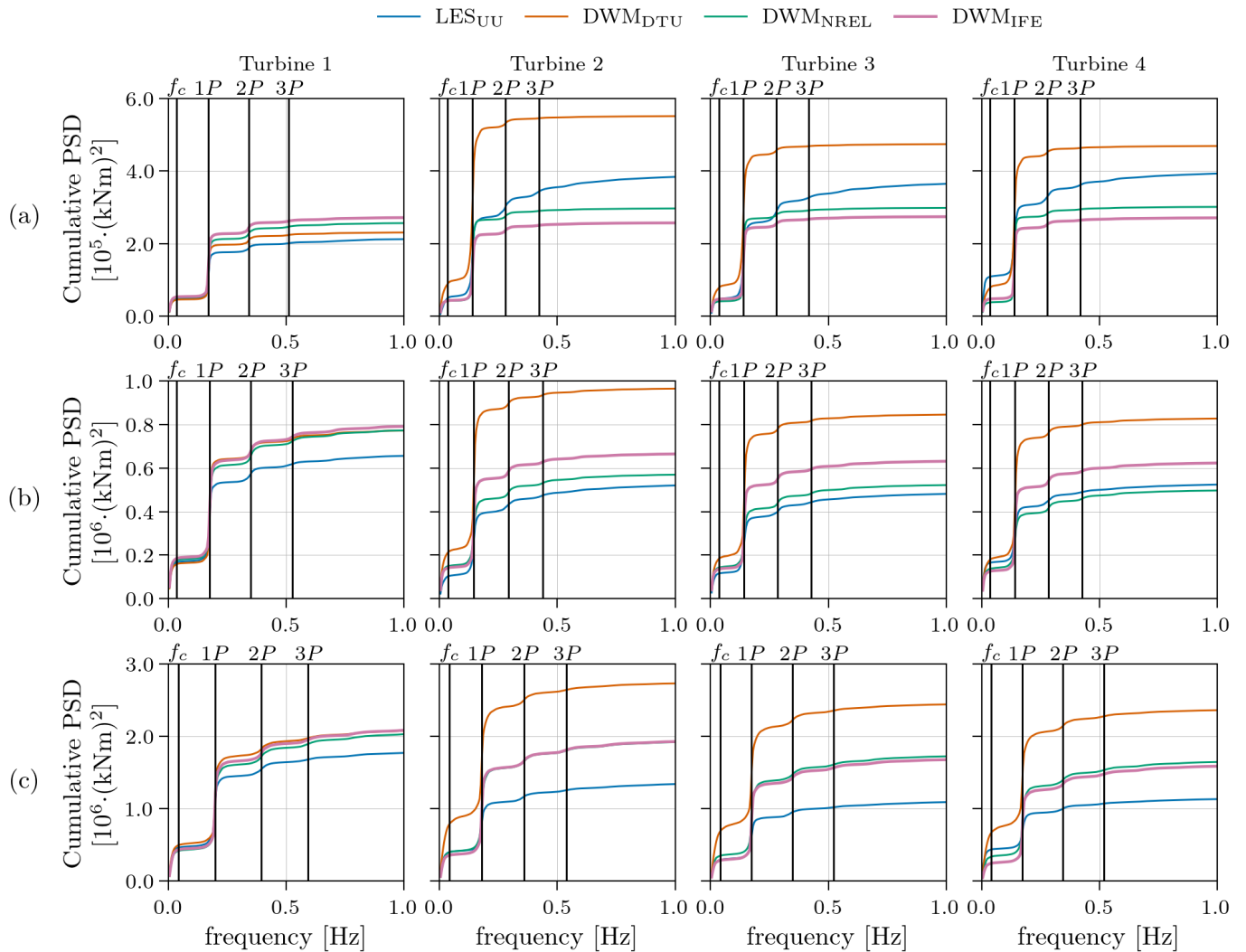


Figure 15. Energy spectra of ~~blade-root-blade-root~~ flapwise bending moment for the aligned incoming wind case with ambient turbulence of (a) $TI_a = 4.6\%$, (b) $TI_a = 8.8\%$, and (c) $TI_a = 12\%$.

cumulative integral correspond to peaks in ~~a normal PSD~~. $f_c = U_\infty / 2D$ ~~the standard PSD~~. $f_c = U_\infty / (2D)$ is the meandering cut-off frequency, and loads associated ~~to-with~~ wake meandering are expected to appear below f_c (Larsen et al., 2008; Larsen and Lio, 2025). ~~Turbine 1, however, sees the undisturbed wind without a meandering wake, so for this turbine the energy levels~~ However, since turbine 1 experiences undisturbed inflow without (no upstream wake), its energy in the PSD below f_c ~~can be seen as the baseline without any~~ represents a baseline without wake meandering energy. Surprisingly, ~~only~~ DWM_{DTU} ~~shows any significant change~~ is the only model consistently estimates a significant increase in energy below f_c ~~between when comparing~~ turbine 1 ~~and-to~~ the turbines operating under waked conditions. LES_{UU} ~~do, however, show increased~~ does show

600 some variation in energy below f_c ~~for some cases~~, for example an increase from turbine 3 to 4 ~~for in~~ the low ambient turbulence case. This change ~~agrees well aligns~~ with the increased meandering ~~seen observed~~ in Fig. 7 ~~especially, particularly~~ in the lateral direction.

DWM_{NREL} and DWM_{IFE} ~~shows show~~ fairly good agreement with LES_{UU} ~~comparing the energy at in terms of energy at~~ the $1P$ frequency. For these models, the $1P$ energy levels ~~seem to scale with the~~ amplitude of the blade force amplitudes of ~~the blade force~~ variations in Figs. 12 ~~13, with 13~~: DWM_{IFE} ~~having the largest and has the highest amplitudes and highest~~ $1P$ energy, and LES_{UU} the lowest ~~amplitudes~~. DWM_{DTU}, however, shows significantly higher $1P$ energy for the turbines ~~operating under waked conditions and (especially for turbine 2) compared to the other models. For DWM_{DTU} the energy at, and the~~ $1P$ frequency energy does not scale ~~as good with the amplitude of the blade force variations. For with the blade force variation amplitude. At~~ frequencies above $1P$, LES_{UU} shows ~~increased levels of energy from turbine higher energy levels in the waked turbines compared to turbine 1 to the turbines operating under waked conditions~~ for the low ambient turbulence case. Energy at the harmonics of $1P$ ($2P$, $3P$, which likely come from $4P$, etc.) arises from asymmetric blade loading (i.e. deviations from purely sinusoidal force variation). In LES_{UU}, the instantaneous wakes can be highly asymmetric and only approximately axisymmetric on average, so turbine 2–4 experience increased energy at these harmonic frequencies compared to turbine 1. In addition, wake-generated turbulence, which has a much smaller length scale than the wake-added turbulence that is known to have a length scale considerably smaller than that of the ambient turbulence (Madsen et al., 2010), and is also seen as increased σ_u in Fig. 4 from the inflow to the waked conditions in front of turbines 2–4². contributes to increased ~~energy at higher frequencies for the turbines operating under waked conditions. None of the DWM models predict a significant increase in high-frequency notable increase in high-frequency energy for the turbines waked turbines. The DWM models assume axisymmetric wakes, which do not directly cause asymmetric blade loading on the turbines operating under waked conditions, only indirectly via meandering. Somewhat unexpectedly, this also holds for DWM_{DTU}, the only DWM implementation in this study that includes a's wake-added turbulence model. For the does not generate the increased high-frequency energy for the~~ waked turbines as was observed in the LES_{UU} results. At higher ambient turbulence cases, even LES_{UU} shows no visible increase in high-frequency energy from turbine 1 to turbines 2–4. This ~~however, is likely due to the fact that the is likely because the~~ wake-added turbulence for these cases are negligible relative to the higher ambient turbulence levels in these cases is negligible compared to the already high ambient turbulence.

625 Even though ~~the DELs estimated by DWM_{DTU} is in good agreement with matches~~ LES_{UU} well in terms of DELs for the low ambient turbulence case, the underlying ~~mechanisms for the development in DELs is rather different for the contributions in the PSD differ between the~~ two models. The increase in DEL for In DWM_{DTU}, the DEL increase from turbine 1 to turbines 2–4 is mainly ~~due to increased energy content driven by higher energy at $1P$ frequency but and~~ also below f_c ~~for all levels of ambient turbulence at all ambient turbulence levels. For LES_{UU}, the DEL increase in the increase in DEL for the low ambient turbulence case is due to comes from~~ a combination of ~~increase in increased~~ energy associated with $1P$ frequency and ~~higher. For the higher ambient turbulence cases, the negligible wake-added turbulence levels and decreasing energy content the~~

²Unfortunately results from LES_{UU} is not shown at $x_{T=i} = -D$, $i = 2, 3, 4$ in this case due to lack of time-resolved data at this axial position. However, $x_{T=i-1} = 5D$ is expected to show similar results.

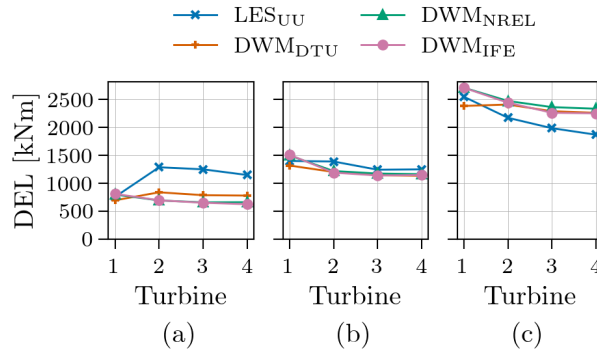


Figure 16. Fatigue of ~~tower-top tower-top~~ yaw moment for the aligned incoming wind case with ambient turbulence of (a) $TI_a = 4.6\%$, (b) $TI_a = 8.8\%$, and (c) $TI_a = 12\%$.

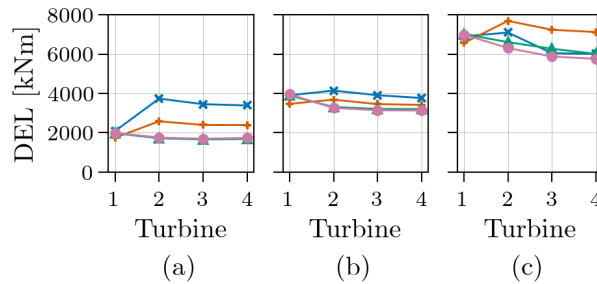


Figure 17. Fatigue of ~~tower-base tower-base~~ fore-aft bending moment for the aligned incoming wind case with ambient turbulence of (a) $TI_a = 4.6\%$, (b) $TI_a = 8.8\%$, and (c) $TI_a = 12\%$. For legend, see Fig. 16.

~~decreasing energy~~ at $1P$ frequency ~~for in~~ LES_{UU} ~~causes a reduction of DEL~~ ~~cause DELs to reduce~~ along the turbine row. For these cases, DWM_{NREL} and DWM_{IFE} ~~follows follow~~ the same trend ~~and~~ are closest to LES_{UU} .

Figures 16 and 17 ~~present show~~ 45-min DELs ~~of for the~~ tower-top yaw moment and tower-base fore-aft bending moment, respectively. ~~A, using a~~ Wöhler coefficient of 3 ~~is applied~~ for the tower. For all cases, the models show good agreement ~~in estimating tower DELs for turbine 1. on turbine 1's tower DELs.~~ For the low ambient turbulence case, LES_{UU} predicts considerably higher ~~tower~~ DELs than the DWM models for ~~the downstream turbines turbines 2-4.~~ Among the DWM ~~implementations models~~, DWM_{DTU} ~~is comes~~ closest to LES_{UU} ~~and~~ is the only ~~DWM model to reproduce the same development of one to reproduce a similar development in~~ DELs along the turbine row. At higher ambient turbulence levels, LES_{UU} and the DWM models are in closer agreement for the turbines operating under waked conditions. Consistent with the ~~blade load results, tower loads increase with ambient turbulence intensity. The cumulative integrals of tower base PSD of the tower-base fore-aft bending moment PSD in Fig. 18 show shows jumps below f_c and at the $3P$ frequency across for all models. Additionally, LES_{UU} shows energy at the harmonics of the also exhibits energy at multiples of $3P$ frequency,~~ visible as small

jumps at $6P$. ~~The energy~~ Energy below f_c contributes more ~~strongly for~~ significantly to tower loads than ~~it did~~ for blade loads shown in Fig. 15. Similar to the blade load results, DWM_{DTU} is the only model consistently predicting higher energy below
645 f_c for turbines ~~2-4~~ 2-4 compared to turbine 1. All models predict ~~comparable energy content at similar~~ $3P$ energy for turbine 1. However, ~~only~~ LES_{UU} ~~is the only model that shows increased energy content at~~ shows increased $3P$ and ~~its harmonics for~~ ~~downstream turbines. This increase diminishes with rising~~ $6P$ energy for the downstream turbines relative to turbine 1. This is ~~likely due to the asymmetric loading caused by the instantaneous LES wakes, as discussed earlier for the blade loads. These~~ ~~increases diminish with higher~~ ambient turbulence, and ~~at by~~ $TI_a = 12\%$, all models predict similar energy ~~content~~ at $3P$ and
650 ~~higher frequencies for all turbines. above for every turbine. The tower-top yaw moment PSD in Fig. A7 in Appendix A shows~~ ~~qualitatively similar behaviour to the tower-base fore-aft moment.~~

3.2 Partially waked case

This section extends the analysis to a more complex inflow scenario ~~by~~ introducing a small misalignment between the mean ~~wind-direction~~ wind direction and the turbine row. The resulting partial-wake configuration better reflects typical operational
655 conditions in wind farms, where turbines are rarely aligned perfectly with the wind. The same ambient conditions as the medium ambient turbulence case in Sect. 3.1 are used, ~~but~~ with a 5° ~~offset angle between the mean wind direction and the~~ ~~inflow angle offset relative to the~~ turbine row and ~~with~~ no yaw misalignment ~~between the rotors and the mean wind of the~~ ~~turbines themselves~~. We evaluate model performance in terms of time-averaged flow fields, wake centre positions, power production, thrust forces, blade loads, and fatigue. The results ~~are used to further investigate~~ ~~allow us to further examine~~ each
660 model's ability to capture asymmetric flow and loading effects.

3.2.1 Mean velocity profiles

Figure 19 shows time-averaged velocity profiles at ~~three axial positions, at the axial positions~~ $-1D$, $2.5D$, and $5D$ ~~relative to the 4 turbines relative to each of the four turbines,~~ for the partially waked case ~~with mean wind direction~~ ~~relative to the~~ ~~row of turbines, and with~~ ambient turbulence $TI_a = 8.8\%$. The upper row shows horizontal profiles at hub height and the lower
665 row shows vertical profiles at the turbine's lateral centre. Horizontal dashed lines indicate the range of the turbine ~~rotor's swept~~ ~~'s rotor-swept~~ area of the ~~closest nearest~~ upstream turbine, and horizontal dash-dot lines ~~indicate at which lateral position~~ ~~mark the lateral positions at which~~ the corresponding vertical profiles are ~~plotted taken~~. Since the ~~ambient conditions of the~~ partially waked case ~~has the same ambient conditions as the~~ ~~match the~~ fully waked case with medium ambient turbulence, ~~also the flow downstream and the flow behind and the~~ response of turbine 1 is similar ~~to this case, with:~~ DWM_{DTU} ~~showing~~
670 ~~shows~~ a distinct near-wake profile, ~~and whereas~~ DWM_{NREL} and LES_{UU} ~~only showing traces of the characteristic near-wake~~ ~~profile. As for show only traces of it. As in~~ the fully waked case, DWM_{IFE} , and to a ~~minor lesser~~ degree DWM_{NREL} , tend to ~~under-predict the deficit at the wake centre~~ ~~underpredict the centreline deficit~~. DWM_{DTU} , ~~however,~~ ~~slightly over-predicts the~~ ~~deficit,~~ ~~by contrast,~~ ~~slightly overpredicts the deficit in turbine 1's wake~~ compared to LES_{UU} ~~in the wake of the first turbine,~~ ~~and then gradually under-predicts the deficit deeper into the,~~ ~~but then gradually underpredicts it further down the~~ turbine row.
675 Do to the asymmetric ~~conditions inflow~~ for turbines 2-4, all models ~~estimate decreased wind speeds on the left side of the the~~

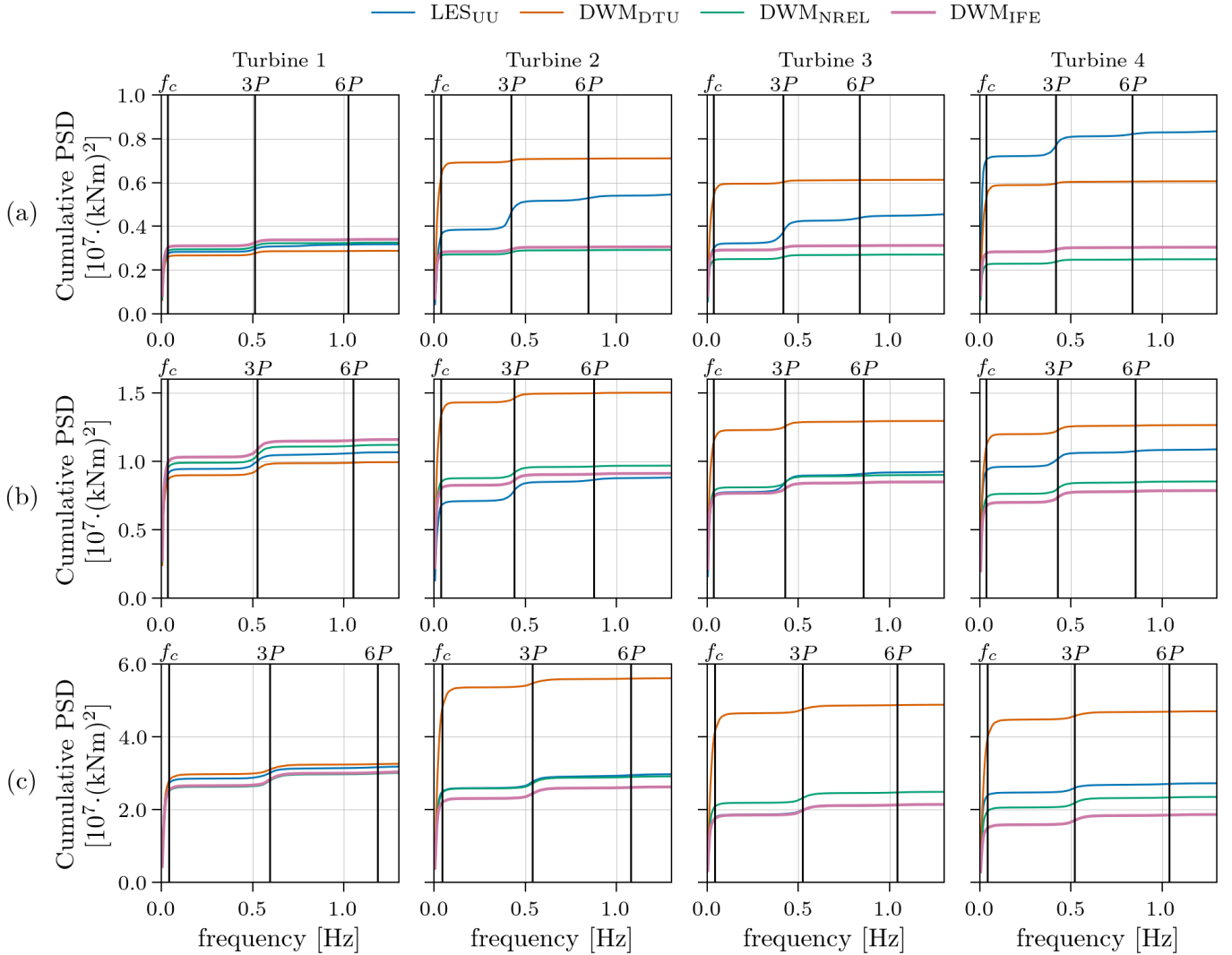


Figure 18. Energy spectra of tower-base tower-base fore-aft bending moment for the aligned incoming wind case with ambient turbulence of (a) $TI_a = 4.6\%$, (b) $TI_a = 8.8\%$, and (c) $TI_a = 12\%$.

wake predict that the wakes of these turbines spread more to the left side when looking downstream for these turbines, but as for. However, as in the fully waked case, LES_{UU} estimates the deficit to the sides shows a greater increase in deficit outside and above the rotor span to increase more than compared to the DWM models deeper into the turbine row.

Figure 20 shows profiles of velocity standard deviation σ_u for the partially waked case. As for in the fully waked case with 680 medium ambient turbulence, LES_{UU} and DWM_{DTU} show much higher levels of σ_u levels than DWM_{NREL} and DWM_{IFE}. DWM_{DTU} shows particularly good agreement with matches LES_{UU} for particularly well in the shear-layer to the right on the

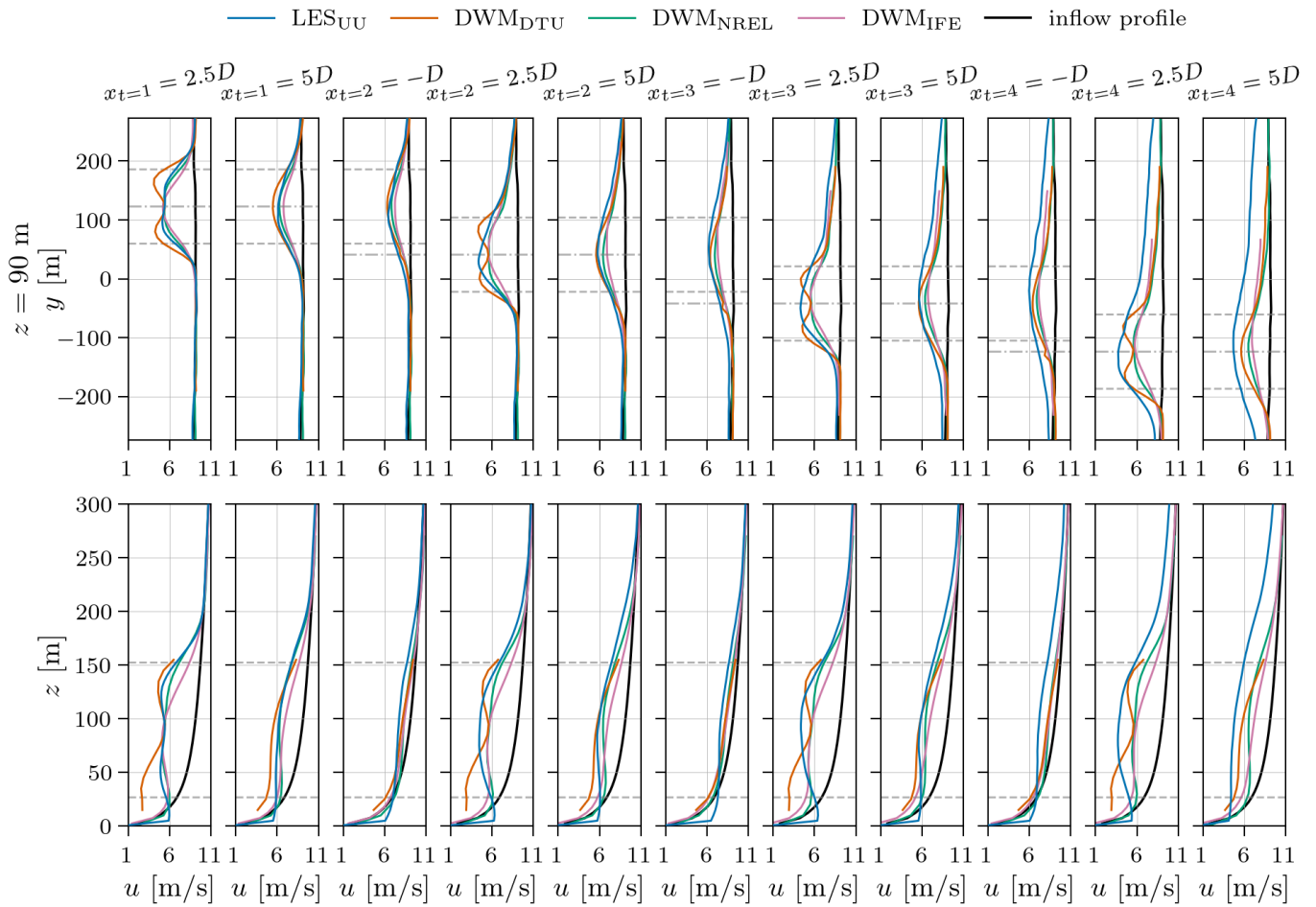


Figure 19. Time-averaged velocity profiles for the partially waked case (5° inflow angle) with medium ambient turbulence ($TI_a = 8.8\%$). Horizontal dashed lines indicate the rotor swept area of the closest upstream turbine, and horizontal dash-dot lines indicate at which lateral position the corresponding vertical profiles are plotted.

right side of the wake when looking downstream, ~~while the left~~ whereas larger differences appear in the left-side shear-layer and in the vertical profiles ~~show larger differences~~.

3.2.2 Wake centre positions

685 Figure 21 shows ~~box-and-whisker-plots-of~~ box-and-whisker plots of the horizontal and vertical wake centre positions at $5D$ downstream of each turbine ~~in the row~~ for the partially waked case. For $LES_{UU,S}$, the wake centre positions are tracked using the ~~python toolbox SAMWICH developed at NREL, described in SAMWICH toolbox~~ (Sect. 2.4. ~~For~~), whereas for the DWM models ~~;~~ the wake centre positions are taken directly from the meandering algorithm in the DWM simulation.

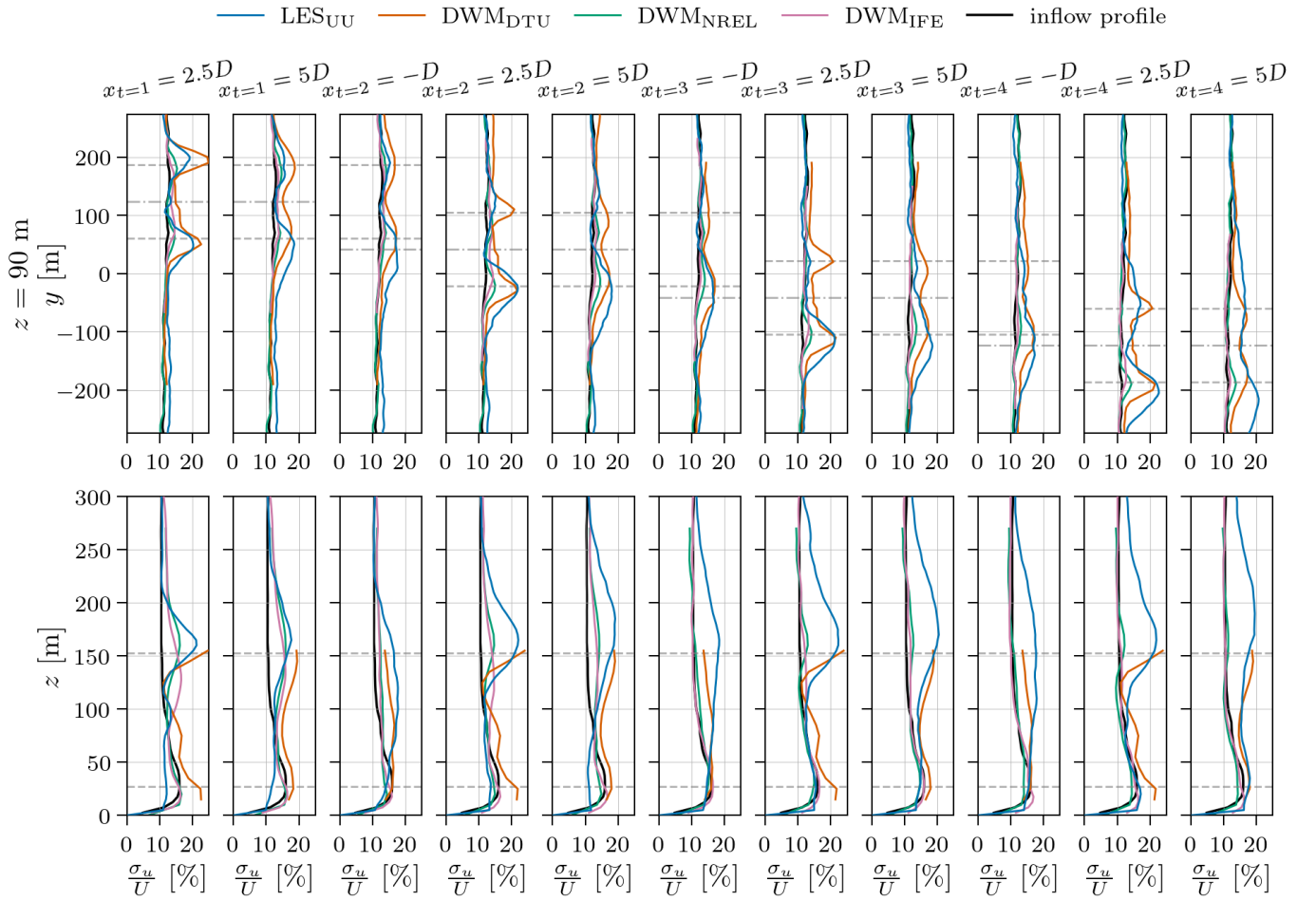


Figure 20. Profiles of velocity standard deviation of velocity for a wind direction for the partially waked case (5° inflow angle) with medium ambient turbulence ($TI_a = 8.8\%$). Horizontal dashed lines indicate the rotor swept area of the closest upstream turbine, and horizontal dash-dot lines indicate at which lateral position the corresponding vertical profiles are plotted.

For turbine 1, all models predict that the median wake centre position ~~has not moved away from~~ stays approximately at the turbine position laterally, ~~i.e.~~ ($y - y_t \approx 0$). For the DWM models ~~this also true~~, this holds for turbines 2–4, ~~while for as well~~, whereas $LES_{UU,S}$ predicts the median wake centre ~~position is positioned~~ positions shifted slightly to the left when looking downstream ($y - y_t > 0$). ~~For the current case with skewed inflow, the turbines are positioned~~ In this skewed inflow setup, each turbine is offset to the left of the ~~their downstream turbines when looking downstream, e.g. one behind it; for example,~~ turbine 1 is positioned $0.65D$, $1.31D$, and $1.96D$ located $0.65D$, $1.31D$, and $1.96D$ to the left of turbine-turbines 2, 3, and 4, respectively. Since ~~the wake tracking algorithm in the SAMWICH toolbox~~ SAMWICH tracks the combined wake from all the upstream turbines, the ~~shift towards left observed~~ leftward shift in the $LES_{UU,S}$ wake centre ~~distribution, can therefore possibly~~

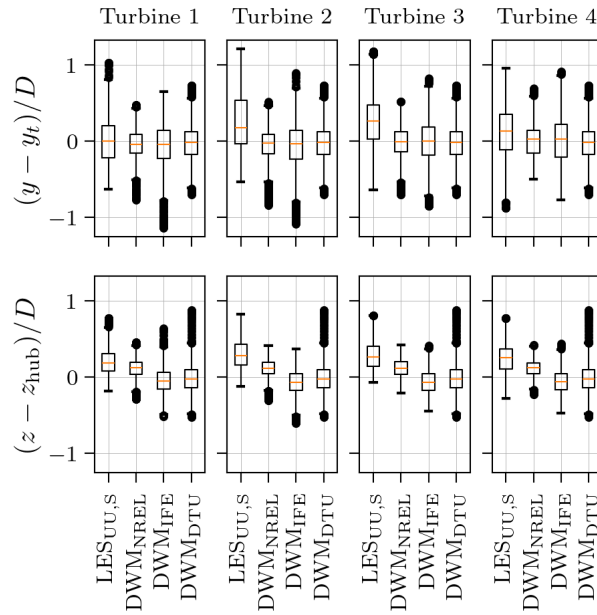


Figure 21. Box ~~plot-plots~~ of horizontal (upper row) and vertical (lower row) wake centre ~~position-positions~~ at $x = 5D$ behind the turbines for the partially waked case (5° inflow angle) with medium ambient turbulence ($TI_a = 8.8\%$).

700 ~~be a result of the impact from the upstream turbines, and not due to a~~ distributions may be influenced by the upstream wakes' position rather than a true deflection of the individual wakes. Alternatively, ~~the asymmetric wake distribution can be explained by wake deflection due to the vertical velocity gradient in the shear flow causing the wake to move horizontally~~ this asymmetry could be caused by the vertical shear in the inflow causing a horizontal wake deflection, as discussed in Sect. 3.1.2. However, ~~this that mechanism~~ does not explain why only the wakes of turbines 2–4 ~~would deflect to the left, show a leftward deflection~~ and not the wake of turbine ~~1, nor why the deflection is in the opposite direction to what was seen in the aligned inflow case.~~

705 As ~~for the aligned cases investigated in in the aligned inflow cases~~ (Sect. 3.1), LES_{UU} and to a ~~smaller lesser~~ extent DWM_{NREL} ~~estimate predict~~ that the wakes deflect ~~upwards upward~~ above hub height ~~due to because of~~ the 5° rotor tilt ~~angle~~. ~~Also. And also~~ in agreement with the previous results, all models show more ~~meandering in~~ horizontal than vertical ~~direction meandering~~. However, ~~the unlike the aligned case, LES_{UU} does not show a large increase in meandering level deeper into the row which was seen for LES_{UU} in the aligned case, is not observed here~~ levels further down the row under partial-wake conditions.

3.2.3 Power and thrust

710 Figure 22 shows time-averaged thrust force and power for ~~the row of turbines for the each turbine in the~~ partially waked case. As expected, ~~all models show turbine 1 exhibits~~ similar thrust and power as the fully waked case with the same medium ambient

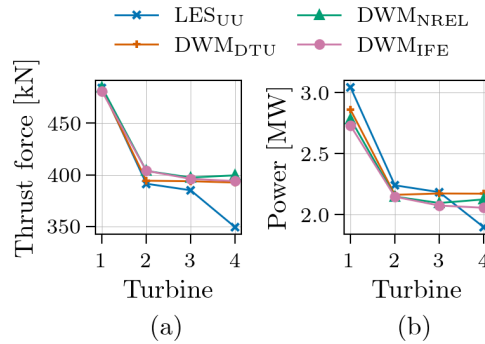


Figure 22. (a) Mean thrust force and (b) mean power for the partially waked case (5° inflow angle) with medium ambient turbulence ($TI_a = 8.8\%$).

turbulence conditions for turbine 1. The small differences seen are due to. However, small differences due appear because of variations in the incoming wind field at the two lateral positions of turbine 1 in the fully waked case ($y = 0$) and in the partially waked case ($y \approx 123$ m). As for in the fully waked case, LES_{UU} shows about 10 % higher power compared to the DWM models for turbine 1. For turbines 2–4 there are good agreement between, the DWM models, while are in good agreement, whereas LES_{UU} shows a significant drop in both thrust and power from between turbine 3 to and 4. This drop comes from the higher deficit upstream deeper deficit in front of turbine 4 as a result of a much wider horizontal wake estimated predicted by LES_{UU}, seen visible at $x_{t=4} = -D$ in Fig. 19.

3.2.4 Blade forces

As for the The time-averaged tangential and normal force distributions along the blade span for the partially waked case (Fig. A8 in Appendix A) show qualitatively similar trends to the fully waked case, there is good agreement between the models for all four turbines in the row when predicting time-averaged tangential and normal force distribution along the radial positions with good agreement among the DWM models, while LES_{UU} shows higher tangential forces in the mid-span region of the blades for the partially waked case (not shown here). In figure 23, Figure 23 presents the azimuthal variation of the normal blade force is presented at four radial positions along the blade for all four turbines in the row under the partially waked case. The models show larger deviations comparing the shapes For turbine 1, the models generally agree on the shape of the force variations, with some amplitude differences near the blade tip. However, larger deviations are seen among the models for turbines 2–4; operating under partially waked conditions. In LES_{UU} predicts, the force minimum to be shifted around is shifted about 90° towards larger ϕ for these turbines, meaning the blades feel the lowest force when pointing turbines 2–4, meaning that the lowest force occurs when the blades point straight to the left. The lowest velocity in the incoming wind field therefore has the lowest velocity is therefore towards the wake of the upstream turbine. For DWM_{IFE}, on the other hand, the minimum force is shifted only slightly towards larger ϕ . Due to the weaker wake deficit estimated by this model Because DWM_{IFE} predicts a

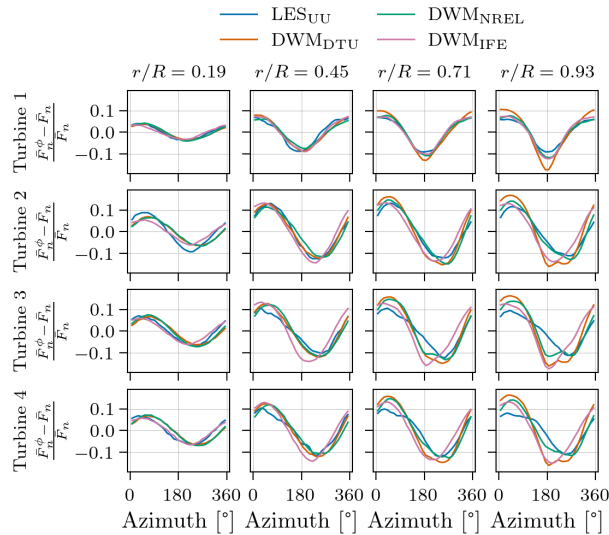


Figure 23. Relative difference between mean normal blade force per azimuthal bin \bar{F}_n^ϕ and total normal force \bar{F}_n for the partially waked case (5° inflow angle) with medium ambient turbulence ($TI_a = 8.8\%$).

weaker wake deficit, the blades feel/experience the lowest force when pointing almost straight down near the bottom of their rotation, where the velocity of the incoming flow is low due to shear. DWM_{DTU} and DWM_{NREL} shows minima located at predict a force minimum at about the same ϕ as the-LES_{UU} minimum for all radial positions of the blade, but towards along the blade. However, at the outer part of the blade, a second minimum appears at approximately the same ϕ as for estimated by DWM_{IFE}. When the blades are pointing down, the tip enters into the regime a blade is pointing downward, its tip passes through a region where the DWM models estimate significantly sharper gradients in the vertical velocity profiles compared to predict significantly sharper vertical velocity gradients than LES_{UU} - as seen in (see Fig. 19. Consequently). As a result, the DWM models predict a force minimum on the outer part of the blades at $\phi \approx 180^\circ$ also for the turbines operating on the outer blade sections, even under partially waked conditions.

3.2.5 Fatigue

Figure 24 shows that all the models estimate comparable levels of blade and tower DELs for the 45-min DELs for (a) blade-root flapwise bending moment, (b) tower-top yaw moment, and (c) tower-base fore-aft bending moment, for the partially waked case. DWM_{DTU} is the only DWM model capturing to capture a similar development along the turbine row as LES_{UU}, but at a slightly higher level for. However, it slightly overpredicts the blade DELs and lower levels for underpredicts the tower DELs compared to LES_{UU}. DWM_{DTU} and LES_{UU} estimate an increase in both estimate increasing DELs from turbine 1 to 2. The In these models, the reduced loads due to an increased wind speed is decreased mean wind are compensated by increased turbulence downstream of turbine 1, modelled in DWM_{DTU} by the wake-added turbulence model. By contrast, DWM_{NREL}

750 and DWM_{IFE} , however, lack such a wake-added turbulence model, with the result that the turbines operating under partially waked conditions show a decrease in DEL compared to turbines 2–4 have lower DELs than turbine 1. By looking at the

The PSDs of the loads presented in Fig. 25, it is clear show that DWM_{DTU} also for the partially waked case shows predicts more energy below f_c for turbines 2–4 than the other models for turbines 2–4, as was also seen in the fully waked case. However, in contrast to the fully waked case, also LES_{UU} shows increased showed no significant change in energy below f_c for turbines 2–4, for the blade-root flapwise bending moment and tower base along the turbine row, whereas here LES_{UU} does exhibit an increase in low-frequency energy from turbine 1 to the waked turbines for both the blade-root flapwise and tower-base fore-aft bending moment. For the blade root moments.

The blade-root flapwise bending moment spectra in Fig. 25 (a) show that the DWM models estimate higher more energy at the $1P$ frequency and its harmonics compared to than the LES_{UU} for all turbines, and which is likely the main reason for cause of the higher DELs estimated by the DWM models. Consistent with As in the fully waked case, the levels of energy at the $1P$ frequency coincides correspond well with the difference in blade force variations blade-force variation amplitudes seen in Fig. 23 for all models except DWM_{DTU} . Again, DWM_{DTU} shows a higher does not show a direct relationship between $1P$ energy and blade-force variation amplitude: it predicts a larger increase in $1P$ energy for the turbines operating under waked conditions than the amplitude in blade force variations indicates. For from turbine 1 to the waked turbines than the blade-force variation amplitude indicates.

In the frequency spectra of tower-top yaw moment moments in Fig. 25 (b), LES_{UU} shows no significant change in energy below f_c , and between the turbines, while the small decrease in $3P$ energy along the turbine row coincides well with the change in DELs along the turbine row. DWM_{NREL} and DWM_{IFE} show a significant decrease in energy below f_c for the turbines operating under waked conditions that, which, together with a decrease in energy at $3P$ frequency, reduce the tower-top yaw moment DELs. Lastly Finally, DWM_{DTU} shows rather nearly constant DELs as a result of a combination of increased energy below f_c and decreased energy at $3P$ frequency for the turbines operating under waked conditions. For DWM_{NREL} and DWM_{IFE} , waked turbines compared to turbine 1.

For the tower-base fore-aft bending moment DELs scale, DWM_{NREL} and DWM_{IFE} show DEL trends that correlate with the energy at $3P$ frequency, while whereas for LES_{UU} and DWM_{DTU} , it is the change changes in energy below f_c that dominates the development in DELs dominate the DEL evolution along the turbine row.

4 Discussion

The comparative evaluation of the three DWM-based wake models against LES reveals generally good agreement in overall wake evolution and turbine performance trends, with notable discrepancies in specific wake features and load predictions.

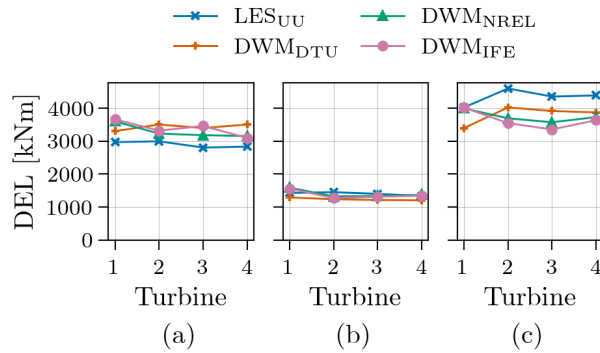


Figure 24. Fatigue of (a) blade-root-blade-root flapwise bending moment, (b) tower-top-tower-top yaw moment, and (c) tower-base-tower-base fore-aft bending moment for the partially waked case (5° inflow angle) with medium ambient turbulence ($TI_a = 8.8\%$).

780 4.1 Wake modelling

All three DWM models capture the qualitative shape and decay of the wake-deficits-wake deficits along the turbine row, but there are systematic differences in deficit magnitude and shape when compared to LES. Immediately downstream of the first turbine, the DWM_{DTU} model produces a more pronounced near-wake profile than observed in the LES, whereas DWM_{NREL} tends to produce a deficit that is more developed towards a Gaussian profile. For the turbines operating under waked conditions, LES_{UU} already shows a Gaussian-like velocity profile at $x = 2.5D$. This is likely due to the-added turbulence in the turbine wakes, which increases the turbulence levels experienced by downstream turbines and enhances wake recovery through faster mixing. Neither DWM_{DTU} nor DWM_{NREL} reflect this change-capture this increase in wake recovery rate between turbine 1 and the downstream turbines operating under waked conditions. Interestingly, DWM_{IFE}'s Gaussian profile therefore tend to outperform the other DWM models in the near-wake of the turbines operating under waked conditionsregion of the waked turbines. Although DWM_{DTU} includes a wake-added turbulence model, it is only applied in the aeroelastic solver and does not influence the-wake development. Consequently, increased wake recovery due to elevated downstream turbulence is not captured in the velocity field. The newly implemented wake-added turbulence model in DWM_{NREL} that-couples wake-added turbulence and meandering (Branlard et al., 2024), though with meandering (Branlard et al., 2024). Although it was not applied in this study, it may improve agreement in future comparisons. Nonetheless, both DWM_{DTU} and DWM_{NREL} exhibit faster wake recovery for at higher ambient turbulence, as expected.

In the far-wake regions for the aligned case (e.g., $x_{t=i} = 5D$, $x_{t=i+1} = -D$), DWM_{DTU} generally slightly-overestimates the centreline deficit slightly, while DWM_{IFE} slightly underestimates it. DWM_{NREL} lies falls in between and is often closest to LES_{UU} in these regions. However, for the partial wake case, DWM_{DTU} seems to be closest to-appears to match LES_{UU} most closely. The DWM_{DTU} model uses as mentioned previously-a superposition method wherein which, under below-rated conditions, the maximum-velocity-deficit-velocity deficit at each point is the maximum-deficit-scanning through all the individual meandered-wake-deficits of upstream turbine is takentaken as the largest deficit among all individual meandering wakes of

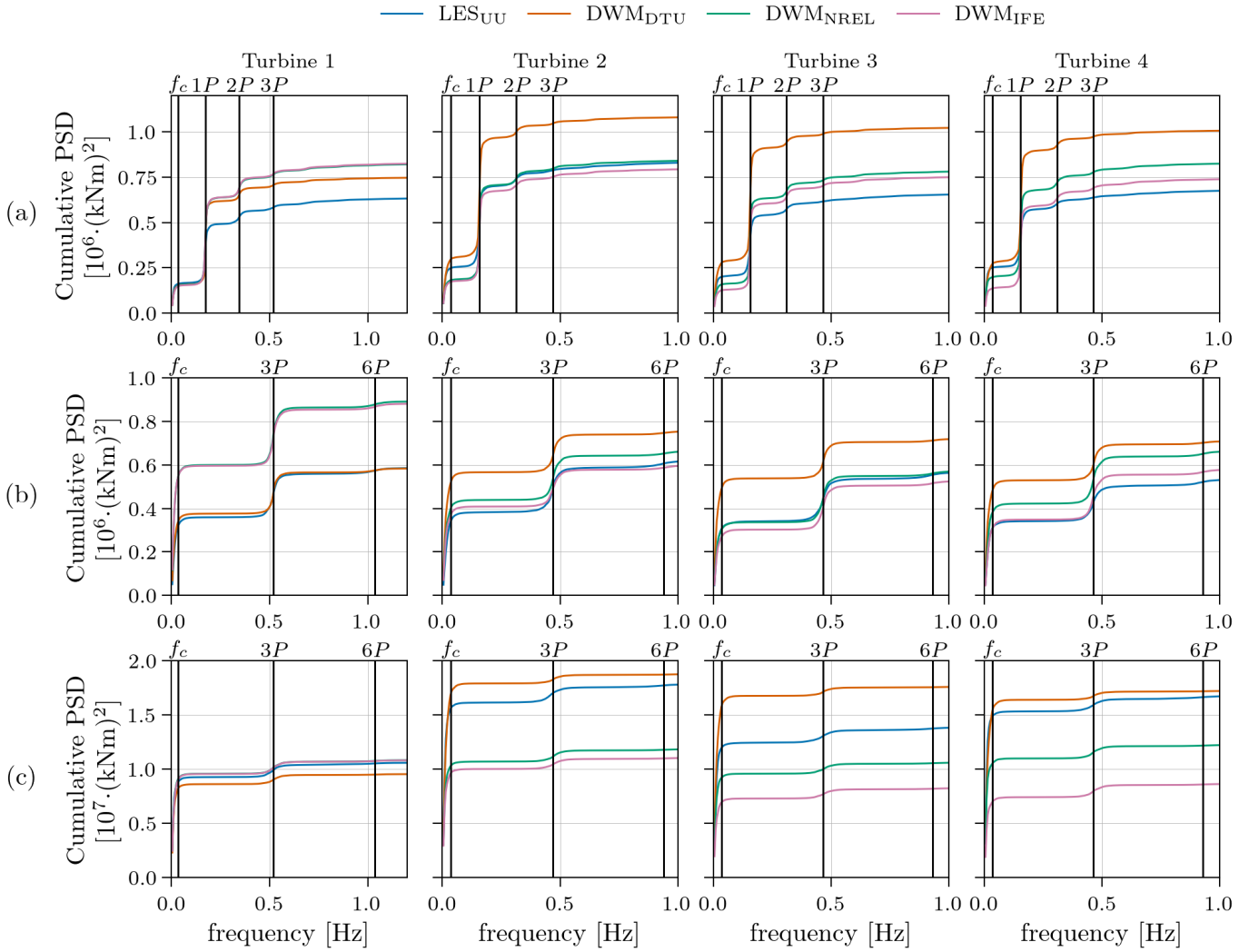


Figure 25. Energy spectra of (a) blade-root-flapwise bending moment, (b) tower-top-yaw moment, and (c) tower-base-fore-aft bending moment for the partially waked case (5° inflow angle) with medium ambient turbulence ($TI_a = 8.8\%$).

upstream turbines. In contrast, DWM_{NREL} and DWM_{IFE} incorporate wake summation schemes where-in which all upstream wakes, calculated sequentially down the row, affect-contribute to the total flow field to different-extent-varying extents. While DWM_{NREL} does not capture the change-in-evolution-of-the flow field along the turbine row significantly better than DWM_{DTU} , DWM_{IFE} demonstrates-shows improved accuracy in the wake periphery, where the build-up-of-LES_UU deficit build-up is substantial. The build-up-of-TI-accumulation-of-turbulence-intensity along the turbine row in the DWM_{IFE} model, affecting-the-which affects its eddy-viscosity closure, can-also-be-a-part-of-the-difference-may-also-contribute-to-the-differences observed relative to the other DWM models. The-performance-of-However, DWM_IFE does, however, degrade-s performance degrades

at higher ambient turbulence, suggesting that the term in ~~the-its~~ eddy viscosity model related to ~~the~~ ambient wind shear scaling
810 with turbulence intensity γ should be calibrated.

Vertical velocity profiles play a critical role in load predictions as they affect the azimuthal variation of the inflow felt by turbine blades, directly influencing blade $1P$ ~~and tower- $3P$~~ loading. Rotor tilt induces an upward wake deflection, which is captured by LES_{UU} and by DWM_{NREL} (the only model that incorporates tilt), but not by DWM_{DTU} or DWM_{IFE} . Notably, LES_{UU} predicts even greater upward ~~deflection-deflections~~ than DWM_{NREL} , ~~which-~~ This deflection increases with down-
815 stream distance and occurs even ~~for the low turbulence case without in the low-turbulence case without any~~ rotor tilt. ~~Also horizontal deflection is~~ Horizontal deflection is also observed in the LES_{UU} results. This suggests that wake rotation and tip vortex effects, which are not accounted for in current DWM formulations, cause additional deflections. The ~~curled-wake model recently implemented in curled-wake extension to~~ DWM_{NREL} (Branlard et al., 2023), ~~though not applied in this study, may improve agreement in future comparisons~~ which was not used in the present simulations, could potentially help reduce these
820 discrepancies.

The box plots of wake centre positions show that the predicted meandering levels for the first turbine in the row agree well among all DWM models and LES_{UU} . Wake meandering is consistently stronger in the horizontal ~~than vertical direction~~ direction than the vertical across all models, consistent with the fact that large-scale vertical turbulence energy ~~being less is lower~~ than large-scale lateral turbulence energy for conventional flat terrain conditions. However, the downstream growth
825 of meandering amplitude ~~downstream~~ is underrepresented: while LES_{UU} shows a 50 % increase from turbine 1 to 2 (~~and continued growth thereafter~~), with continued growth beyond, the DWM models maintain nearly constant meandering levels. This ~~might result from their~~ discrepancy may result from the models' reliance on the same ambient turbulence field for all wakes, without accounting for the ~~increased additional~~ turbulence from upstream ~~wake interactions~~ wakes, which leads to underprediction of wake spreading in deep turbine arrays. Hanssen-Bauer et al. (2023) suggest that this could be addressed
830 by coupling the wake-added turbulence model with the meandering routine, so that both ambient and wake-added turbulence contribute to wake motion. In fact, ~~this is what is implemented in~~ the new wake-added turbulence model in DWM_{NREL} (Branlard et al., 2024) implements this approach. However, if ~~the~~ wake-added turbulence ~~is in fact contributing significantly~~ does significantly contribute to wake meandering, it is in conflict with the traditional DWM assumption that meandering is driven only by large-scale turbulence γ , while wake-added turbulence captures smaller scales. Nevertheless, important future
835 work is to check this assumption by testing the new DWM_{NREL} wake-added turbulence model.

As shown in the ~~profiles of σ_u profiles~~ (Figs. 4-6, ~~6~~ and 20), the ~~DWM_{DTU} 's inclusion of a~~ wake-added turbulence model in DWM_{DTU} clearly improves its turbulence predictions. DWM_{NREL} and DWM_{IFE} , lacking such a scheme, significantly underpredict σ_u in the turbine wakes across all cases. The influence of wake turbulence on the flow field is evident in snapshots of instantaneous velocity profiles. In the low ambient turbulence case in Fig. A1, DWM_{NREL} and DWM_{IFE} show relatively
840 smooth wake profiles, whereas LES_{UU} and DWM_{DTU} produce more turbulent profiles. In the high ambient turbulence case shown in Fig. A2 the wakes do not dominate the flow field as much due to the already high background turbulence, and differences between the models are less pronounced.

Even with a wake-added turbulence model, DWM_{DTU} still shows discrepancies relative to LES_{UU} , which may stem partly from differences in wake shape influencing that influence the added turbulence through via the velocity gradient input. However, the lack of Furthermore, DWM_{DTU} clearly lacks a model for turbulence build-up across the row of turbines is evident, especially for the case with along the turbine row, especially evident in the low ambient turbulence case. Here LES_{UU} indicates shows increasing σ_u along the row, even as the mean deficit and velocity gradients decrease, which contradicts the wake-added turbulence formulation given in Eq. 7. A possible reformulation of the present added wake current wake-added turbulence approach could be to consider treat Eq. 7 as a source term of wake added turbulence (which it is) and then combine it with an accumulation term and a decay term. The DWM modelling improvement improvements by Keck et al. (2015) should also be considered as it both includes they account for the impact of the ambient vertical wind gradient on the shear on eddy viscosity and models model the build-up of the wake added wake-added turbulence. Comparisons with ALM simulations show a reduction of that including these improvements can reduce turbulence intensity deviations by up to 40 % in the deviation on turbulence intensity after the by the eighth turbine in a row by including this improvement (Keck et al., 2015).

855 4.2 Power and thrust predictions

Despite the differences in flow details, all three DWM-based models reproduce the general trends in time-averaged turbine power and thrust observed in the LES benchmark, and stay within 5–10 staying within 5–10 % deviation of the LES results. Surprisingly, while the DWM models show excellent good agreement in power estimation prediction for turbine 1 where the inflow is identical for all models, LES_{UU} consistently predicts approximately about 10 % higher power output. This comes from discrepancy arises because LES_{UU} predicts higher tangential forces in the middle sections of the blades estimated by LES_{UU} compared to the DWM models, likely due to differences in the aeroelastic solver. If this discrepancy seen in the turbine model is consistent for all velocities turbine-model discrepancy is consistent across all wind speeds, its impact can be adjusted for by normalizing all turbine powers with that of turbine 1. This would result in the power from by the power of turbine 1, as shown in Fig. 26 (see Appendix B for further discussion of this approach's validity). With this normalization, LES_{UU} generally aligns its power output generally aligns well with DWM_{NREL} for all turbines, while DWM_{DTU} and especially DWM_{IFE} typically estimate slightly higher power outputs overestimate the power for turbines 2–4. However, The exception is the partially waked case with a 5° angle between the inflow and the turbines rows shows inflow angle relative to the turbine row, which reveals the consequence of the DWM models not capturing the significant build-up of failing to capture the significant velocity-deficit to the sides of the build-up outside the rotor span. This In LES_{UU} , this build-up causes a drop in power from turbine 3 to turbine 4 in the LES_{UU} results which that is not captured by the DWM models. For turbine 4, LES_{UU} estimates the power to be 17–18 % lower than in the DWM models. This highlights the importance of accurate prediction of lateral accurately predicting wake spreading, particularly under real-world conditions, where perfect alignment is rare, as it can cause. Failing to capture wake spreading can lead to a non-negligible overshoot of the estimated overestimation of a wind farm's annual energy production of a wind farm. In this regard, the momentum-conserving superposition method applied in DWM_{IFE} is a promising approach, as it produces greater wake spreading and a more accurate increase in the off-rotor-span deficit, particularly in the low ambient turbulence case. However, the generally poor performance of this DWM implementation in estimating wake-deficit strength

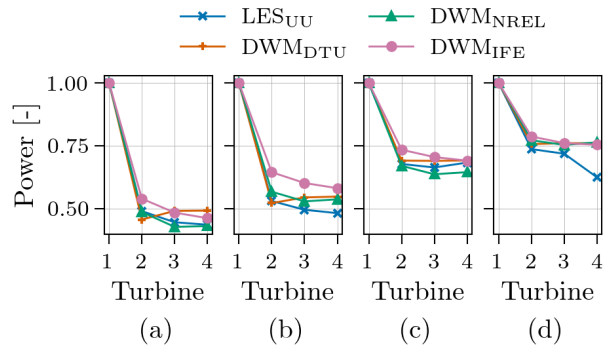


Figure 26. Mean power for the aligned incoming wind case with (a) low ($TI_a = 4.6\%$), (b) medium ($TI_a = 8.8\%$), (c) high ($TI_a = 12\%$) ambient turbulence, and (d) for the partially waked case (5° inflow angle) with medium ambient turbulence ($TI_a = 8.8\%$). For each model, the power outputs are normalized by the power of turbine 1.

for the medium and high ambient turbulence cases, prevents us from seeing the full potential of the momentum-conserving summation method in the partially waked scenario.

4.3 Fatigue-load predictions

880 Fatigue-load predictions represent the area of greatest divergence between the DWM and LES results, underscoring the challenges involved in of modelling wake-induced unsteady inflow conditions and their structural consequences. While all three DWM models are able to reproduce the general trends in time-averaged loads (e.g., mean blade forces and mean thrust), their predictions of damage equivalent loads (DELs) vary substantially, particularly for DELs vary substantially. The deviations are largest for the turbines operating under waked conditions, though differences are also evident for turbine 1, which likely originate from differences in the aeroelastic solvers. As with power, the influence of the aeroelastic solver can be limited by normalizing all turbine DELs by the DEL of turbine 1 (see Appendix B for a discussion of this approach's validity). The resulting normalized DELs for the blade-root flapwise bending moment and the tower-base fore-aft bending moment are shown in Figs. 27 and 28, respectively. Even though the normalization reduces the spread between the models slightly, the overall picture is the same. For the low ambient turbulence case, the DWM models tend to estimate lower blade loads and especially lower tower loads for the waked turbines compared to LES. For this case, DWM_{DTU} is closest to LES_{UU} in terms of DEL magnitude and its development along the turbine row. For higher ambient turbulence, the deviations between DWM and LES_{UU} are smaller. The DWM models predict a larger increase in DELs with rising ambient turbulence compared to LES_{UU}. Consequently, in the high ambient turbulence case the DWM models, and especially DWM_{DTU}, predict higher DELs than LES_{UU}, particularly for blade loads.

895 Spectral analysis reveals that all DWM models tend to overestimate the energy content at the $1P$ frequency for the blade loads. This has shown to be related to the higher estimated azimuthal blade force variations is related to higher azimuthal

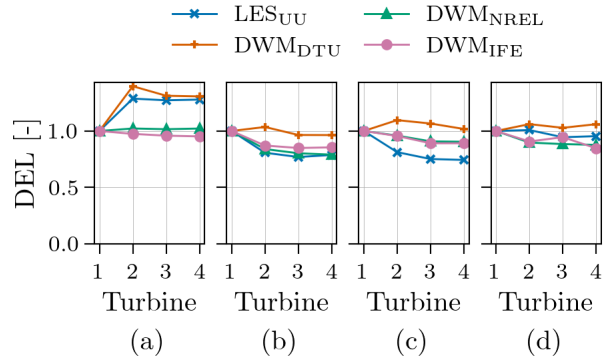


Figure 27. Fatigue of blade-root flapwise bending moment for the aligned incoming wind case with ambient turbulence of (a) $TI_a = 4.6\%$, (b) $TI_a = 8.8\%$, (c) $TI_a = 12\%$, and (d) for the partially waked case (5° inflow angle) with medium ambient turbulence ($TI_a = 8.8\%$). For each model, the DELs are normalized by the DEL of turbine 1.

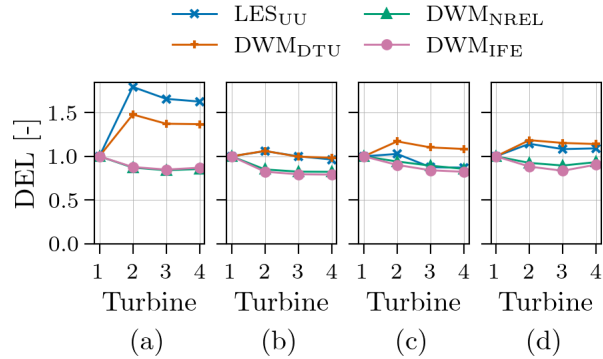


Figure 28. Fatigue of tower-base fore-aft bending moment for the aligned incoming wind case with ambient turbulence of (a) $TI_a = 4.6\%$, (b) $TI_a = 8.8\%$, (c) $TI_a = 12\%$, and (d) for the partially waked case (5° inflow angle) with medium ambient turbulence ($TI_a = 8.8\%$). For each model, the DELs are normalized by the DEL of turbine 1.

blade-force variations predicted by the DWM models, which is a direct consequence of the shape-of-the-shapes of their predicted wake velocity profiles. However, for some of the models, especially DWM_{DTU} , the blade force variation azimuthal blade-force variations seen in Figs. 12–13 and 23, and do not scale with the energy at $1P$ frequency do not scale as expected. As explained in Hanssen-Bauer et al. (2023), this mismatch likely comes from a wake meandering effect. When upstream wakes meander, the wake—an upstream wake meanders, it moves normal to the wind direction. This causes additional velocity gradients to appear—when a wake covers only parts of the only partially covers a downstream turbines’ swept-rotor area. These partially waked conditions, caused by wake meandering, last for several blade rotations since the meandering motion is slower than the blade rotation ($f_c < 1P$). The effect will is to a large extent not be visible in the blade force variation plots as blade-force

905 ~~variation plots, because~~ the forces are averaged in each azimuthal bin over the ~~whole-entire~~ simulation. However, ~~the-plots-of~~
~~wake-centre-positions-reveal~~ ~~wake-centre-position-plots-show~~ that DWM_{DTU} does not ~~estimate-higher-levels-of-meandering~~
~~predict-higher-meandering-levels~~ than the other models. Still, the ~~loads-load~~ spectra for DWM_{DTU} clearly show a significant
increase in energy at ~~the-low-frequencies~~ ~~low-frequencies~~ (associated with meandering ~~for-the-turbines-operating-under-waked~~
~~conditions,-which-~~) ~~for-the-waked-turbines-relative-to-turbine-1.~~ This behaviour is not seen ~~for-in~~ the other models ~~-This~~
910 ~~suggests-that-for-and-suggests-that-in~~ DWM_{DTU} , ~~the-meandering-has-a-higher-effect-on-the-loads-compared-to-meandering~~
~~affects-the-loads-more-strongly-than-in~~ the other models, possibly ~~due-to-the~~ ~~because~~ DWM_{DTU} produces more distinct deficits
with sharper radial gradients ~~in- DWM_{DTU} 's-case.~~

Consistent with ~~prior~~ findings for above-rated conditions ~~in-by~~ Hanssen-Bauer et al. (2023), we find that all DWM mod-
els tend to underestimate ~~the-fatigue-loading~~ ~~fatigue-loading~~ on downstream turbines, especially on the tower, if important
915 turbulence-generation mechanisms are neglected. In the present below-rated cases, the DWM_{DTU} model with ~~a-its~~ wake-added
turbulence model is the only DWM implementation that roughly captures the ~~increase-in-fatigue-damage-for~~ ~~increased-fatigue~~
~~damage-on~~ the turbines exposed to upstream wakes ~~for-relative-to-turbine-1-in~~ the low ambient turbulence case. However,
the magnitude of the increase in tower loads remains ~~under-predicted.~~ ~~For-the-cases-with~~ ~~underpredicted.~~ For higher ambient
turbulence, the trend is ~~not-so-clear,-but-for-the-blade-loads~~ ~~less-clear.~~ For blade loads, LES_{UU} shows a decrease in ~~DEL's-DELS~~
920 along the turbine row, ~~while-whereas~~ DWM_{DTU} still ~~estimates-an-increase-in-DEL's~~ ~~predicts-an-increase~~ from turbine 1 to
2. ~~The-reason-for-this~~ ~~inconsistency-can-be-due-to-the~~ ~~different-mechanisms-behind-the-increased-DEL's-estimated-by-This~~
~~inconsistency-appears-to-stem-from-different-mechanisms-causing-the-increased-DELS-in~~ DWM_{DTU} ~~and-versus~~ LES_{UU} for
the ~~turbines-operating-under-waked-conditions.~~ ~~For-waked-turbines.~~ In LES_{UU} , the high-frequency content of the load spec-
tra is ~~affected,-probably-directly-by-elevated,~~ ~~likely-due-to~~ the higher small-scale turbulence in the wake. This ~~effect~~ is most
925 pronounced in the ~~case-with~~ low ambient turbulence ~~case,~~ since the relative increase ~~here-is-higher~~ ~~in-small-scale-turbulence~~
~~is-greatest.~~ DWM_{DTU} , ~~by-contrast,~~ seems to affect the loads more indirectly ~~through-via~~ wake meandering, as described in
the previous paragraph. ~~The-wake-added-turbulence-can-possibly~~ ~~Wake-added-turbulence-could-also~~ play a role ~~here,-causing~~
~~meandering-of-the-wakes-to-have-an-increased-effect-on-the-loads-when-the-wakes-including-enhanced-turbulence-~~, ~~as-it-might~~
~~cause-the-meandering-wakes-with-enhanced-turbulence-to-have-a-greater-effect-on-loads-when-they~~ move in and out of the
930 ~~rotor's-swept-area.~~ ~~For-rotor-swept-area.~~ At higher ambient turbulence ~~levels,~~ the wake-added turbulence ~~seems-appears~~ to
play a smaller role in the fatigue-loading development along the turbine row ~~for-in~~ LES_{UU} , while for DWM_{DTU} the ~~increased~~
~~enhanced~~ meandering effect on loading ~~keeps-dominating~~ ~~continues-to-dominate.~~

Another important factor explaining the divergence between the DWM and LES fatigue results is the fact that the DWM
models ~~predict-assume~~ axisymmetric wakes that meander, whereas the instantaneous LES wakes can be highly asymmetric
935 and only approximately axisymmetric on average (~~as-seen-in-velocity-profiles-~~ ~~This-difference-is-clearly-illustrated-by-the~~
~~snapshots-of-instantaneous-velocity-profiles-for-the-low-ambient-turbulence-case~~ in Figs. 1-3 and 19). ~~This-deviation-from~~
~~symmetry-introduced-by-the-wake-in-the-LESA1.~~ While for the DWM models the shapes of the instantaneous wake deficits
~~can-be-recognised-from-the-time-averaged-ones-in-figure-1-for-all-turbines-in-the-row,~~ the LES wakes differ much more
~~in-shape.~~ This asymmetry in the LES_{UU} ~~results-is-likely~~ ~~flow-is~~ an important driver ~~on-the-tower-loads,-and-is-likely-to~~

940 ~~contribute to the underprediction of tower loads in the DWM models.~~ of loads, especially in the low ambient turbulence case, and appears as energy at higher harmonics of the blade rotational frequency, i.e. $2P$, $3P$, etc., for blade loads and $3P$, $6P$, etc. for tower loads. This phenomenon contributes to the DWM models' underprediction of loads. It aligns with the findings of Bernard et al. (2024), who investigated loads on a turbine under low-turbulence offshore conditions. Also here the traditional DWM models with axisymmetric wake deficits failed to capture the increased higher-harmonic content in the tower-top load spectra under waked conditions compared to free-inflow conditions. However, when a wake-distortion component was added to produce a non-axisymmetric wake in the DWM model, it showed better agreement with the measured load spectra and DELs.

An interesting observation is that LES_{UU} , ~~which~~ showed no significant change in energy below f_c for the fully waked case, but estimates increased energy below f_c ~~for the turbines operating under partially waked conditions from turbine 1 to turbines 2–4 in the partially waked case.~~ This was seen for the ~~blade-root blade-root~~ flapwise bending moment and tower-base fore-aft bending moment, but not ~~for~~ the tower-top yaw moment. ~~Since the upstream wakes on average are positioned to the side of the turbines operating in partial wake, combined with the fact that there is most meandering in lateral direction, results relatively often in the case where the wake moves completely~~ For turbines 2–4 in the partially waked conditions, the upstream neighbours are not directly ahead but offset laterally. As a result, lateral meandering relatively often moves the wake entirely away from the downstream turbines ~~sideways~~. This causes large ~~changes in the blade-root moment and the fluctuations in blade-root and tower fore-aft moment~~ ~~to appear in on~~ the meandering time-scale ($f < f_c$).

Overall, all DWM models struggle to capture the full range and ~~correct~~ intensity of wake-driven loading observed in LES. ~~Better~~ ~~A better~~ representation of turbulence evolution and its interaction with wake dynamics is crucial ~~to improve~~ ~~for improving~~ fatigue-load predictions in DWM frameworks.

4.4 Weaknesses of the present study

960 While the comparative analysis provides valuable insights into the performance of DWM-based wake models, several limitations of the present study must be acknowledged.

First, all simulations were conducted at a single below-rated wind speed with the turbines ~~running at constant~~ ~~operating at fixed~~ RPM and pitch. This constrains the ~~generalizability~~ ~~generalisability~~ of the findings to other operational regimes, particularly near rated or cut-out wind speeds, where aerodynamic and control responses differ significantly. At higher wind speeds, turbine control strategies such as blade pitch and generator torque regulation may alter wake characteristics and structural responses in ways ~~that are not captured here~~ ~~not captured in this study~~.

Second, the inflow conditions in both the LES and DWM simulations assume a neutral atmospheric boundary layer over homogeneous terrain, without thermal stratification. In reality, wind farms operate under more complex atmospheric conditions, including stable and unstable stratification, wind veer, and heterogeneous surface roughness. These factors influence turbulence intensity, wake deflection, and recovery, and may lead to larger discrepancies between engineering-fidelity models and field measurements.

970 Third, the modelled wind farm layout consists of a single row of four identical turbines with uniform spacing. While this configuration provides a controlled environment for model comparison, it lacks the complexity of real-world wind farms, where

turbines are arranged in staggered rows or irregular layouts and are subject to multi-directional wake interactions. Moreover, the only non-aligned inflow condition tested involved a ~~small~~ ~~modest~~ 5° offset, which is ~~modest~~ ~~small~~ relative to real-world offsets caused by wind-direction variability or ~~wake-steering~~ ~~wake-steering~~ control strategies. Larger inflow angles, including turbine yaw misalignments, could lead to more complex wake dynamics that challenge current DWM formulations.

Fourth, the simulation durations were finite, ~~and so~~ some load and flow statistics may be affected by sampling limitations (Liew and Larsen, 2022).

~~Finally~~ ~~Fifth~~, validation against field measurements was not part of this study. While high-fidelity LES-ALM provides a physically consistent ~~and~~, high-resolution reference, ~~the simulations are not necessarily reflecting these simulations do not necessarily reflect~~ one-to-one full-scale measurements (Asmuth et al., 2022; Sood et al., 2022). The actuator-line method used in the LES ~~model—though~~ ~~model – though~~ widely accepted as a high-fidelity ~~approach—introduces~~ ~~approach – introduces~~ its own approximations. The method represents blades as line forces rather than resolving blade-resolved flow features, which limits its accuracy in modelling near-wake vorticity, dynamic stall, and fine-scale unsteadiness. ~~The lack of an elastic turbine model also means that structural Eigenmodes are not captured, which is particularly important for tower dynamics.~~ Comparing model predictions against full-scale SCADA ~~or lidar, lidar, and strain~~ data would further strengthen the conclusions and reveal model limitations under real operational conditions.

~~Finally, the present comparison evaluates each DWM framework as a complete modelling system. Because several sub-models (e.g., wake-deficit formulations, wake-summation methods, meandering methods, and turbulence treatments) differ between implementations, differences in results cannot be attributed to any single modelling choice. As a consequence, some interpretations of the causes behind model discrepancies remain qualitative. The present intercomparison reflects the combined effects of multiple sub-model differences. A more rigorous assessment would require controlled sensitivity studies where individual sub-models are varied or exchanged within a single framework to isolate their influence.~~

Future work should address these limitations by considering a broader ~~set range~~ of operating conditions, ~~implementing including~~ variable atmospheric stability and wind shear, and ~~by~~ evaluating model performance in more complex ~~wind~~ farm layouts. ~~Enhanced turbulence modelling—including coupling of~~ ~~In addition, controlled sensitivity studies should be carried out to further disentangle the contributions of each modelling choice. Furthermore, improved turbulence modelling – both related to~~ wake-added turbulence ~~with meandering and more flexible wake-merging strategies—remains a~~ ~~in individual wakes and turbulence development across a wind farm related to turbulence build-up and increased meandering levels – remains a~~ key area for development in DWM frameworks. ~~Asymmetries in turbine wakes, both in the instantaneous wake deficit and in a time-averaged sense due to wake deflections, also appear to be important drivers to fatigue damage that are not captured by current DWM models.~~ Ultimately, continued benchmarking against both LES and high-quality field data is essential to advance the reliability of engineering-fidelity wake models for design and certification.

1005 5 Conclusions

This study presents a comprehensive comparison of three DWM-based wake models ~~—(the DTU, IFE, and NREL implementations—)~~ against high-fidelity LES for a row of four wind turbines operating under below-rated wind conditions. The main findings indicate that all three engineering-fidelity models capture the general wake evolution and turbine performance with reasonable accuracy in terms of mean values. ~~However, notable discrepancies arise in wake shape and unsteady load~~
1010 ~~predictions.~~ Specifically, the time-averaged turbine thrust force and aerodynamic power outputs ~~predicted by~~ from the DWM models generally ~~aligned~~ align with the LES benchmarks (often within ~~5–10~~ 5–10 %), suggesting that the DWM framework is broadly reliable for estimating wind farm energy yield ~~estimation in at~~ below-rated wind speeds ~~for a variety of~~ across various ambient turbulence intensities.

~~Nonetheless, the models~~ However, the DWM models still exhibit limitations in capturing ~~wake shapes~~ the wake shape, unsteady wake dynamics, and cumulative downstream effects observed in ~~the~~ LES, and ~~their~~ each implementation show distinct strengths and weaknesses ~~vary between the different DWM implementations.~~ Accurate modelling of far-wake shape is particularly important, as it influences both power output and structural loads on downstream turbines. For instance, the pronounced deficit build-up observed in the peripheral regions of the LES wake may significantly affect power ~~estimation~~ estimates under partially waked conditions. In this regard, the IFE model's wake superposition approach and ~~its~~ treatment of turbulence
1020 build-up via an eddy viscosity formulation appear to outperform the other models under low ambient turbulence conditions. At higher ambient turbulence levels, however, the benefit of these improvements is veiled by the IFE model's underprediction of wake-deficit strength. A more extensive calibration of the IFE model may therefore be necessary to enhance its performance under such conditions. In contrast, the DTU and NREL implementations with different wake summation models produce weaker wake expansion and less variation in incoming velocity among turbines 2–4, yet show better agreement with LES in
1025 terms of wake deficit strength and resulting power predictions for turbines operating under fully waked conditions. Another key observation is the presence of relatively small wake deflections in the LES, even without turbine yaw. These deflections, likely resulting from rotor tilt and three-dimensional wake effects, are crucial for predicting blade loading on downstream turbines ~~—The NREL model most closely replicates this behaviour, capturing also captures~~ the upward wake deflection ~~—Moreover, accurate representation of the increased turbulence in the turbine wakes—both spatial variation and spectral content—as~~
1030 ~~well as the progression of turbulence and meandering throughout the wind farm, is essential. Among the models, the DTU implementation, with its wake-added turbulence model, is closest to LES in capturing these turbulence characteristics. for turbines with rotor tilt, although not to the same extent as observed in LES.~~

Of critical concern are the substantial discrepancies in ~~fatigue-relevant load~~ fatigue-load predictions between the DWM models and ~~the LES. While all the LES. Under low ambient turbulence conditions, all~~ DWM implementations tend to ~~under-predicted~~
1035 ~~fatigue-damage~~ underpredict fatigue damage on downstream turbines ~~in low ambient turbulence and over-predict in~~ (especially in tower loads), whereas under high ambient turbulence they tend to overpredict fatigue loads. However, the DTU model is generally best at capturing the trend of varying loads along the row implementation, which includes a wake-added turbulence model, is generally the closest to LES in predicted fatigue load levels and best captures the load variations along the turbine

1040 row. These findings highlight the importance of accurately representing the increased turbulence in turbine wakes – both spatial variation and spectral content – as well as the downstream progression of turbulence and wake meandering across the wind farm. The current study also confirms previous findings that DWM’s underprediction of fatigue damage at low ambient turbulence is partly due to the assumption of an axisymmetric wake deficit, which prevents the model from capturing important asymmetric load effects on downstream turbines.

1045 ~~The implications for wind farm modelling and design are significant. On the positive side, DWM-based models offer a computationally efficient method for simulating wakes and can reasonably predict average flow deficits and power production across many scenarios. This makes them well-suited for wind farm layout optimization, control strategy development, and operational assessments, where full LES remains infeasible. The general agreement in power and thrust predictions supports the use of these engineering-fidelity tools for estimating energy production and first-order loads under below-rated, aligned inflow conditions. However, discrepancies in wake modelling performance present potential risks. If applied without careful validation, some DWM models may underestimate fatigue loads or overestimate downstream performance, potentially resulting in non-conservative designs.~~

1050 ~~In conclusion, while~~ While DWM models strike a favourable balance between accuracy and computational cost, further ~~refinement is necessary to~~ refinements are needed to address the shortcomings identified in this study so that these models can support all aspects of wind farm design and certification with confidence. ~~Continued development and calibration of these engineering-fidelity models, informed by~~ Future work should include continued development, calibration, and validation of DWM models against high-fidelity benchmarks and field measurements ~~, are essential. Addressing under a broader range of operating conditions and more complex farm layouts. Additionally, controlled sensitivity studies are recommended to isolate the contributions of each DWM sub-modelling choice. By addressing~~ the identified shortcomings ~~will enable~~, future DWM-based models will be able to more accurately represent complex wake interactions, ~~thus enhancing thereby improving~~ predic-
1060 tions of both energy yield and structural loads in large wind farms.

Author contributions. All authors: proposed the methodology, formal analysis, and investigation. ØWHB: simulated the test cases and submitted the DWM_{IFE} results. PD: simulated the test cases and submitted the DWM_{NREL} results. HAaM: simulated the test cases and submitted the DWM_{DTU} results. HA: Produced the LES inflow wind fields, simulated the test cases and submitted the LES_{UU} results. ØWHB: post-processed (except for the wake centre tracking) and visualized the data from the numerical models. PD: conducted the SAMWICH wake
1065 tracking and post-processing. ØWHB: wrote the manuscript draft. All authors: reviewed and edited the paper.

Competing interests. The authors declare that they have no conflict of interest.

Acknowledgements. This work has been funded by the Norwegian Research Council, through the project NEXTFARM: Engineering speed modelling of realistic fatigue for all the individual turbines in wind parks by representative pre-calculations, Grant No. 281020.

1070 This work was authored in part by the National Renewable Energy Laboratory for the U.S. Department of Energy (DOE) under Contract No. DE-AC36-08GO28308. The views expressed in the article do not necessarily represent the views of the DOE or the U.S. Government. The U.S. Government retains and the publisher, by accepting the article for publication, acknowledges that the U.S. Government retains a nonexclusive, paid-up, irrevocable, worldwide license to publish or reproduce the published form of this work, or allow others to do so, for U.S. Government purposes.

References

- 1075 Asmuth, H., Diaz, G. P. N., Madsen, H. A., Branlard, E., Forsting, A. R. M., Nilsson, K., Jonkman, J., and Ivanell, S.: Wind turbine response in waked inflow: A modelling benchmark against full-scale measurements, *Renew. Energ.*, 191, 868–887, <https://doi.org/10.1016/j.renene.2022.04.047>, 2022.
- Bartl, J., Mühle, F., Schottler, J., Sætran, L., Peinke, J., Adaramola, M., and Hölling, M.: Wind tunnel experiments on wind turbine wakes in yaw: effects of inflow turbulence and shear, *Wind Energ. Sci.*, 3, 329–343, <https://doi.org/10.5194/wes-3-329-2018>, 2018.
- 1080 Bernard, V., Andersen, S. J., Leon, J. M., Beaudet, L., Verelst, D., and Iliopoulos, A.: Observation and modelling of asymmetric loading on large offshore wind turbines in wake conditions, in: *Journal of Physics: Conference Series, The Science of Making Torque from Wind*, Florence, Italy, 29-31 May, 2024, 092092, vol. 2767, <https://doi.org/10.1088/1742-6596/2767/9/092092>, 2024.
- Bossuyt, J., Scott, R., Ali, N., and Cal, R. B.: Quantification of wake shape modulation and deflection for tilt and yaw misaligned wind turbines, *J. Fluid Mech.*, 917, A3, <https://doi.org/10.1017/jfm.2021.237>, 2021.
- 1085 Branlard, E., Martínez-Tossas, L. A., and Jonkman, J.: A time-varying formulation of the curled wake model within the FAST.Farm framework, *Wind Energy*, 26, 44–63, <https://doi.org/10.1002/we.2785>, 2023.
- Branlard, E., Jonkman, J., Platt, A., Thedin, R., Martínez-Tossas, L. A., and Kretschmer, M.: Development and Verification of an Improved Wake-Added Turbulence Model in FAST. Farm, in: *Journal of Physics: Conference Series, The Science of Making Torque from Wind*, Florence, Italy, 29-31 May, 2024, 092036, vol. 2767, <https://doi.org/10.1088/1742-6596/2767/9/092036>, 2024.
- 1090 Clayton, B. R. and Filby, P.: Measured effects of oblique flows and change in blade pitch angle on performance and wake development of model wind turbines, in: *Proceedings of the fourth BWEA Wind Energy Conference*, BHRA Fluid Engineering, Cranfield, Bedford, UK, 214–224, 1982.
- de Vaal, J. B. and Muskulus, M.: Simplified wake modelling for wind farm load prediction, in: *Journal of Physics: Conference Series, EERA DeepWind'2021*, Trondheim, Norway, 13-15 January 2021, 012012, IOP Publishing, <https://doi.org/10.1088/1742-6596/2018/1/012012>, 2021.
- 1095 Doubrawa, P., Barthelmie, R. J., Wang, H., and Churchfield, M. J.: A stochastic wind turbine wake model based on new metrics for wake characterization, *Wind Energy*, 20, 449–463, <https://doi.org/10.1002/we.2015>, 2017.
- Doubrawa, P., Annoni, J. R., and Jonkman, J. M.: Optimization-Based Calibration of FAST.Farm Parameters against SOWFA, 2018 Wind Energy Symposium, Kissimmee, Florida, USA, 8–12 January 2018, <https://doi.org/10.2514/6.2018-0512>, 2018.
- 1100 Doubrawa, P., Shaler, K., and Jonkman, J.: Difference in load predictions obtained with effective turbulence vs. a dynamic wake meandering modeling approach, *Wind Energ. Sci.*, 8, 1475–1493, <https://doi.org/10.5194/wes-8-1475-2023>, 2023.
- Fleming, P. A., Gebraad, P. M., Lee, S., van Wingerden, J.-W., Johnson, K., Churchfield, M., Michalakes, J., Spalart, P., and Moriarty, P.: Evaluating techniques for redirecting turbine wakes using SOWFA, *Renew. Energ.*, 70, 211–218, <https://doi.org/10.1016/j.renene.2014.02.015>, 2014.
- 1105 Glauert, H.: *Airplane Propellers*, in: *Aerodynamic Theory*, Springer, Berlin, Heidelberg, Germany, 169–360, 1 edn., https://doi.org/10.1007/978-3-642-91487-4_3, 1935.
- Hanssen-Bauer, W., De Vaal, J. B., Tutkun, M., Asmuth, H., Ivanell, S., and Stenbro, R.: Dependence of wind turbine loads on inlet flow field, in: *Journal of Physics: Conference Series, Wind Energy Science Conference*, Cork, Ireland, 17–20 June 2019, 062065, <https://doi.org/10.1088/1742-6596/1618/6/062065>, 2020.

- 1110 Hanssen-Bauer, W., Doubrawa, P., Madsen, H. A., Asmuth, H., Jonkman, J., Larsen, G. C., Ivanell, S., and Stenbro, R.: Comparison of three DWM-based wake models at above-rated wind speeds, in: *Journal of Physics: Conference Series, Wake Conference, Visby, Sweden, 20–22 June 2023*, 012054, <https://doi.org/10.1088/1742-6596/2505/1/012054>, 2023.
- International Electrotechnical Commission: *Wind energy generation systems - Part 1: Design requirements*, IEC 61400-1:2019, <https://webstore.iec.ch/en/publication/26423>, (last access: 5 February 2021), 2019.
- 1115 Jonkman, J., Butterfield, S., Musial, W., and Scott, G.: *Definition of a 5-MW reference wind turbine for offshore system development*, Tech. Rep., National Renewable Energy Laboratory, Golden, CO, USA, 2009.
- Jonkman, J., Doubrawa, P., Hamilton, N., Annoni, J., and Fleming, P.: *Validation of FAST. Farm Against Large-Eddy Simulations*, in: *Journal of Physics: Conference Series, The Science of Making Torque from Wind, Milan, Italy, 20-22 June 2018*, 062005, vol. 1037, <https://doi.org/10.1088/1742-6596/1037/6/062005>, 2018.
- 1120 Jonkman, J. M., Annoni, J., Hayman, G., Jonkman, B., and Purkayastha, A.: *Development of FAST. Farm: a new multi-physics engineering tool for wind-farm design and analysis*, 35th Wind Energy Symposium, Grapevine, Texas, USA, 9-13 January 2017, 0454, <https://doi.org/10.2514/6.2017-0454>, 2017.
- Keck, R.-E., Madsen, H. A., Larsen, G. C., Veldkamp, D., Wedel-Heinen, J. J., and Forsberg, J.: *A consistent turbulence formulation for the dynamic wake meandering model in the atmospheric boundary layer*, Ph.D. thesis, Technical University of Denmark, Lyngby, Denmark, 1125 2013.
- Keck, R.-E., de Maré, M., Churchfield, M. J., Lee, S., Larsen, G., and Madsen, H. A.: *Two improvements to the dynamic wake meandering model: including the effects of atmospheric shear on wake turbulence and incorporating turbulence build-up in a row of wind turbines*, *Wind Energy*, 18, 111–132, <https://doi.org/10.1002/we.1686>, 2015.
- Larsen, G. C. and Lio, A. W.: *Low-pass filtering of meandering scales*, in: *Journal of Physics: Conference Series, Wake Conference, Visby, Sweden, 10–12 June 2025*, 012020, vol. 3016, p. 012020, <https://doi.org/10.1088/1742-6596/3016/1/012020>, 2025.
- 1130 Larsen, G. C., Madsen, H. A., Thomsen, K., and Larsen, T. J.: *Wake meandering: a pragmatic approach*, *Wind Energy*, 11, 377–395, <https://doi.org/10.1002/we.267>, 2008.
- Larsen, G. C., Ott, S., Liew, J., van der Laan, M. P., Simon, E., Thorsen, G. R., and Jacobs, P.: *Yaw induced wake deflection - a full-scale validation study*, in: *Journal of Physics: Conference Series, The Science of Making Torque from Wind, Online, 28 September - 2 October*, 1135 2020, 062047, vol. 1618, IOP Publishing, <https://doi.org/10.1088/1742-6596/1618/6/062047>, 2020.
- Larsen, T. J., Madsen, H. A., Larsen, G. C., and Hansen, K. S.: *Validation of the dynamic wake meander model for loads and power production in the Egmond aan Zee wind farm*, *Wind Energy*, 16, 605–624, <https://doi.org/10.1002/we.1563>, 2013.
- Larsen, T. J., Larsen, G. C., Madsen, H. A., and Petersen, S. M.: *Wake effects above rated wind speed. An overlooked contributor to high loads in wind farms*, *EWEA Annual Conference and Exhibition, Paris, France, 17 - 20 November 2015*, 95–99, 2015.
- 1140 Larsen, T. J., Larsen, G. C., Pedersen, M. M., Enevoldsen, K., and Madsen, H. A.: *Validation of the Dynamic Wake Meander model with focus on tower loads*, in: *Journal of Physics: Conference Series, Wake Conference, Visby, Sweden, 30 May - 1 June 2017*, 012027, <https://doi.org/10.1088/1742-6596/854/1/012027>, 2017.
- Liew, J. and Larsen, G. C.: *How does the quantity, resolution, and scaling of turbulence boxes affect aeroelastic simulation convergence?*, in: *Journal of Physics: Conference Series, The Science of Making Torque from Wind, Delft, Netherlands, 1-3 June 2022*, 032049, vol. 2265, 1145 <https://doi.org/10.1088/1742-6596/2265/3/032049>, 2022.
- Liu, L., Franceschini, L., Oliveira, D. F., Galeazzo, F. C., Carmo, B. S., and Stevens, R. J. A. M.: *Evaluating the accuracy of the actuator line model against blade element momentum theory in uniform inflow*, *Wind Energy*, 25, 1046–1059, <https://doi.org/10.1002/we.2714>, 2022.

- Machefaux, E., Larsen, G. C., Troldborg, N., Hansen, K. S., Angelou, N., Mikkelsen, T., and Mann, J.: Investigation of wake interaction using full-scale lidar measurements and large eddy simulation, *Wind Energy*, 19, 1535–1551, <https://doi.org/10.1002/we.1936>, 2016.
- 1150 Madsen, H. A., Larsen, G. C., and Thomsen, K.: Wake flow characteristics in low ambient turbulence conditions, *Copenhagen Offshore Wind*, Copenhagen, Denmark, 26-28 October 2005, 2005.
- Madsen, H. A., Larsen, G. C., Larsen, T. J., Mikkelsen, R., and Troldborg, N.: Wake deficit-and turbulence simulated with two models compared with inflow measurements on a 2MW turbine in wake conditions, *European Wind Energy Conference and Exhibition*, Brussels, Belgium, 31 March – 3 April 2008, 48-53, 2008.
- 1155 Madsen, H. A., Larsen, G. C., Larsen, T. J., Troldborg, N., and Mikkelsen, R.: Calibration and validation of the dynamic wake meandering model for implementation in an aeroelastic code, *Journal of Solar Energy Engineering J. Sol. Energy Eng.*, 132, 041014, <https://doi.org/10.1115/1.4002555>, 2010.
- Madsen, H. A., Larsen, T. J., Larsen, G. C., and Hansen, K. S.: Wake flow characteristics at high wind speed, in: *34th Wind Energy Symposium*, San Diego, California, USA, 4-8 January 2016, 1522, <https://doi.org/10.2514/6.2016-1522>, 2016.
- 1160 Madsen, H. A., Larsen, T. J., Pirrung, G., Li, A., and Zahle, F.: Implementation of the Blade Element Momentum Model on a Polar Grid and its Aeroelastic Load Impact, *Wind Energ. Sci.*, 5, 1–27, <https://doi.org/10.5194/wes-2019-53>, 2020.
- Meyer Forsting, A. R., Pirrung, G. R., and Ramos-García, N.: A vortex-based tip/smearing correction for the actuator line, *Wind Energ. Sci.*, 4, 369–383, <https://doi.org/10.5194/wes-4-369-2019>, 2019.
- Michelsen, J. A.: Basis3D - a platform for development of multiblock PDE solvers, *Tech. Rep.*, Technical University of Denmark, Lyngby, Denmark, 1994a.
- 1165 Michelsen, J. A.: Block structured multigrid solution of 2D and 3D elliptic PDE's, *Tech. Rep.*, Technical University of Denmark, Lyngby, Denmark, 1994b.
- Monin, A. S., A. M. O.: Basic laws of turbulent mixing in the surface layer of the atmosphere, *Nauk SSSR Geophys. Inst.*, 24, 163–187, 1954. NREL: OpenFAST, <https://www.nrel.gov/wind/nwtc/openfast>, last access: 22 August 2025, 2025.
- 1170 Nygaard, T. A., De Vaal, J., Pierella, F., Oggiano, L., and Stenbro, R.: Development, verification and validation of 3DFloat; aero-servo-hydro-elastic computations of offshore structures, in: *Journal of Physics: Conference Series*, EERA DeepWind'2016, Trondheim, Norway, 20-22 January 2016, 425–433, vol. 94, <https://doi.org/10.1016/j.egypro.2016.09.210>, 2016.
- RCN: Engineering speed modelling of realistic fatigue for all the individual turbines in wind parks by representative pre-calculations - *Prosjektbanken*, <https://prosjektbanken.forskningsradet.no/project/FORISS/281020>, last access: 25 August 2025, 2025.
- 1175 Rychlik, I.: A new definition of the rainflow cycle counting method, *Int. J. Fatigue*, 9, 119–121, [https://doi.org/10.1016/0142-1123\(87\)90054-5](https://doi.org/10.1016/0142-1123(87)90054-5), 1987.
- Shaler, K. and Jonkman, J.: FAST.Farm development and validation of structural load prediction against large eddy simulations, *Wind Energy*, 24, 428–449, <https://doi.org/10.1002/we.2581>, 2021.
- Sood, I., Simon, E., Vitsas, A., Blockmans, B., Larsen, G. C., and Meyers, J.: Comparison of large eddy simulations against measurements from the Lillgrund offshore wind farm, *Wind Energ. Sci.*, 7, 2469–2489, <https://doi.org/10.5194/wes-7-2469-2022>, 2022.
- 1180 Sørensen, J. N. and Shen, W. Z.: Numerical modeling of wind turbine wakes, *J. Fluids Eng.*, 124, 393–399, <https://doi.org/10.1115/1.1471361>, 2002.
- Sørensen, N. N.: General purpose flow solver applied to flow over hills, *Ph.D. thesis*, Risø National Laboratory, Roskilde, Denmark, 1995.
- Trujillo, J.-J., Bingöl, F., Larsen, G. C., Mann, J., and Kühn, M.: Light detection and ranging measurements of wake dynamics. Part II: two-dimensional scanning, *Wind Energy*, 14, 61–75, <https://doi.org/10.1002/we.402>, 2011.
- 1185

Zong, H. and Porté-Agel, F.: A momentum-conserving wake superposition method for wind farm power prediction, *J. Fluid Mech.*, 889, A8, <https://doi.org/10.1017/jfm.2020.77>, 2020a.

Zong, H. and Porté-Agel, F.: A point vortex transportation model for yawed wind turbine wakes, *J. Fluid Mech.*, 890, A8, <https://doi.org/10.1017/jfm.2020.123>, 2020b.

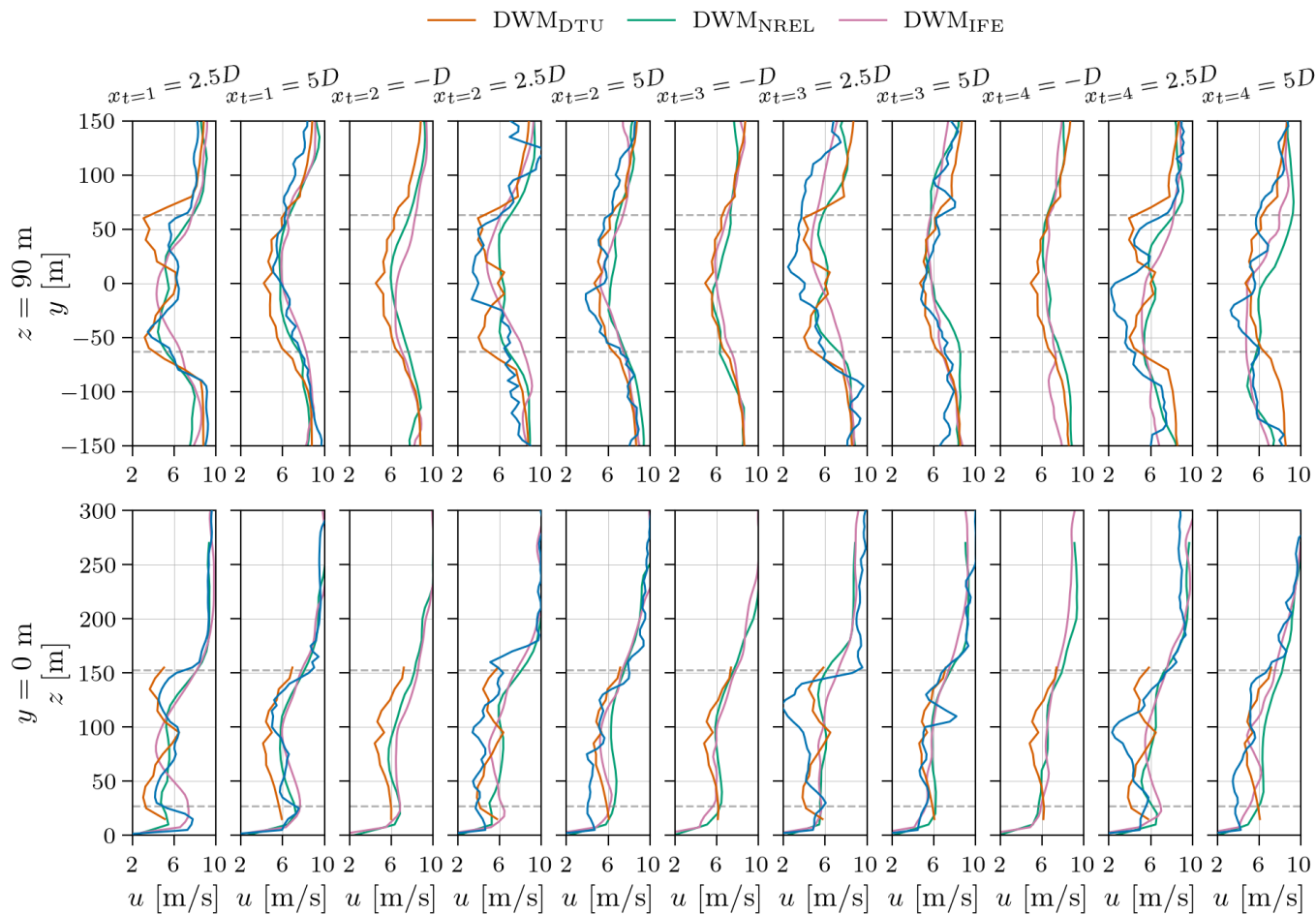


Figure A1. [Instantaneous velocity profiles at \$t = 100\$ s for the aligned incoming wind case with low ambient turbulence \(\$TI_a = 4.6\$ %\).](#) [Horizontal dashed lines indicate the rotor swept area. \$LES_{UU}\$ is missing at \$x_{t=i} = -D\$, \$i = 2, 3, 4\$ due to lack of time-resolved data at this axial position.](#)

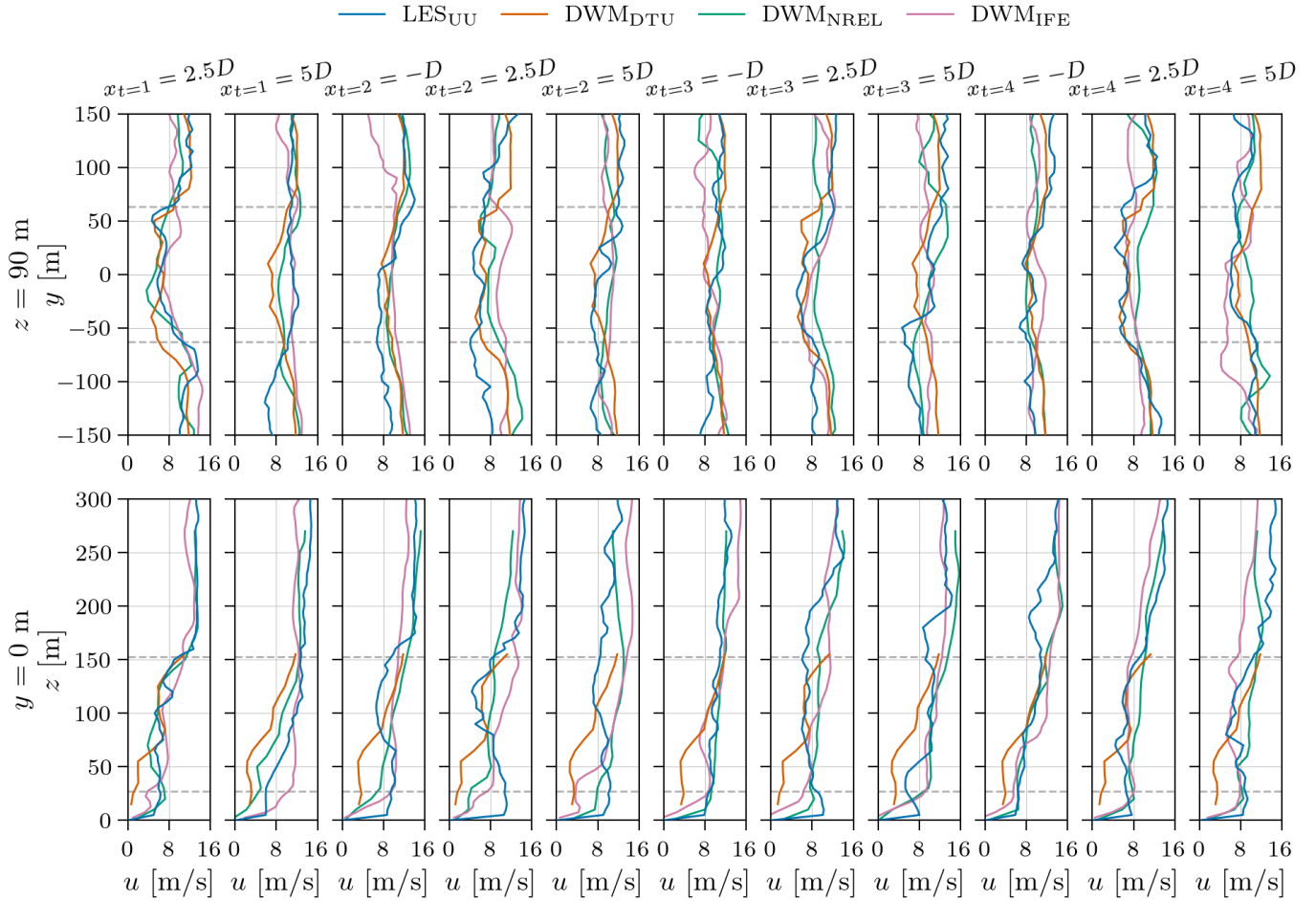


Figure A2. Instantaneous velocity profiles at $t = 100$ s for the aligned incoming wind case with high ambient turbulence ($TI_a = 12.0\%$). Horizontal dashed lines indicate the rotor swept area.

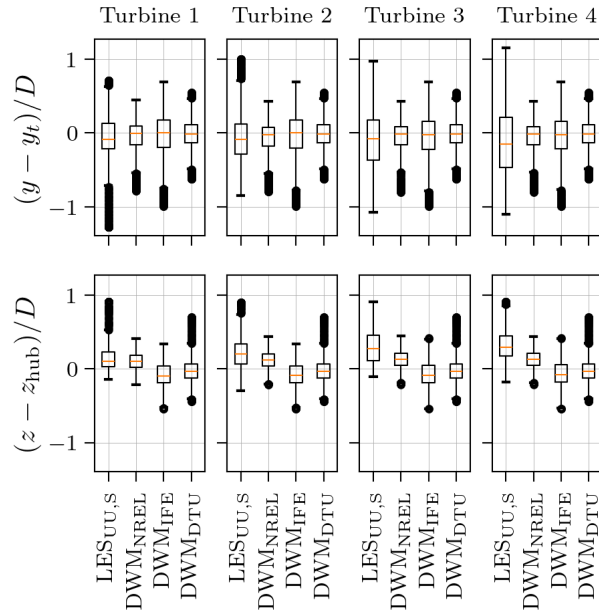


Figure A3. Box plots of horizontal (upper row) and vertical (lower row) wake centre positions at $x = 5D$ behind the turbines, for the aligned incoming wind case with medium ambient turbulence ($TI_a = 8.8\%$).

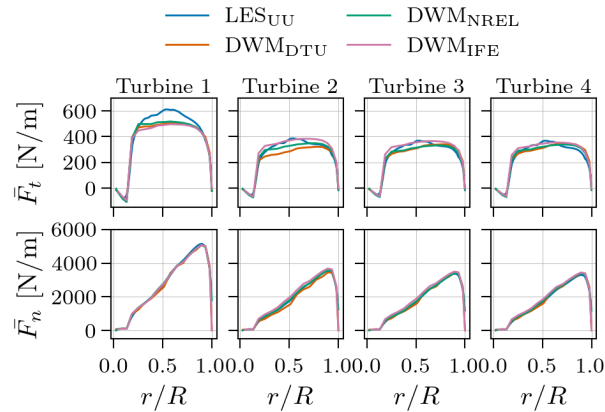


Figure A4. Time-averaged blade force as function of blade radius for the aligned incoming wind case with medium ambient turbulence ($TI_a = 8.8\%$).

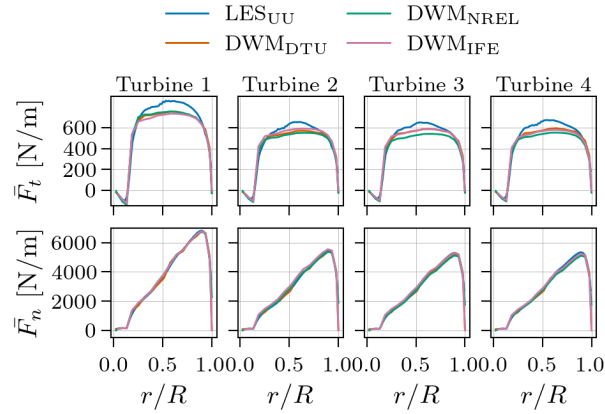


Figure A5. Time-averaged blade force as function of blade radius for the aligned incoming wind case with high ambient turbulence ($TI_a = 12\%$).

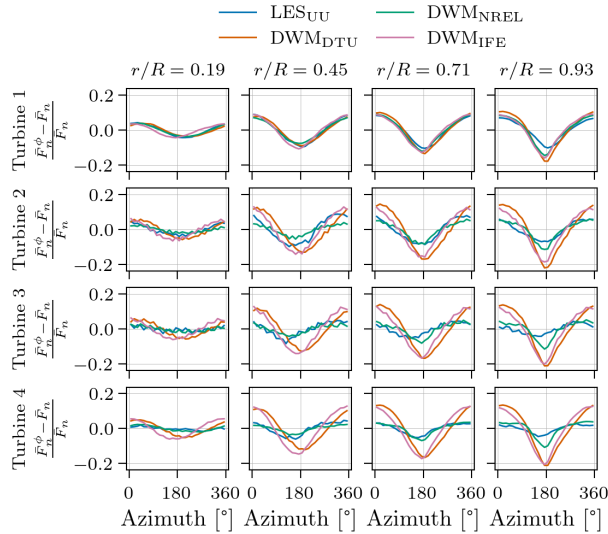


Figure A6. Relative difference between mean normal blade force per azimuthal bin \bar{F}_n^ϕ and total normal force \bar{F}_n , for $TI_a = 8.8\%$.

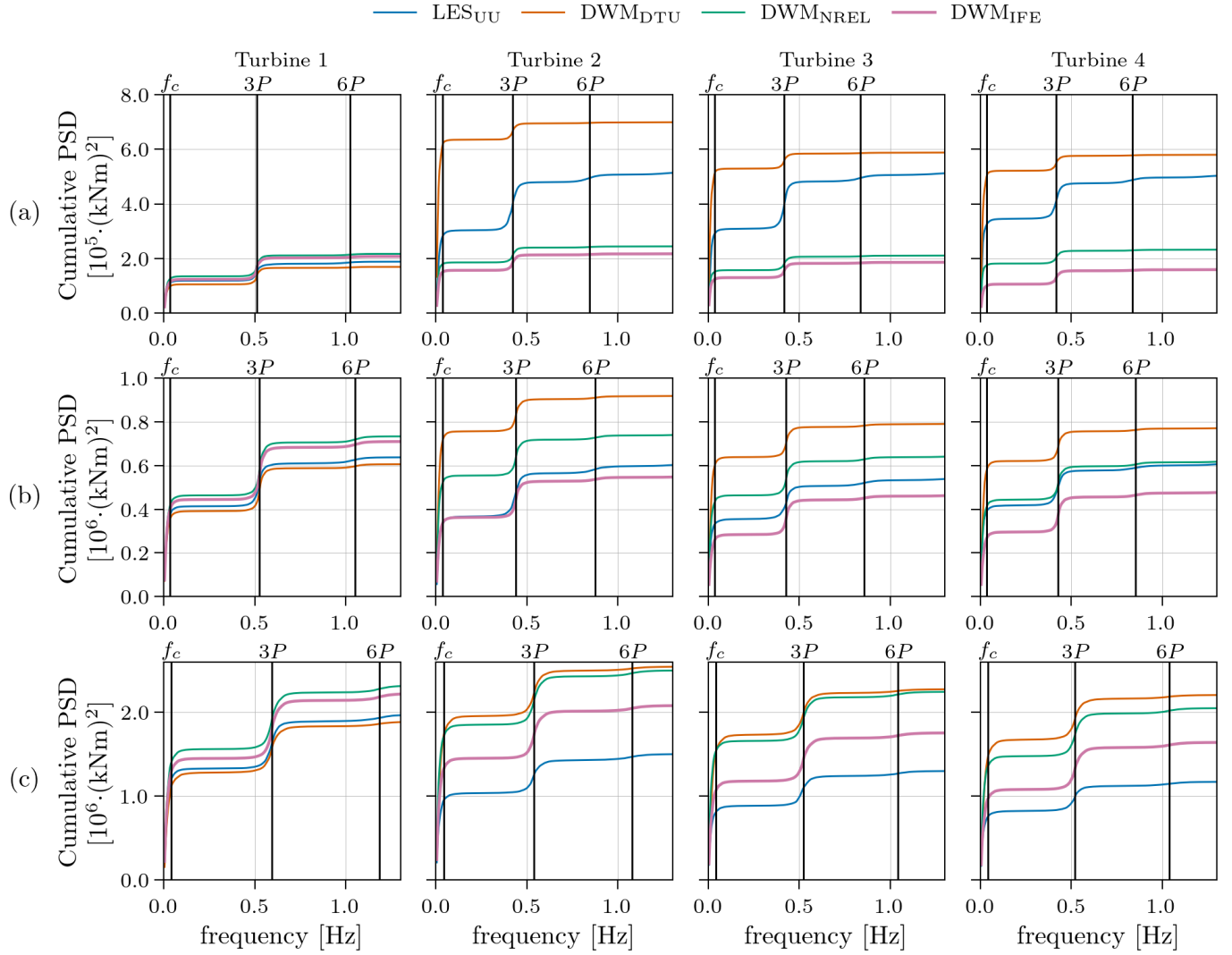


Figure A7. Energy spectra of tower-top yaw moment for the aligned incoming wind case with ambient turbulence of (a) $TI_a = 4.6\%$, (b) $TI_a = 8.8\%$, and (c) $TI_a = 12\%$.

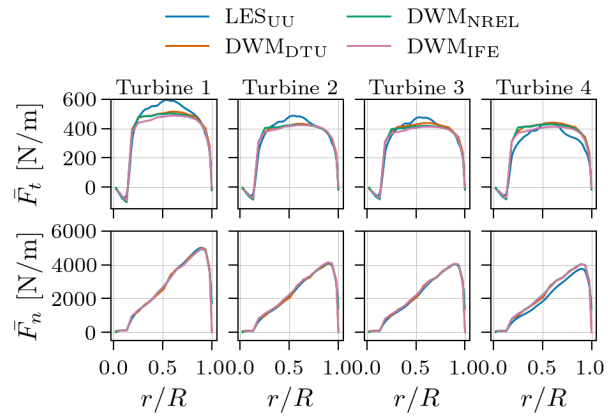


Figure A8. Time-averaged blade force as function of blade radius for the partially waked case, 5° inflow angle and medium ambient turbulence ($TI_a = 8.8\%$).

Appendix B: Aeroelastic solver sensitivity analysis

1195 Since the inflow to turbine 1 is identical across all models, any differences in response for this turbine likely originate from the aeroelastic solvers to which the different wake models are coupled, rather than from the wake models themselves – the primary focus of this study. Ideally, to isolate the impact of the wake models, all simulations should be performed using the same aeroelastic solver. However, this would require code modifications and rerunning the simulations.

1200 Alternatively, if the discrepancies between the aeroelastic solvers are consistent across wind speeds, the solver effect can be mitigated by normalizing all turbine outputs by the value of turbine 1. To test this assumption with minimal additional simulations, the flow fields from DWM_{NREL} and DWM_{IFE} at $x_t = -D$ were converted and used as input to 3DFloat, the aeroelastic solver from IFE. The resulting mean thrust force and aerodynamic power are shown in Fig. B1 for the aligned inflow case with medium ambient turbulence ($TI_a = 8.8\%$). The original results from DWM_{NREL} and DWM_{IFE} are also included for comparison.

1205 As expected, thrust and power outputs for turbine 2–4 are lower in the simulations using flow fields at $x_t = -D$, compared to the original simulations where the inflow has recovered for $1D$ longer. However, while the original DWM_{NREL} results were generated using NREL’s aeroelastic solver OpenFAST, the three other simulations all used 3DFloat. Because the reductions in thrust and power between the simulations using the wake model by NREL and for the simulations using the wake model by IFE are similar, we can conclude that the aeroelastic solvers have a negligible effect on the reduced results.

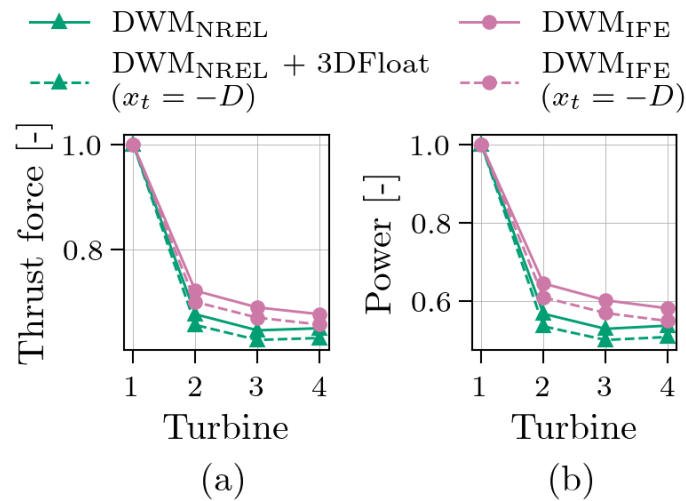


Figure B1. (a) Mean thrust force and (b) mean power for the aligned incoming wind case with medium ambient turbulence ($TI_a = 8.8\%$). For each model, the thrust and power outputs are normalized by the value of turbine 1.

Similarly, the DELs of the blade-root flapwise bending moment, tower-top yaw moment, and tower-base fore-aft bending moment are shown in Fig. B2 for both the new and original simulations. Here, the DELs for turbine 2-4 are higher in the

1210 simulations using the flow fields at $x_t = -D$, as expected, since the inflow in the original simulations has recovered for $1D$ longer and become less turbulent. Also for the DELs, the reductions are similar for the simulations using the wake model by NREL and for the simulations using the wake model by IFE, even though some slightly larger deviations are observed than for the mean values. Still, it seems like an acceptable conclusion that also for the fatigue damage the aeroelastic solvers have a negligible effect on the results when normalized by the value of turbine 1.

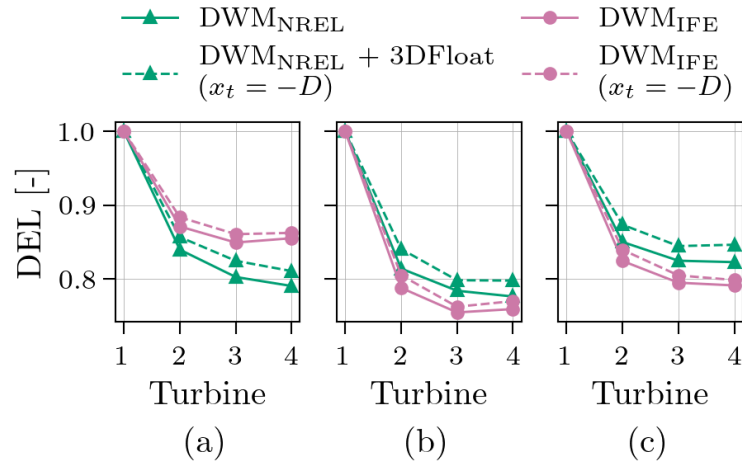


Figure B2. Fatigue of (a) blade-root flapwise bending moment, (b) tower-top yaw moment, and (c) tower-base fore-aft bending moment for the aligned incoming wind case with medium ambient turbulence ($TI_a = 8.8\%$). For each model, the DELs are normalized by the DEL of turbine 1.